(2)

Quarterly Report

on

Long Endurance Underwater Power System

January 1989 - March 1989

Contract No. N00014-87-C-0335

Aquanautics Corporation
980 Atlantic Avenue, #101
Alameda, CA 94501
April 24, 1989

Table of Contents

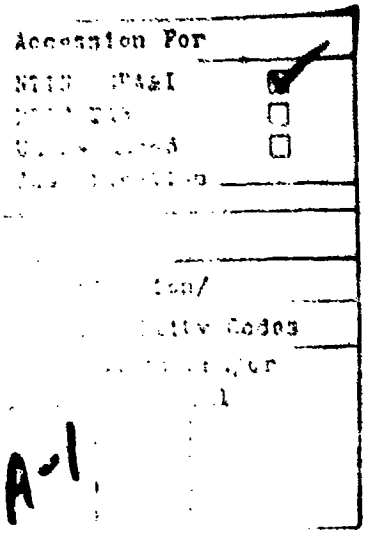

1.0 SUMMARY

The work carried out from January 1989 through March 1989 under the present contract is described in this report. Major activities undertaken in this quarter can be categorized as follows:

a) Direct Feed of Oxygen Carrier into Fuel Cell: Previous work carried out with carrier in a half-cell has been extended to a fuel cell where H_2 has been incorporated as the fuel. The positive power obtained (0.17 V @ 10 mA/cm^2) in the fuel cell is in itself a major achievement. Performance analysis points to the possibility of improvement in the hydrogen anode and the carrier, as well as a reduction in IR losses.

b) Gill: For operation at depth, gill membrane elements need to be of a solid type rather than microporous. Another requirement being that hollow fiber membranes are necessary, implies a very limited number of sources of supply. Aquanautics has been able to identify a source and has already tested a cartridge from them. The microporous control cartridge and solid membrane had roughly similar oxygen flux characteristics, and the difference was attributable to the geometry of the cartridges. Oxygen transport through the membranes has been modelled and the results are expected to yield design equations enabling selection of gill geometry and design parameters.

c) Hydrogen Generator: Subsequent to the feasibility study of hydrogen generation by reacting seawater with aluminum, Alupower, Inc. has delivered a 1W-1 month Al-Seawater battery/hydrogen generator. The system is compact and will be tested.

Based on the work done in this quarter, the system volume targets for a one kilowatt system operating continuously for a period of one year have been formulated.

They are as follows:

H_2 Generator	4000 l
Aquanautics Gill	500 l
Fuel Cell	400 l
Other	100 l
Total System Volume	5000 l

Activities planned for the next quarter are as follows:

1) Fuel cell performance improvement via,

   a) H_2 - anode modification,
   b) Lower IR drop via better contact, better bonding of H_2 - anode and membrane, and
   c) Carrier study leading to lower cathodic losses.

2) Gill: A solid gill membrane packaged into a design suitable for oxygen transfer will be procured for testing. Gill sizing models will be developed and calibrated using experiments on packaged gills of the appropriate geometry.

3) H_2 Generation: Testing of the Alwatt battery will be carried out to characterize its performance.

4) Integration: A small-scale integration of gill and fuel cell will be carried out preparatory to a 10 W integration that is scheduled for later on in the program.

2.0 UNDERWATER POWER SOURCE (UPS): OVERALL SCHEMATICS

Figure 1 shows the schematic diagram for a long endurance UPS with direct carrier feed fuel cell (CFFC) process. In this scheme, three basic units are shown:

1. Alwatt hydrogen generator
2. Hybrid fuel cell
3. Gill

The gill and the right half of the fuel cell in the figure represent the contribution of Aquanautics' technology. The Alwatt H_2 generator is produced by Alupower, Inc., Bernardsville, New Jersey. The design of Alwatt will be modified to suit UPS needs. The fuel cell is of a special type being jointly developed by Aquanautics and a fuel cell manufacturer named Giner, Inc., Waltham, Massachusetts. The gill design and requirements are being met jointly with Applied Membrane Technology, Minnetonka, Minnesota. The oxygen carrier is an integral part of Aquanautics' patented technology.

2.1 Process

1. Gill

At the gill, oxygen dissolved in seawater at a concentration of approximately 3 ml/l of seawater is transferred through a membrane packaged into a gill. Proper packaging of the membrane is essential to provide:

i) low volume/unit oxygen transferred
ii) low seawater drag losses
iii) low carrier pumping cost

It has been concluded that a rectangular gill package with a hollow fiber membrane will be the design choice with carrier flowing inside the hollow fiber and seawater flowing outside. More detailed results of gill experimentation can be found in Section 5.0.

The driving force for O_2 diffusion is the difference in oxygen concentration between the seawater and carrier.

2. Fuel Cell

The carrier picks up oxygen at the gill, and in the fuel cell oxygen gets reduced. The exact chemical reaction mechanism is not yet known, but the overall reaction is deduced to be:

$$(LM)_2 - O_2 + 2H_2O + 4e^- \text{---> } 2LM + 4OH^-$$

To counteract the OH^- generated, electrochemical oxidation of hydrogen is employed on the other side of a cation-exchange membrane. The hydrogen ion generated comes across the membrane and neutralizes the OH^-. The reaction at the anode is,

$$2H_2 \text{ ---> } 4H^+ + 4e^-$$

The hybrid fuel cell design is a new concept. Details, progress and status of the fuel cell testing can be found in Section 4.0.

FIGURE 1
Schematic Diagram for Proposed UPS

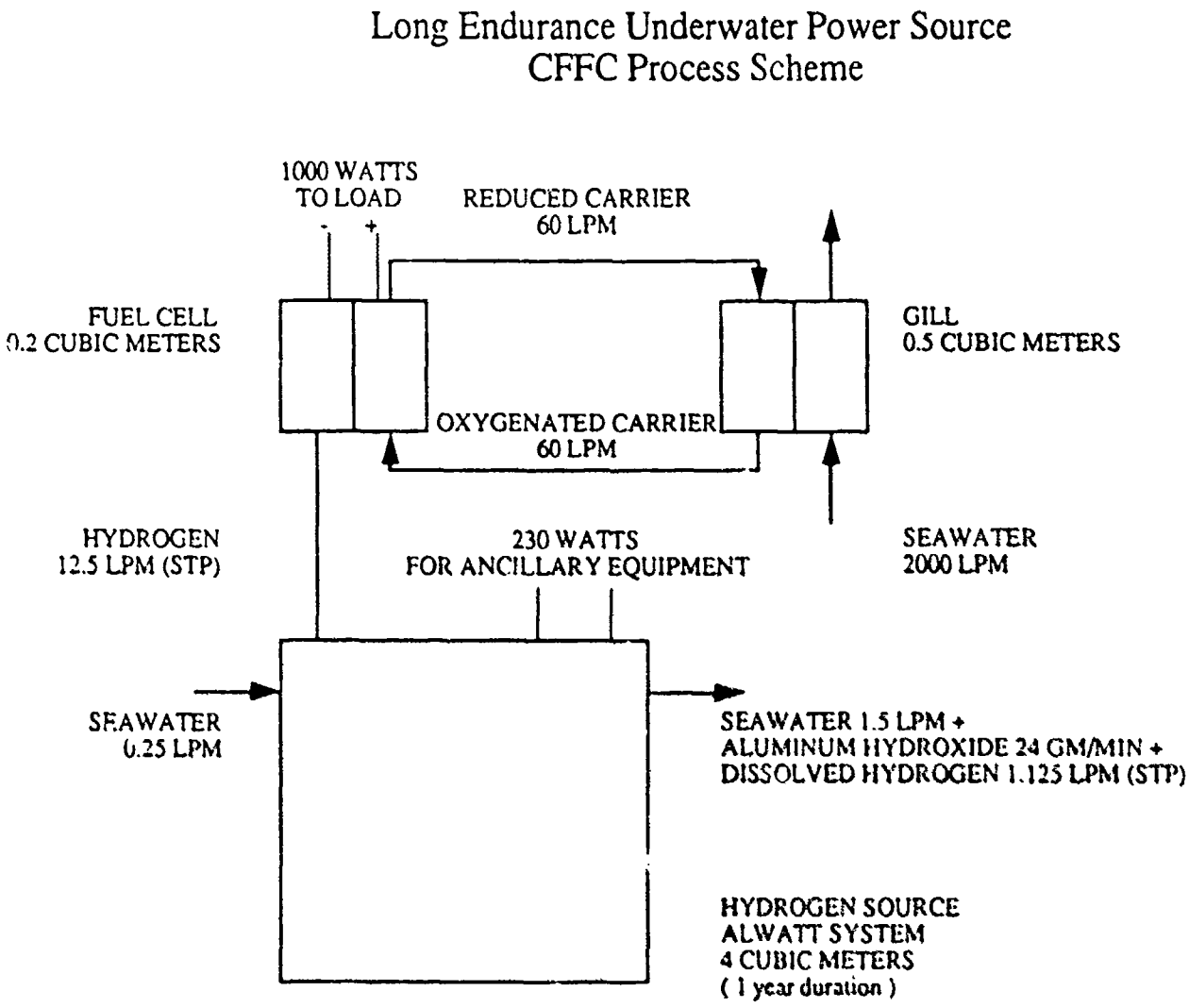

3. Alwatt Hydrogen Generator

Although the source of Hydrogen can be cryogenic Hydrogen, Aquanautics has already reported that the Alwatt system provides a much safer and volumetrically superior option for the UPS. Aluminum is reacted with seawater in a corrosion cell and provides some power as well.

The overall reaction is:

$$Al + 3H_2O \text{ ---> } AL(OH)_3 + \frac{3}{2} H_2$$

More details of the Alwatt system can be found in Section 6.0.

2.2 Performance Targets

The specifications for the operation of an UPS are dictated by the site of operation which is expected to be at ocean depths of up to 6000 m. Conditions of operation are likely to be as follows:

1. Depth ≈6,000 meters or 600 atmospheres pressure,
2. Temperature 0 - 3°C,
3. O_2 concentration 3 ml/l of seawater,
4. Biological Fouling almost non-existent, and
5. Geological Fouling is to be determined.

The objective of this program is to develop a system that is superior to that provided by competing technologies and to provide the Navy with a viable option for its needs. On the basis of a 1 kw-yr system a comparison between existing technologies and the expected Aquanautics system is depicted in Table 1. Use of standard fuel cells with stored reactants was not considered owing to the need for expensive and cumbersome pressure vessels.

TABLE 1
Comparison of Viable Systems

	Vol. m^3	Weight, T
Alwatt Battery	14.6	19.5
AL/Peroxide	14.6	14.6
$Li/SOCl_2$	14	20
Aquanautics	5	5-8

Table 2 lists the breakdown of system volume by component. The volumes shown here represent performance targets that have to be established in order to attain viability as shown in Table 1.

TABLE 2
Performance Targets

Item	Parameters	Vol/KW or KW-YR liters
Alwatt	<0.0006 l/l of H_2	4000
Gill	<80 l/lpm of O_2	500
Fuel Cell	>160 w/lpm of O_2 >80 w/lpm of H_2	
volume.	<200 l/kw	220
Controls, etc.		100
Total System Volume		4820

Table 3 shows the volumes of the various components under the best case scenario. These represent theoretical limits implied by the thermodynamics of the various processes as well as the current state-of-the-art in the case of gill design.

TABLE 3
Theoretical Limits

Alwatt	0.0003 l/l of H_2	1000
Gill	40 l/lpm of O_2	240
Fuel Cell	320 w/lpm O_2 160 w/lpm H_2 30 l/kw[1]	30

2.3 Model

Detailed modeling was carried out under a separate Defense SBIR program (contract #DAAH01-88-C-0413). The essence of that model is given here. The model has been updated with new information available, mainly from Alupower. Table 1 shows the performance target components of a 1 kw-yr. UPS.

[1]Based on Published data for Standard Fuel Cells.

Figure 2 shows the sensitivity of the component volumes with respect to fuel cell voltage. This is the single most important factor determining the overall volume of the power source. The principle of this power source is that Aquanautics is trying to utilize the hydrogen generated by the Alwatt system. The amount of hydrogen consumed will determine the amp-hours and when multiplied by voltage will give the watt-hours. Therefore to obtain a given watt-hour, the amount of hydrogen needed will be inversely proportional to voltage of the individual fuel cell. Consequently volume of Alwatt is inversely proportional to the voltage of the fuel cell. It is quite clear that the gill volume and fuel cell volume are much smaller than the Alwatt volume. They are also inversely proportional to fuel cell voltage. The current density of the fuel cell has an important bearing on the fuel cell only. It reduces the total volume of the fuel cell which will directly reflect on the cost. The fuel cells will be the most expensive component on a unit volume basis. Current density will have another important effect. Higher operating current density will reduce the fuel cell separator area and thereby reduce the loss of hydrogen from the anode side of the fuel cell to the cathode side and therefore to the sea through the gill.

FIGURE 2
Results of System Modelling

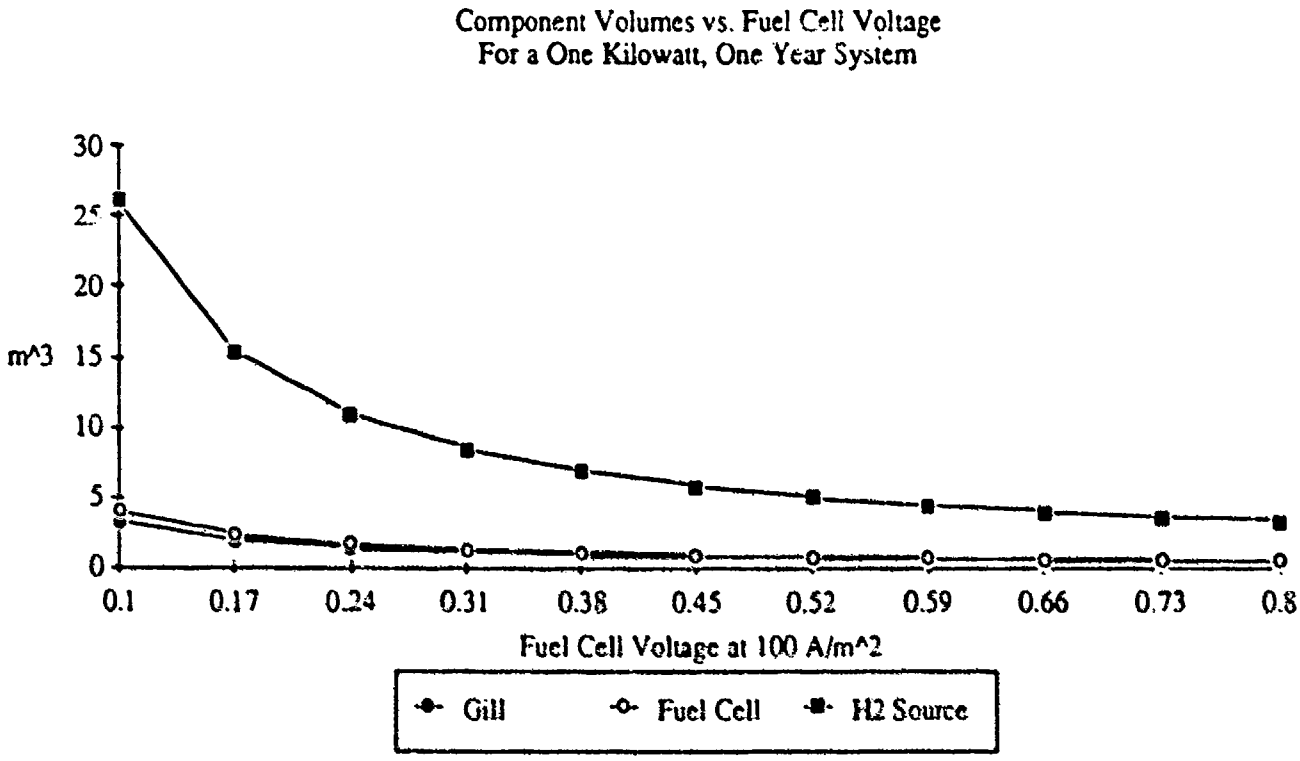

3.0 OVERALL PLAN

The overall plan for this year's work is shown in a PERT chart (Figure 3) where the major activities are laid out. Each activity also has a few sub-activities that are shown in this plan. Major milestones where integration will be undertaken are as follows:

Small-Scale Integration: This is to test a 25 cm^2 fuel cell with a small solid gill membrane cartridge providing the required oxygen.

10 Watt Demonstration: This would involve integrating the gill, fuel cell and the Alwatt into a 10 Watt power generation device.

The activities represented in shaded boxes have already been completed. The numbers at the top left side of the activity box indicate the scheduled starting date of the activity. In addition to the above milestones, work shall also proceed on the following technical issues.

Carrier Longevity and Kinetics Study: This is a program that is being worked out with Aquanautics' industrial partner who is interested in oxygen generation on land. The results of this program are directly applicable to the present program. The object of this program will be to obtain a carrier stable up to one year or more at the end of 1991.

Fuel Cell Related Activities: This area is the most revolutionary aspect of the program. The program objective is to obtain 0.4V, 10 mA/cm^2 this year and next year the target would be 0.6V at 30 mA/cm^2.

Gill Related Activities: Aquanautics needs to procure a bigger custom-made gill for the 10W demonstration as well as to check for volume and power requirements of the gill. Experimental results shall be used to verify design equations that will be developed.

Hydrogen Generator: This activity relates to obtaining a bigger Alwatt hydrogen generator and testing it.

FIGURE 3
Overall DARPA V Program

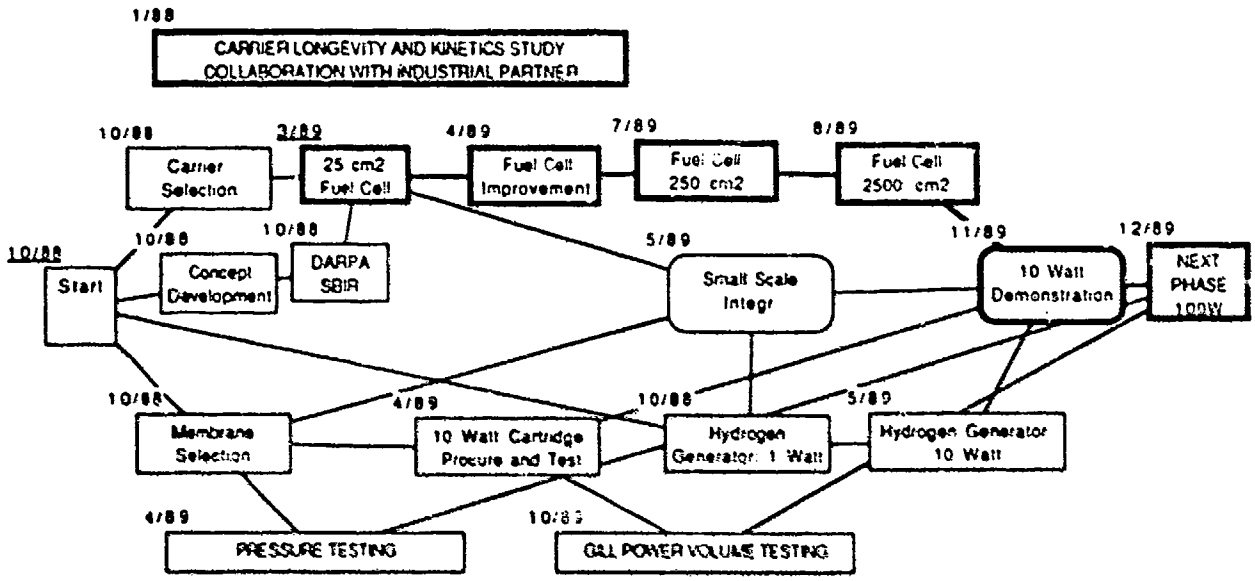

4.0 FUEL CELL

4.1 Introduction

In an earlier contract sponsored by DARPA (Contract #DAAH01-88-C-0413), the feasibility of carrier being fed directly to a half-cell equivalent of the cathode in a fuel cell had been established. This section describes experiments involving the integration of Aquanautics' carrier technology and a real fuel cell employing hydrogen.

These results are to be construed as preliminary in the sense that the fuel cell design is revolutionary and much different than that of a standard fuel cell and the reactants are very different. There is, thus scope of much further improvement and this will be followed up in future work.

4.2 Thermodynamics of H_2/O_2 Fuel Cell

A fuel cell involving H_2 and O_2 leads to the following overall reaction:

$$2H_2\,(g) + O_2\,(g) \text{---> } 2H_2O(l),\ \Delta G^o,\ = 113.38 \text{ kcal/mole} \qquad (1)$$

The relationship of emf. (E^o) to the Gibb's free energy (ΔG^o) is as follows:

$$\Delta G^o = -nFE^o$$

This yields a voltage of 1.23 volts at atmospheric pressure and a temperature of 298°K. Using an oxygenated carrier, the above equation has to be changed to:

$$2H_2\,(g) + (L\text{-}M)_2^{2+}\,O_2 \text{---> } H_2O + 2L\text{-}M^2,\ \Delta G_2^o \qquad (2)$$

To calculate ΔG_2^o, ΔG^o of the following equation has to be known:

$$2L - M^{2+} + O_2 \text{---> } (L - M)_2^{2+} - O_2,\ \Delta G_3^o = 15 \text{ kcal/mole} \qquad (3)$$

From previous studies it has been determined that ΔG^o is of the order of 10-15[3] kcal/mole.

$$\Delta G_2^o = \Delta G_1^o - \Delta G_3^o$$

$$\cong -98 \text{ kcal/mole}$$

Therefore the emf., $E^o = 1.06V$

The lower temperature of operation and higher pressure of hydrogen will lead to a further increase in the potential[2]. The slopes of potential vs. temperature and pressure are:

---

[2]Tilak, B.V., Yeo, R.S., and Srinivasan, S., "Electrochemical Energy Conversion - Principles," *Comprehensive Treatise of Electrochemistry*, 3, Plenum, New York (1981).

$$\frac{\partial \Delta G}{\partial T} = -0.84 \text{ mv/}^{o}\text{C} \quad (4)$$

$$\frac{\partial \Delta G}{\partial \log P} = 45 \text{ mV} \quad (5)$$

Therefore, the potential E^{o} at 100 atmosphere and $O^{o}C$ will definitely be higher by another 100 mV or so.

This leads to $E^{o} \cong 1.16V$ compared to 1.23V for land use of a SPE (solid polymer electrolyte) type fuel cell.

4.3 Operation of a Fuel Cell

Unfortunately, the fuel cell does not operate at the thermodynamic point as there are losses encountered due to polarization and cell resistance. These losses depend on the current density of operation. The operational schematic of a typical land-based SPE fuel cell is shown in Figure 4. The operating characteristics of such a cell are depicted in Figure 5. It can be seen that a fuel cell should operate at around 0.85V for 300 A/ft^2 or 322 mA/cm^2. A direct feed fuel cell should therefore operate at around 0.70V at this current density if all the losses are eliminated.

4.4 Fuel Cell Design

Simple integration of a standard fuel cell with Aquanautics' carrier is not expected to function properly. All the standard fuel cells are designed to use gaseous oxygen as feed to the cathode side. In Aquanautics' system the liquid oxygenated carrier flows through the cathode side. So far, Aquanautics has been using a high surface area cathode in its fuel cell experiments and this seems to work quite favorably.

Another reason that Aquanautics had to change the fuel cell design is that previously researchers had determined that Nafion type (a product from Dupont) ion-exchange membranes react with the carrier. Most of the SPE fuel cell electrodes that have been manufactured to date are made of Nafion type membranes. Aquanautics' researchers have identified another membrane called RAI4010 manufactured by RAI Research Corporation, that functions without adverse reactions with the carrier solution.

These two modifications were incorporated in the new design and experiments were carried out to observe the performance of a fuel cell. Towards the end, the performance of this fuel cell was analyzed to determine improvements that are needed. The schematic of a direct feed fuel cell are shown in Figure 6. Requests for supply of the fuel cell electrodes were sent to four companies. They were:

1. Giner, Inc., Waltham, Massachusetts,
2. Ergenics, Inc., Wyckoff, New Jersey,
3. Treadwell Corporation, Thomaston, Connecticut, and
4. Ballard Technologies, Vancouver, Canada.

Two proposals were received and Giner, Inc. was asked to supply the fuel cell anode pressed onto a RAI4010 membrane.

FIGURE 4

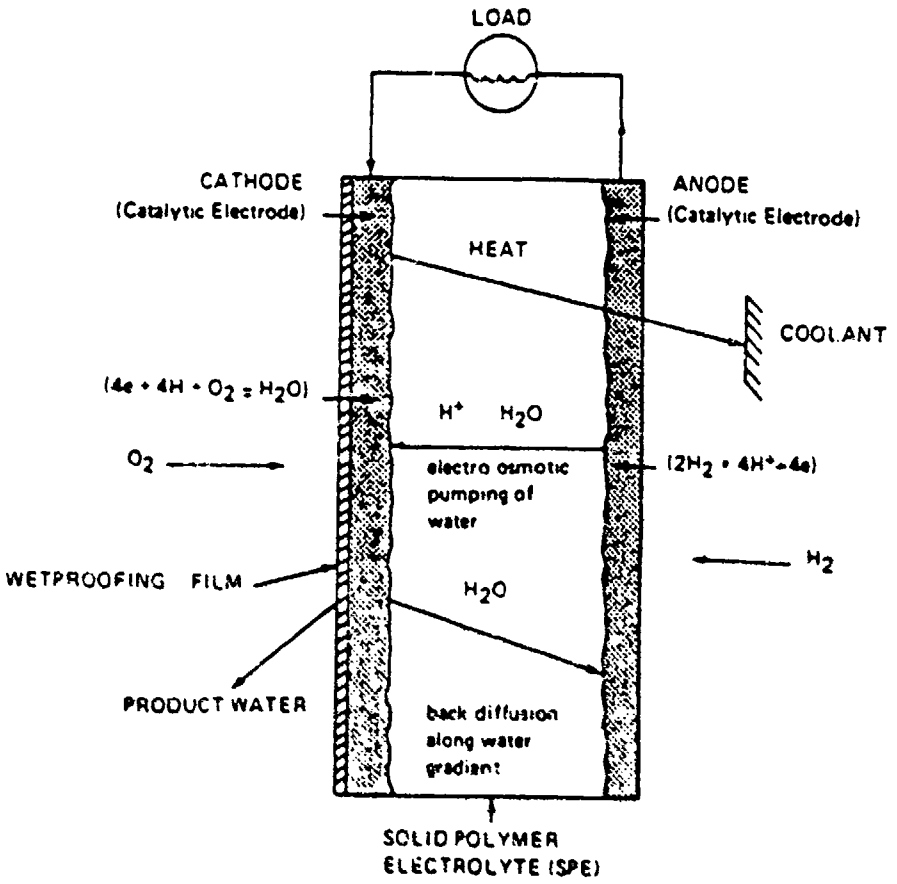

THE BASIC STRUCTURE IN THE FUEL CELL MODULE

FIGURE 5

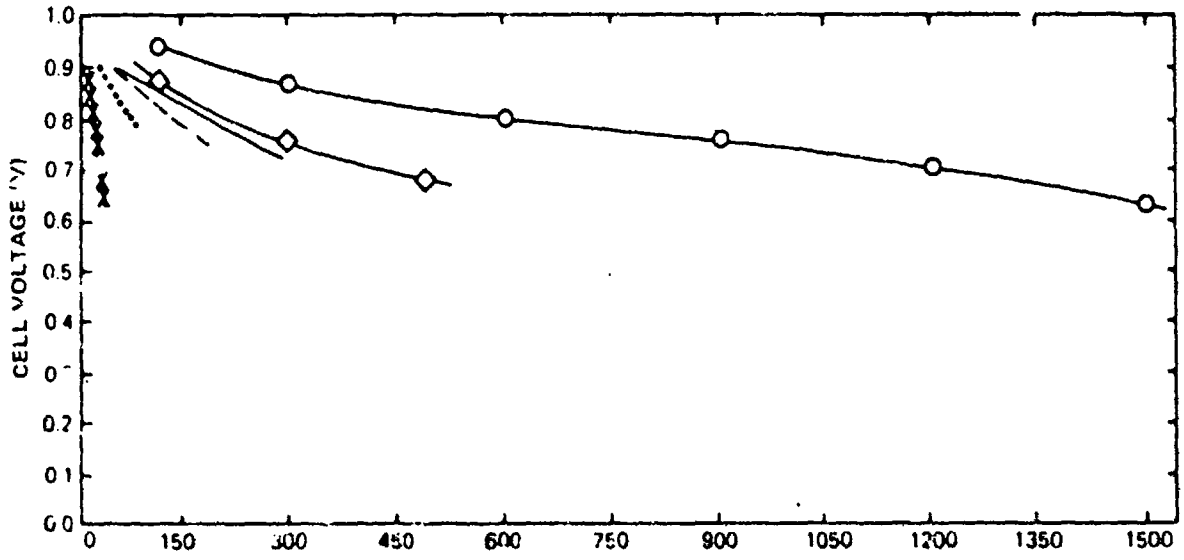

GENERAL ELECTRIC/HAMILTON STANDARD
FUEL CELL PERFORMANCE (O_2/H_2)

FIGURE 6

Title: Schematic of Direct Feed Fuel Cell

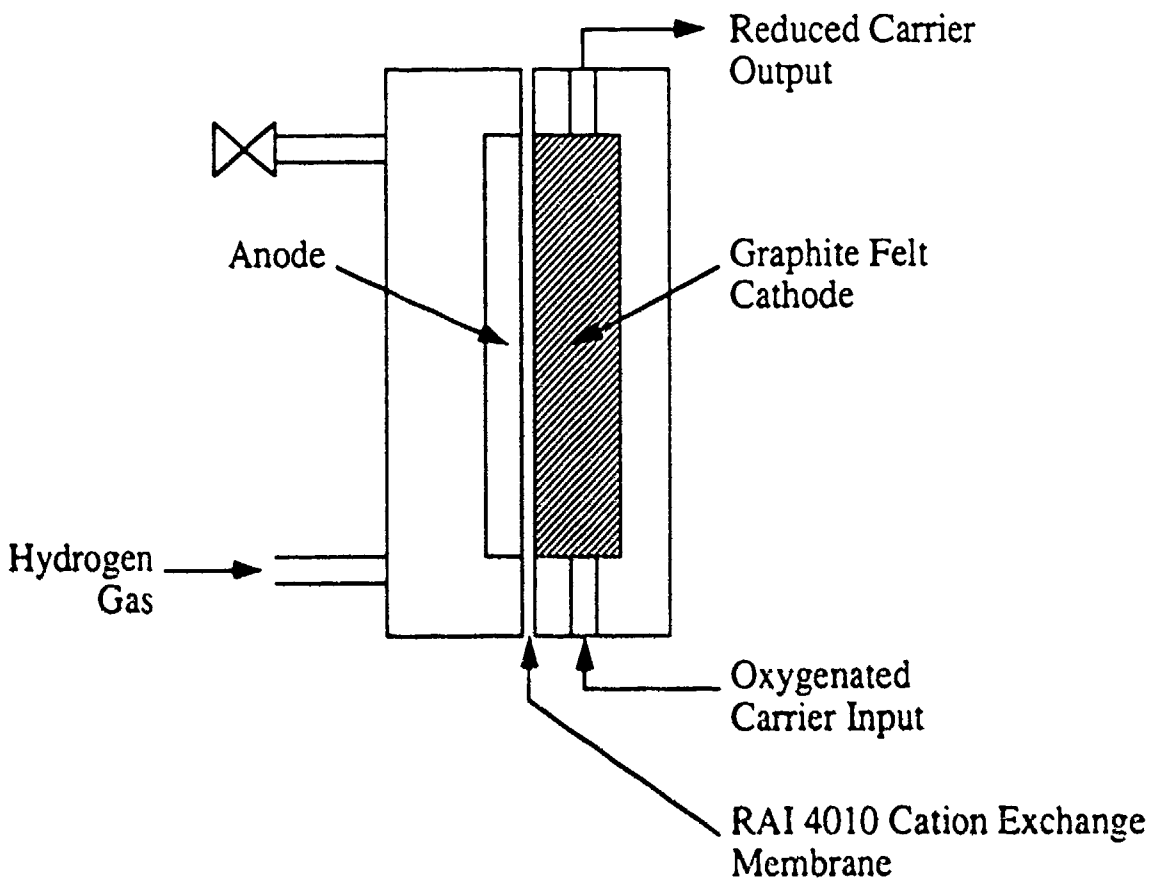

4.5 Direct Feed Fuel Cell Experiments

SUMMARY

The experimental work done thus far has shown:

1) A working fuel cell produces power when fed with hydrogen and an oxygen carrier solution.

2) The hydrogen anodes custom-made by Giner, Inc. are much more effective than a platinized titanium mesh used with the same ion exchange membrane as in the Giner, Inc. anodes.

3) The oxygen carrier solution,when reduced with a hydrogen anode performed as predicted by previous studies (DARPA SBIR Contract #DAAH01-88-C-0413) which reduced the carrier with an acid anolyte.

4) Oxygen carriers offer a significant improvement in cell performance over an aqueous salt solution.

5) Carrier solutions using acetate, perchlorate, chloride and fluoride anions have been used in the experimental cell. Although the chloride solution has the best cell performance to date, the other anions show promise of improved hydrogen anode performance.

While the cell performance achieved to date, 171 mV at 10 mA/cm^2, is short of the intermediate goal of 400 mV at 10 mA/cm^2, there is considerable room for improvement in the performance of the hydrogen anode and some improvement can also be expected in carrier performance and reduction of ohmic losses.

EXPERIMENTAL APPARATUS

The experimental apparatus used in these studies is shown schematically in Figure 7. The electrochemical cell has current collectors measuring 2.5 cm. perpendicular to the direction of fluid flow and 10 cm. along the direction of current flow. The electrode on the cathode side is a carbon felt compressed to a depth of 0.5 cm. with a titanium current collector. The anode consists of the Giner hydrogen electrode backed with a current collector made of a platinized titanium mesh welded to a platinized titanium plate. The cell is housed in an acrylic body. The reference electrode in the catholyte was either a silver wire insulated except for the tip which was coated with silver chloride, or a Microelectrode Inc. Model 22710 silver / silver chloride reference electrode. In either case the reference electrode was mounted at the catholyte entrance to the cell just below the felt electrode. Several different anode reference electrode configurations were used with mixed results. Consequently the anode voltages reported here are calculated with respect to the reference electrode in the catholyte for consistency. Voltages between the anode and cathode, anode and anode reference, anode reference and cathode reference, and cathode and cathode reference were all recorded. The cell current was controlled with a Princeton Applied Research Model 363 potentiostat /galvanostat. The catholyte was aerated after the cell by employing a Hoechst-Celanese microporous membrane module (catalog number 50101010) which provides 1.2 square meters of gas-liquid contact area. Hydrated air was supplied to the membrane module at approximately 100 milliliters per minute.

FIGURE 7

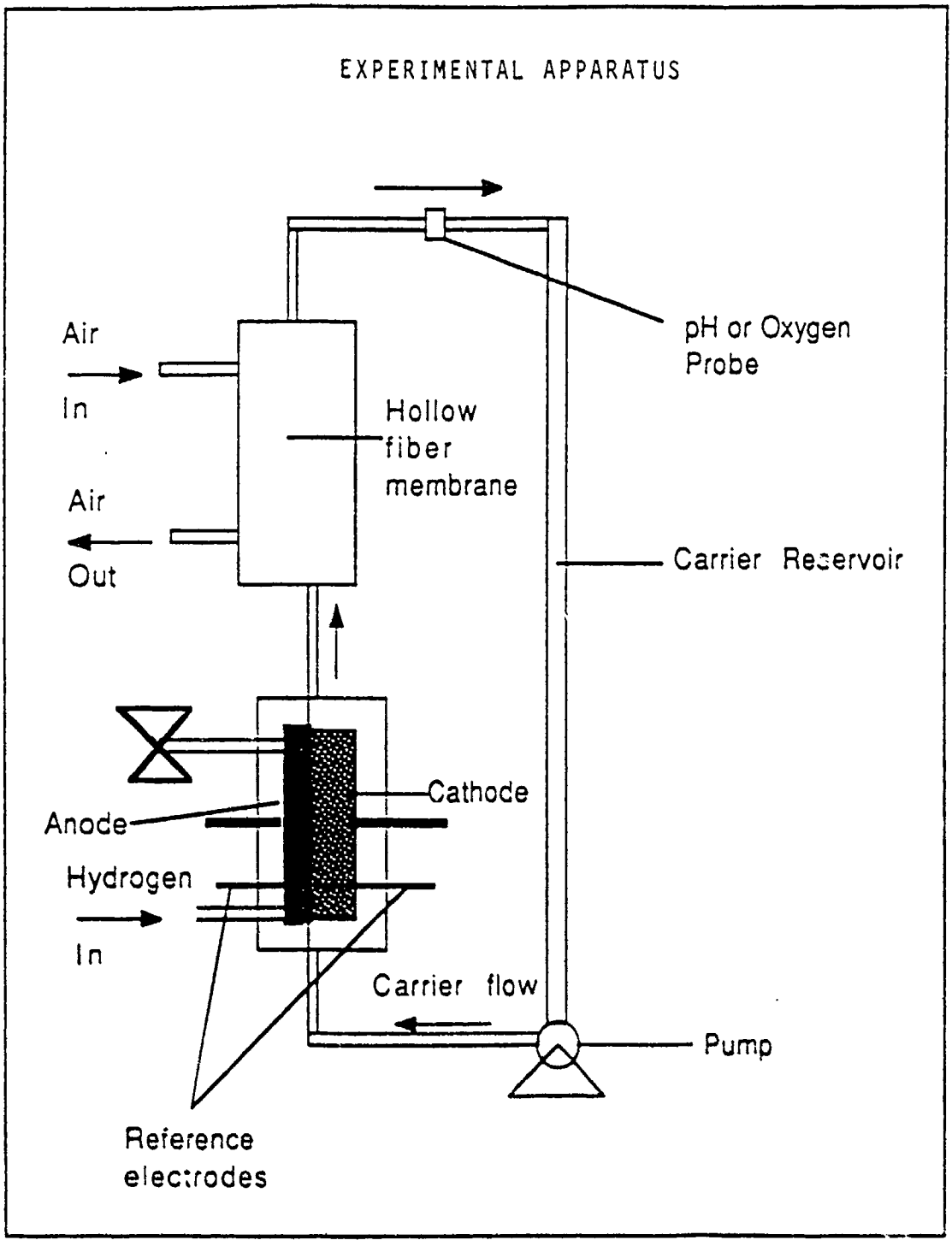
EXPERIMENTAL APPARATUS
Air
In
Air
Out
Hollow
fiber
membrane
pH or Oxygen
Probe
Carrier Reservoir
Cathode
Anode
Hydrogen
In
Carrier flow
Pump
Reference
electrodes

A pH probe was located in the catholyte downstream from the membrane module. Hydrogen flowed past the anode at a rate of approximately 2 milliliters per minute. The carrier flow rate was 40 milliliters per minute. The standard experiment recorded cell voltages and catholyte pH averaged over one minute periods at the end of each one minute period. Current was stepped up every 12 minutes. The entire current range was covered two or three times for each solution.

EXPERIMENTAL PROCEDURE AND RESULTS

There have been five areas of investigation in the experimental work done thus far. Each of these will be discussed in more depth in the following paragraphs.

1) The first experiments investigated the effectiveness of the hydrogen anodes custom-fabricated by Giner, Inc. for this project. Earlier work at Aquanautics indicates that the Nafion membranes normally used in hydrogen anodes may not be compatible with the oxygen carrier solution. Consequently, Giner, Inc. was asked to fabricate a hydrogen anode using an RAI 4010 cation exchange membrane, which previous work at Aquanautics had shown to be compatible with carrier solutions. Four experiments, two using 0.5 molar potassium fluoride as catholyte and the other two using 0.5 molar lithium perchlorate as catholyte, were performed using either platinized titanium mesh covered with the RAI membrane or the Giner, Inc. electrode as the hydrogen anode. As Figures 8 and 9 show, the Giner, Inc. electrode dramatically improved the cell voltage, and the voltage of the hydrogen anode with respect to a silver/silver chloride reference electrode as current densities were increased. This was found to be true of both electrolytes.

2) The second set of experiments was intended to confirm that the carrier performance found in earlier work done by Aquanautics for the DARPA SBIR could be reproduced using a hydrogen anode instead of a hydrochloric acid anolyte. Figure 10 shows the catholyte potentials with respect to a silver / silver chloride reference electrode for 0.4 molar 23 Suzy P/cobalt chloride in 1.5 molar potassium chloride. These potentials were within or above the zero to 0.17 volt range found with such a solution in the previous experiments conducted with the acid anolyte.

3) The third subject of investigation was the performance of the cell and oxygen carrier when the oxygen carrier solution was made using anions other than chloride. Aquanautics' consultant, Dr. Elton Cairns, indicates that chloride ions are detrimental to the effectiveness of the platinum catalyst in the hydrogen anode. Aquanautics has, therefore, tested carrier solutions using fluoride, acetate, perchlorate as well as chloride as anions. A carrier solution could not be made using the ligand and cobalt perchlorate due to the very low solubility of the resulting complex. Carrier solutions using fluoride and acetate as anions, although beneficial to the performance of the hydrogen anode, have not yet performed as well overall as those with the chloride ion. No definitive conclusion about the performance of carrier solutions made using the fluoride and acetate anions can be drawn from the work done so far, since: 1) due to a short supply of ligand in free base form, solutions with matching carrier complex concentrations have not been compared; and 2) carrier solutions with conductivities as high as the chloride solution have not yet been evaluated.

FIGURE 8

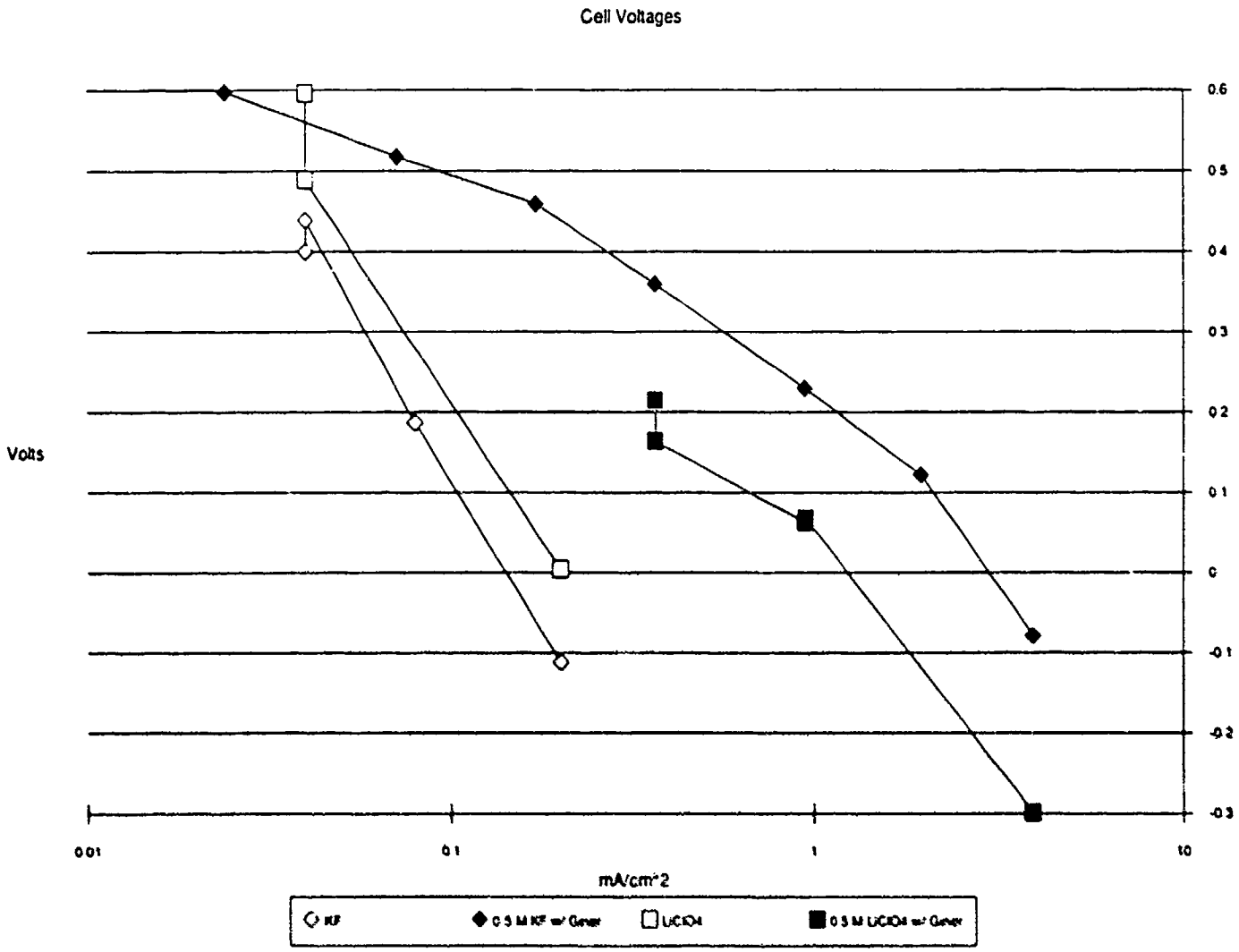
Cell Voltages
Volts
0.6
0.5
0.4
0.3
0.2
0.1
0
-0.1
-0.2
-0.3
0.01
0.1
1
10
mA/cm^2
KF
0.5 M KF w/ Gelatin
LiClO4
0.5 M LiClO4 w/ Gelatin

FIGURE 9

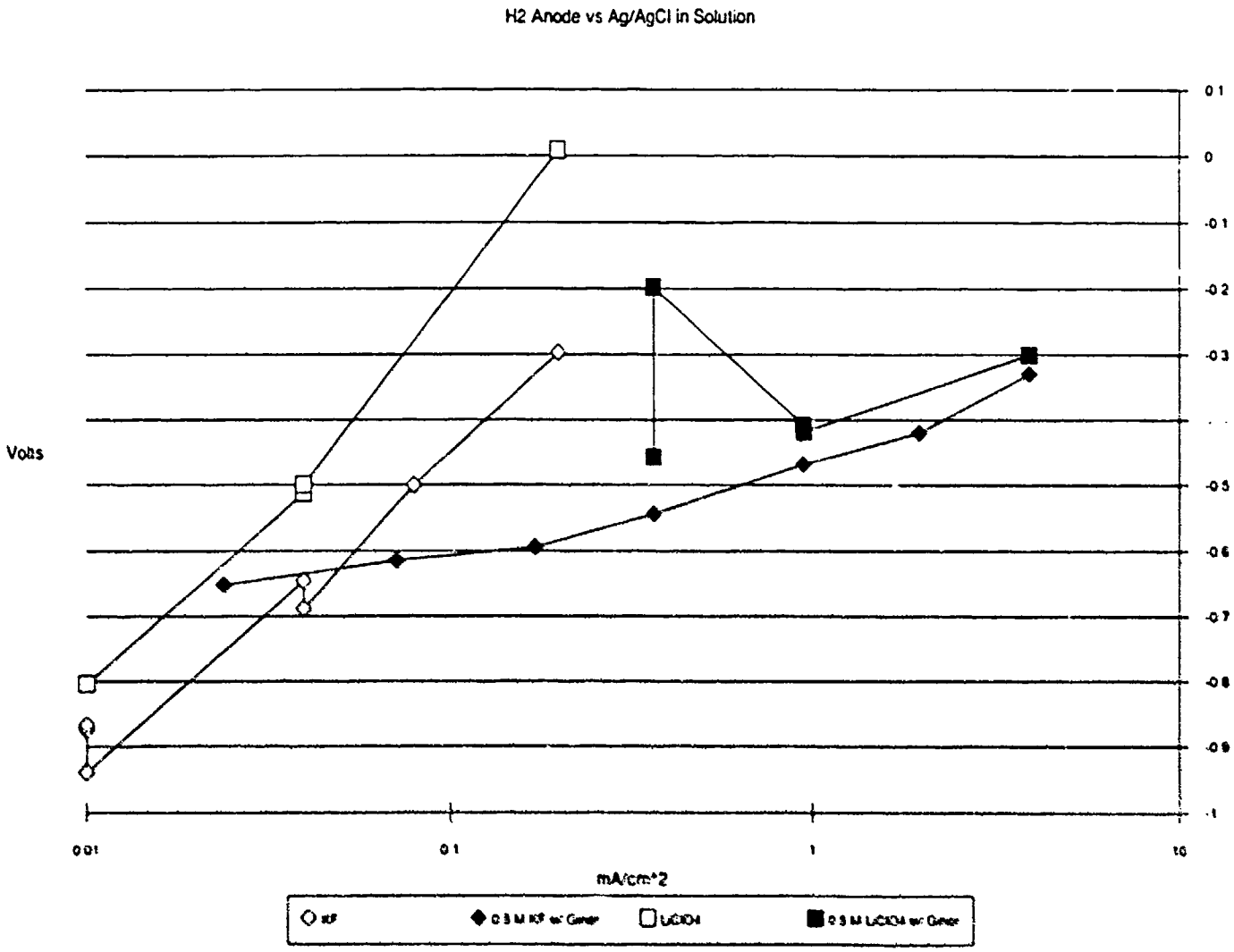
H2 Anode vs Ag/AgCl in Solution
Volts
0.1
0
-0.1
-0.2
-0.3
-0.5
-0.6
-0.7
-0.8
-0.9
-1
0.01
0.1
1
10
mA/cm^2
KF
0.5 M KF w/ Gelat
LiClO4
0.5 M LiClO4 w/ Gelat

4) In conjunction with the evaluation of alternate anions, salt solutions without the oxygen carrier were run to provide background information. In every case oxygen carriers significantly improved cell performance over a salt solution alone. Figures 10 and 11 show the improvement in cathode and cell performance when comparing solutions of potassium fluoride, sodium acetate and potassium chloride salts with solutions using the same salt and an oxygen carrier. The graphs show that the improvement in cell performance comes primarily from improvement in the cathode performance. The anode potentials shown in Figure 12 do not show such clear improvement when carrier solutions are employed instead of salt solutions.

5) Experiments were done using a current interrupt technique to measure the ohmic losses in the cell. The accompanying graph (Figure 13) shows that 100 to 120 mV of ohmic loss are present at 10 mA/cm^2. This represents 25% of the intermediate design cell goal of 0.4 V and indicates that there is substantial room for improvement in reducing contact drop losses and other ohmic losses.

PERFORMANCE ANALYSIS

It is instructive to compare the distribution of voltage losses found in the direct feed fuel cell experiment with the published performance of a gaseous hydrogen-oxygen fuel cell. Figure 14 compares the voltage losses at a current density of 10 mA/cm^2 for a gaseous cell[3] with losses found at the same current density in two direct feed fuel cell experiments using oxygen carriers. The performance of the gaseous cell, shown as "Standard" in the figure, and representing the fruits of several decades of research and development, shows that the voltage losses amount to only about 20% of the total cell voltage with the majority of the losses in the cathode. Anode losses in the Standard cell are negligible at this current density. In contrast the output voltage in the cell which used potassium chloride as the supporting electrolyte (designated "Chloride" in the figure) amounts to less than 15% of the total cell voltage. Anode, cathode and ohmic losses all offer significant room for improvement. In the case where sodium acetate was used as the supporting electrolyte the voltage losses are so large that the cell output voltage is negligible. Note that if the anodic and ohmic losses in the Chloride case were reduced to the same magnitude as in the Standard of the cell terminal voltage would be about 0.55 volts. This is well above the 0.4 volt intermediate goal and does not require any improvement at all in the performance of the oxygen carrier on the cathode side.

PLAN FOR NEXT QUARTER

This quarter's plan is to improve the performance of the fuel cell by:

1) Investigating fuel cell design options with companies like Giner, Electrochem and Treadwell, Inc.

2) Performing carrier work described in the Carrier Section.

---

[3]Kordesch, K., "Electrochemical Energy Storage," *Comprehensive Treatise of Electrochemistry*, **3**, Plenum, New York (1981).

FIGURE 10

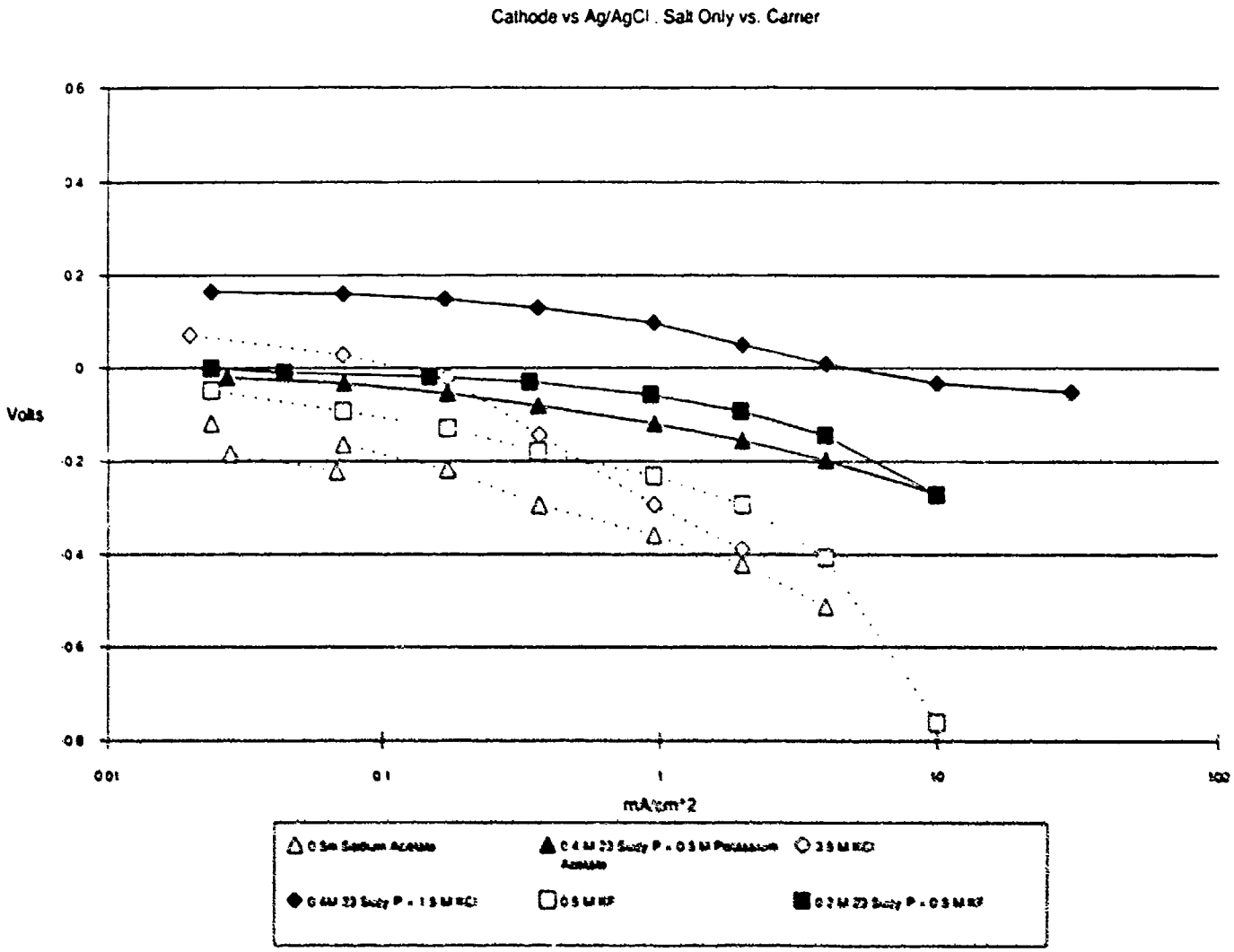
Cathode vs Ag/AgCl . Salt Only vs. Carrier
0.6
0.4
0.2
0
-0.2
-0.4
-0.6
-0.8
Volts
0.01
0.1
1
10
100
mA/cm^2

FIGURE 11

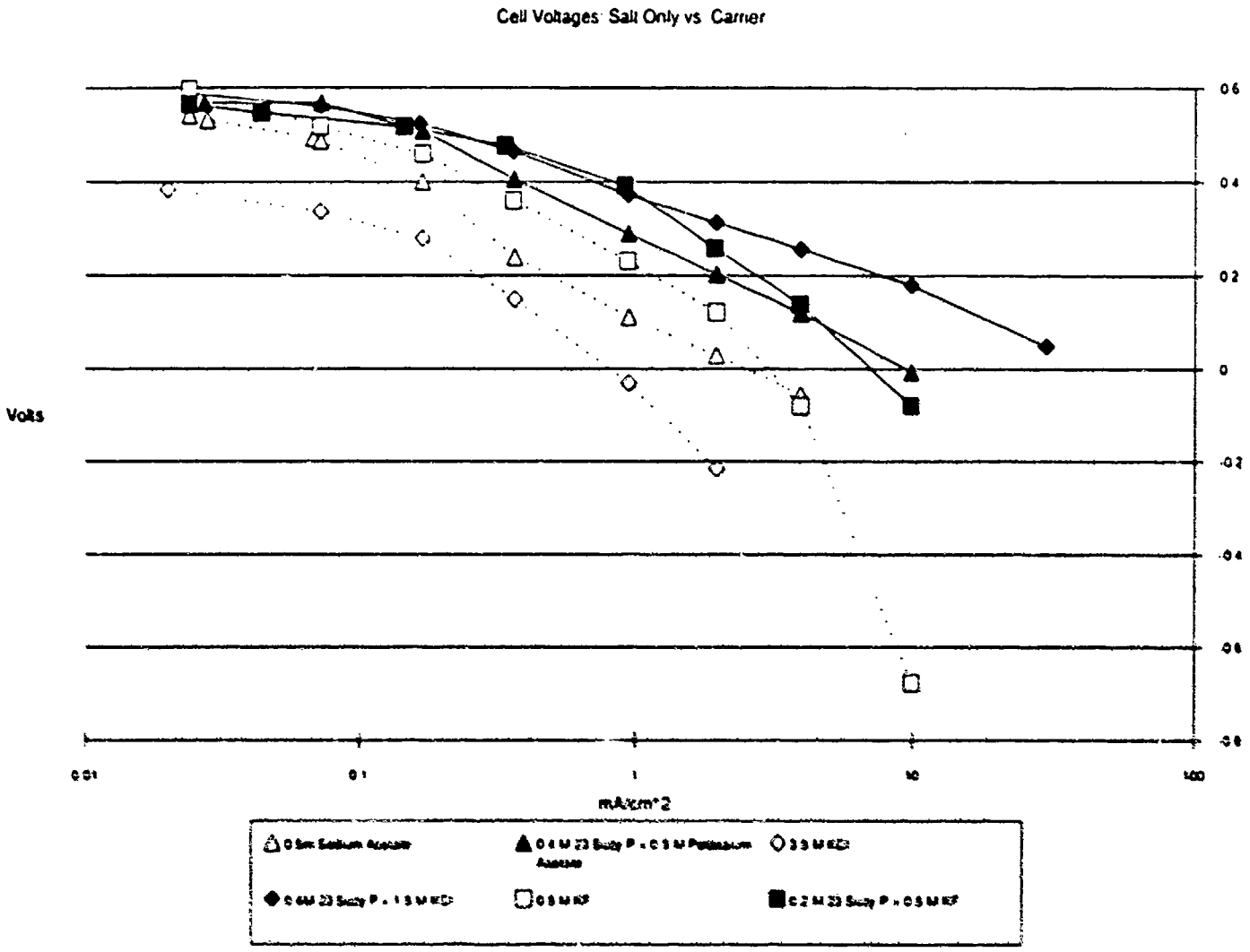
Cell Voltages Salt Only vs Carrier
Volts
mA/cm^2
0.6
0.4
0.2
0
-0.2
-0.4
-0.6
-0.8
0.01
0.1
1
10
100

FIGURE 12

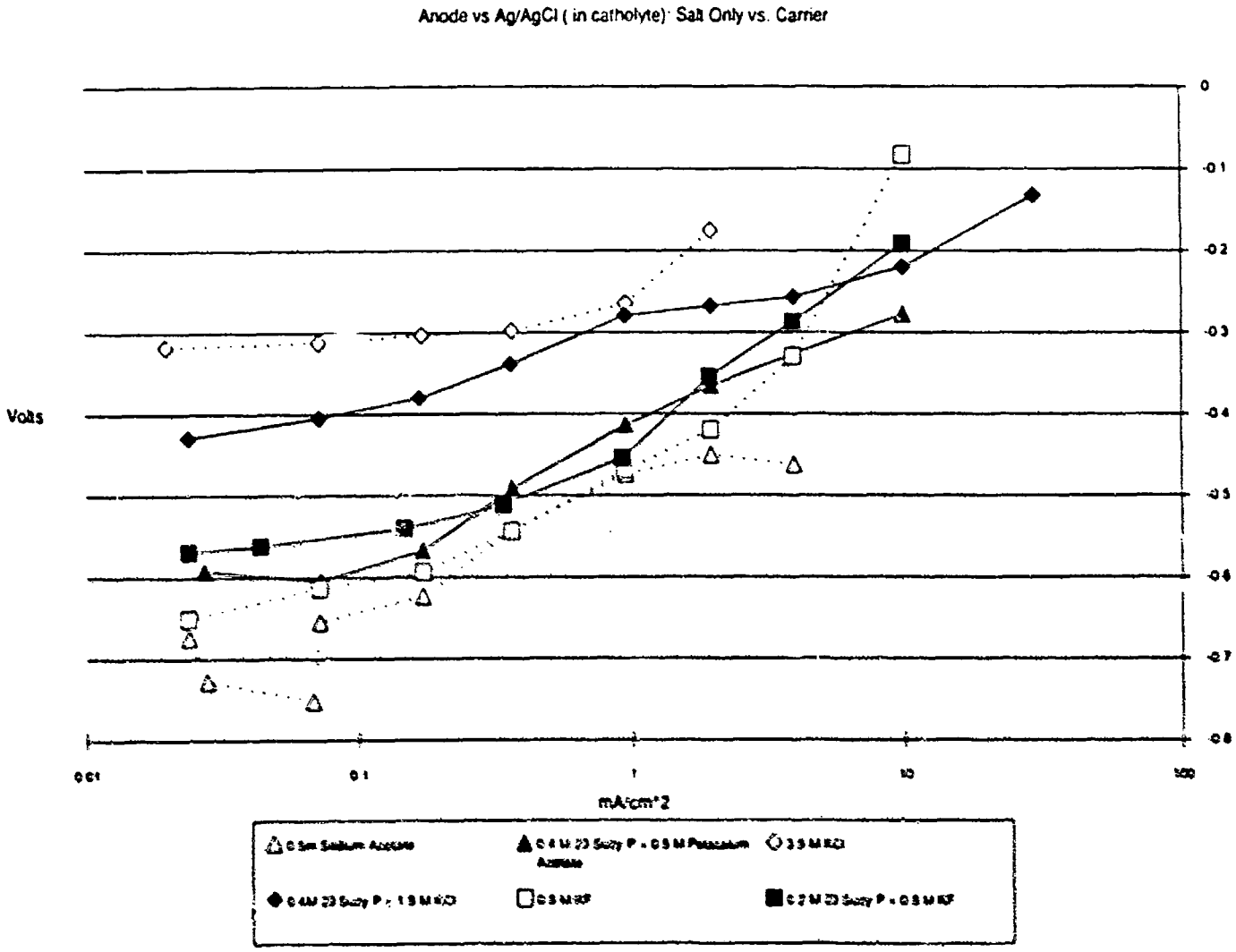
Anode vs Ag/AgCl (in catholyte) Salt Only vs. Carrier
Volts
0
-0.1
-0.2
-0.3
-0.4
-0.5
-0.6
-0.7
-0.8
0.01
0.1
1
10
100
mA/cm^2

FIGURE 13

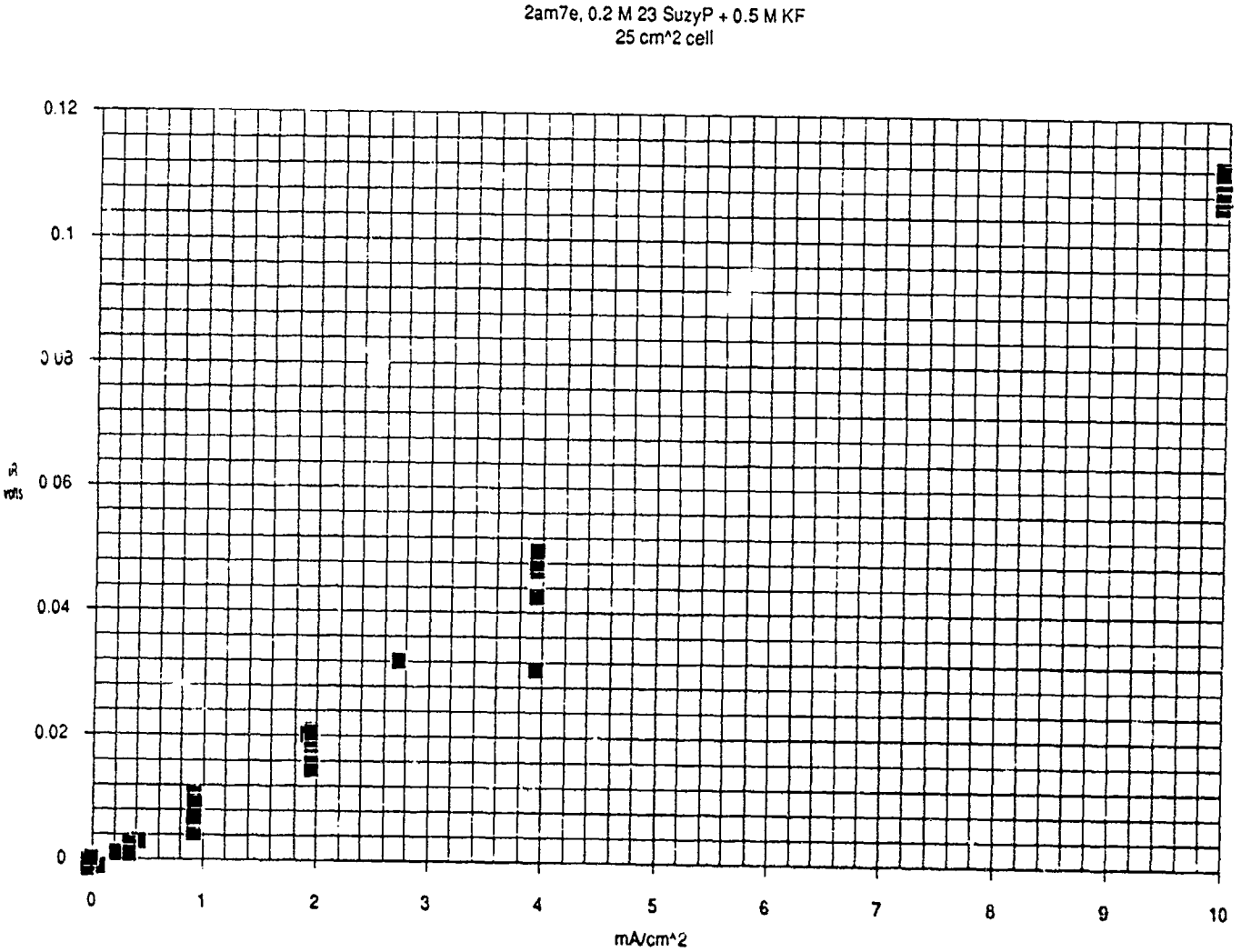
2am7e, 0.2 M 23 SuzyP + 0.5 M KF
25 cm^2 cell
0.12
0.1
0.08
0.06
0.04
0.02
0
0
1
2
3
4
5
6
7
8
9
10
mA/cm^2

FIGURE 14

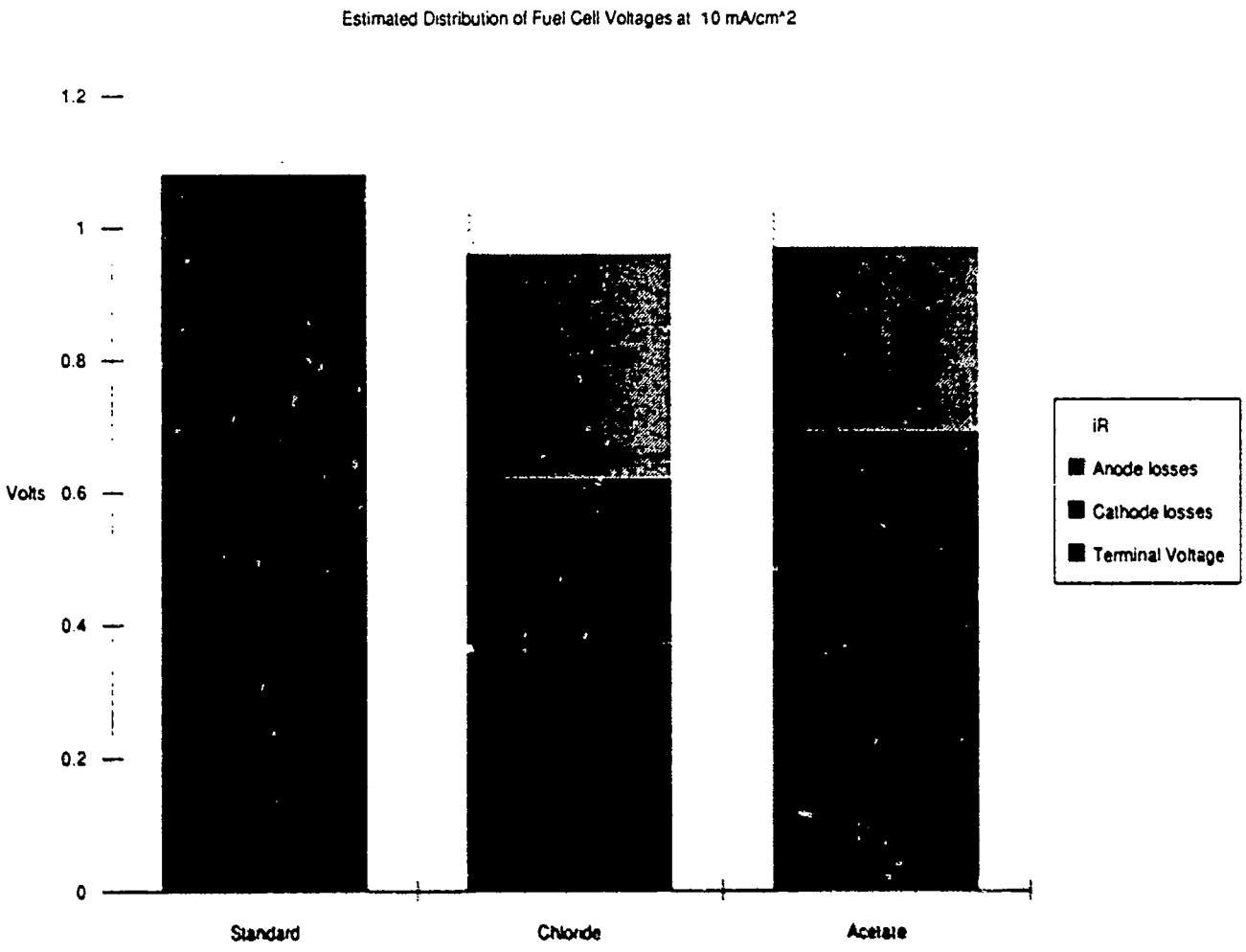
Estimated Distribution of Fuel Cell Voltages at 10 mA/cm^2
1.2
1
0.8
Volts 0.6
0.4
0.2
0
Standard
Chloride
Acetate
iR
Anode losses
Cathode losses
Terminal Voltage

5.0 GILL

5.1 Membrane Permeability Evaluation by Measuring Oxygen Transport from Air to Nitrogen

INTRODUCTION

This section describes experiments undertaken to evaluate the oxygen permeabilities of flat sheet samples of solid membranes using gas flow on both sides of the membrane. These experiments were undertaken with a view towards computing the actual membrane permeability by eliminating the predominance of hydrodynamic limitations encountered in the case of oxygen diffusion through liquids. It is hoped that by modelling the mass transport process using published correlations, it will be possible to calculate the approximate oxygen permeability of different membrane samples. These experiments were undertaken as part of a broader effort towards identifying suitable solid membranes for use in the gill of an underwater power source that also employs the Aquanautics technology of oxygen binding chemicals.

This report shall deal primarily with the methods employed in the experiments conducted towards this goal and also discuss the results obtained from them. The experiments under discussion here were carried out between February 23 and March 29, 1989.

BACKGROUND

CFFC Scheme

The background for this work is a study into the feasibility of using the Aquanautics oxygen binding carriers to extract dissolved oxygen from seawater and generate electrical power from the extracted oxygen. The application of such a power source calls for capabilities of operating at ocean depths of up to 6000 meters which corresponds to overburden pressures of up to 600 atmospheres. Figure 1 depicts the schematic of a system that would employ the Aquanautics carriers to generate power from the dissolved oxygen in seawater.

Importance of the Gill Design

One crucial element of this system is the gill, which is used to bring the seawater and oxygen absorbing carrier in close vicinity without physical contact since mixing would dilute the carrier. The seawater and carrier are therefore separated by a membrane through which the oxygen dissolved in seawater is transported to the carrier where it is absorbed by the carrier molecules in a chemical reaction. The oxygen affinity of the proprietary carrier ensures that the dissolved oxygen content of the carrier solution is zero. This causes an oxygen concentration gradient across the membrane which is the driving potential for oxygen transport.

The carrier is then fed to a fuel cell where the oxygen is stripped out to react with hydrogen from a separate source to generate power as described in an earlier section. The partially deoxygenated carrier is then returned to the gill where it absorbs fresh oxygen from the seawater. The advantage of this system lies in the fact that the carrier contains high concentrations of oxygen by virtue of its ability to reversibly bind it. Typically, up to 4.5 standard liters of oxygen can be bound in one liter of carrier solution. For systems producing small units of kilowatts of power, the oxygen transport required is in the range of 5 to 20 standard liters per minute. This transport takes place through the gill and thus

gill design is an important feature of the system. In order for the Aquanautics system to retain any competitive advantage over other power producing systems, such as Magnesium-seawater batteries or use of stored reactants, it is important for the volume and weight of such a system be as small as possible. The gill, because of the low oxygen concentrations in seawater and the large quantities of oxygen required to produce the necessary power, forms a significant portion of the overall system volume. Therefore, any attempt to optimize system size would have to proceed by investigating ways of decreasing gill size while retaining the ability to facilitate transport of the required quantities of oxygen.

In addition to this, power consumed in pumping seawater through the gill constitutes a major source of parasitic loss of net power. It is therefore, imperative that the gill design be optimized to enable maximum extraction of oxygen from the seawater and to ensure that power consumed in pumping does not form a proportionately large portion of the energy budget. The design of such a gill proceeds in two steps, firstly the selection of a material and secondly the actual design of a configuration in which this material is employed. The hollow fiber configuration that has been widely used at Aquanautics, prior to this point, supports a large interfacial or surface area within a small volume. Commercial designs of hollow fiber membranes have achieved packing densities in excess of 2000 sq. meters of surface area per cubic meter of volume. These designs therefore provide the requisite performance insofar as the optimization of configuration is concerned.

The material employed in the gill is another important component of the gill design. For applications at low or atmospheric pressures, microporous hollow fiber membranes have exhibited excellent oxygen transport capabilities. Laboratory experiments at Aquanautics have largely been conducted with the help of microporous hollow fiber devices. Since these membranes have porosities of up to 40%, they provide the transported oxygen with a large area of gas space to diffuse through. The membrane permeabilities have therefore not been an issue since the diffusion of oxygen though the seawater is four orders of magnitude slower than that of oxygen through the gas spaces. It has therefore been established that in the case of microporous membranes, the membranes do not control oxygen flux or even contribute significantly to the resistance to oxygen flux.

In deep water applications, the use of microporous membranes becomes infeasible due to the high overburden pressures encountered. These pressures, which increase at the rate of approximately one atmosphere for every 10 meters of depth, would result in the membrane being subject to high hydraulic pressures. Gas pores, being inherently more compressible than liquids, would be crushed and liquid to liquid contact across the membrane would result. This leads to physical mixing that the membranes were initially intended to prevent. The solution to this would be to use membranes with no pores. However, non-porous separators, by definition, have a very high resistance to oxygen flux, or in other words a low oxygen permeability. The compromise therefore, is to use composite solid membranes that are built by depositing ultra-thin solid layers on a support substructure constituted by a microporous membrane.

Membrane Product Review

In keeping with this objective, Mr. Benedict of Aquanautics initiated a membrane product review with the intent of identifying a membrane that would meet the above criteria. Most of the positive respondents presented flat sheet samples, though one hollow fiber device was also procured for initial evaluation and testing. The flat sheet samples were tested in special fixtures built for that purpose. Two flat sheet samples were tested in this batch of experiments in addition to a hollow fiber prototype device. The first flat sheet sample was from SciMed Life Systems and shall be hereafter referred to as the SciMed membrane.

This membrane was constructed using a silicone layer deposited on a nylon mesh. The second sample was obtained from Membrane Technology Research, Inc. and was constructed by the deposition of a 1 micron thick poly(dimethylsiloxane) layer on a conventional microporous support substructure. The prototype hollow fiber solid membrane cartridge was obtained from Applied Membrane Technology, Inc. and was constructed by the ultra-deposition of a proprietary solid layer on 20% porosity microporous hollow fibers manufactured by Hoechst-Celanese.

OBJECTIVE

The objective of this experiment was to evaluate the oxygen flux through the flat sheet solid membrane samples as well as the solid membrane hollow fiber prototype cartridge that was procured as a result of the product review. The testing was to determine the flux of oxygen from a feed of air at one atmosphere pressure to a sink of nitrogen at the same pressure. The use of gases as the feed and sink allowed for large oxygen fluxes thus reducing the effect of measurement errors. Also, the use of gases ensured that the oxygen flux was affected by the actual permeability of the membranes in addition to the diffusion boundary layers on either side of the membrane. The flux through the various membranes could then be compared and the differences in membrane permeabilities computed. The measurements were also repeated for various flow rate values (for both the feed air and the sweep nitrogen) to ensure that the effects of the two diffusion boundary layers could be modelled and the actual membrane permeabilities computed from the data. Moreover, the experiments are expected to establish a data base for membrane permeabilities and set up a protocol for experiments on further samples of membranes and for comparing the data acquired using the various membrane samples.

EXPERIMENTAL SET-UP

System Schematic

Figure 15 depicts the apparatus used in this experiment and the schematic of the system assembly.

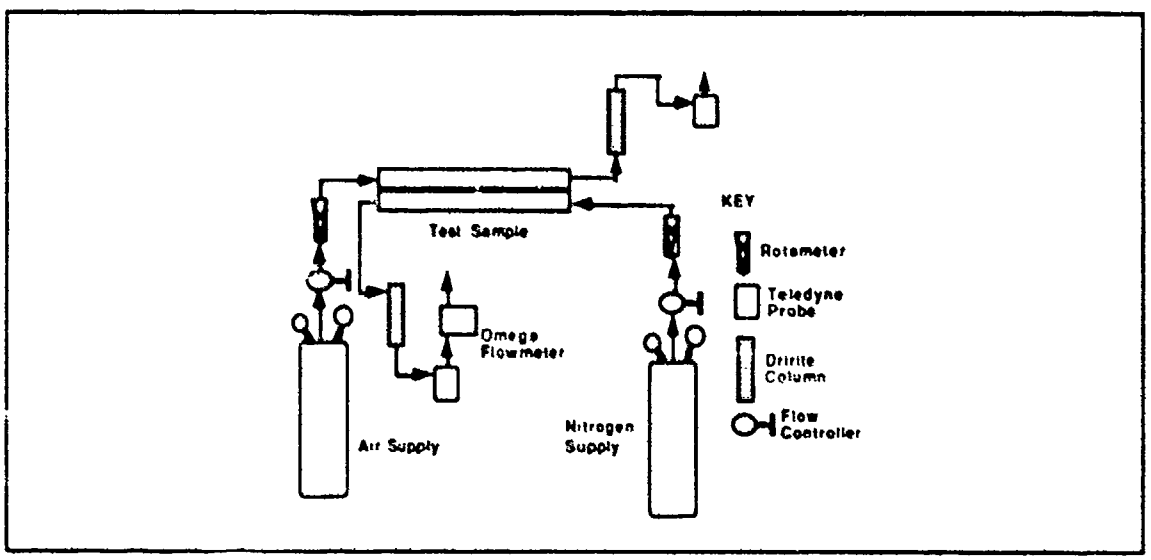

FIGURE 15
Schematic of Experimental Setup

Description of Components

As can be seen from Figure 15, the apparatus basically consisted of the test sample, which was either the flat sheet membrane testing fixture or the hollow fiber cartridge, connected to the gas sources through rotameters which were used to set the flow rates of the gases. Veriflo flow controllers were used for this purpose and these were connected directly to the needle valves in the laboratory-wide gas system. Instrumentation was added on the downstream side of the fixtures or cartridge. This consisted of a Teledyne probe at the air exit to measure the oxygen content of the exhaust air. A Teledyne probe as well as an Omega gas flowmeter were located at the nitrogen exit to measure the oxygen content of the nitrogen sweep as well as to enable calculation of the oxygen transported from the air stream to the nitrogen sweep in the membrane. The Omega flowmeter used with the flat sheet membranes had a full scale range of 0 to 1 l/min and a full scale output of 0 to 5 V. The flowmeter used with the hollow fiber prototype had a full scale range of 0 to 5 l/min. Dririte columns were used in both gas streams prior to the probes to scrub the gases of any moisture that may have been present in the gas bottles. In addition to the instrumentation mentioned above, a differential pressure sensor was applied across the inlets to both sides of the test sample to measure excess of total pressure on either side. The pressure difference data was used in the calculation of the log mean concentration difference which in turn was used to calculate the overall mass transfer coefficient of the system.

The fixtures were plate and frame devices that had an interfacial area of approximately 500 cm^2 or 0.05 m^2. The depth of the flow channel was approximately 5 mm and the flow path was filled with nylon mesh to support the membranes and prevent them from billowing out and blocking a flow channel. These membrane fixtures were originally intended to be used with carrier and seawater on either sides of the membranes, but did not yield measurable rates of oxygen transport when used in that configuration. This was due to the small interfacial area as well as the fact that the diffusion of oxygen through the liquids is too slow to provide identifiable flux. The use of these fixtures for that purpose was therefore abandoned and the membranes used with gases instead to evaluate their efficacy.

The prototype hollow fiber solid membrane cartridge that was tested using this method was also intended for use with carrier and seawater and had an interfacial area of approximately 0.37 m^2. This cartridge yielded measurable quantities of oxygen transport in the intended experiment with carrier and seawater, but initial evaluation was also performed on this cartridge with the apparatus described above.

PROCEDURE

Instrument Calibration

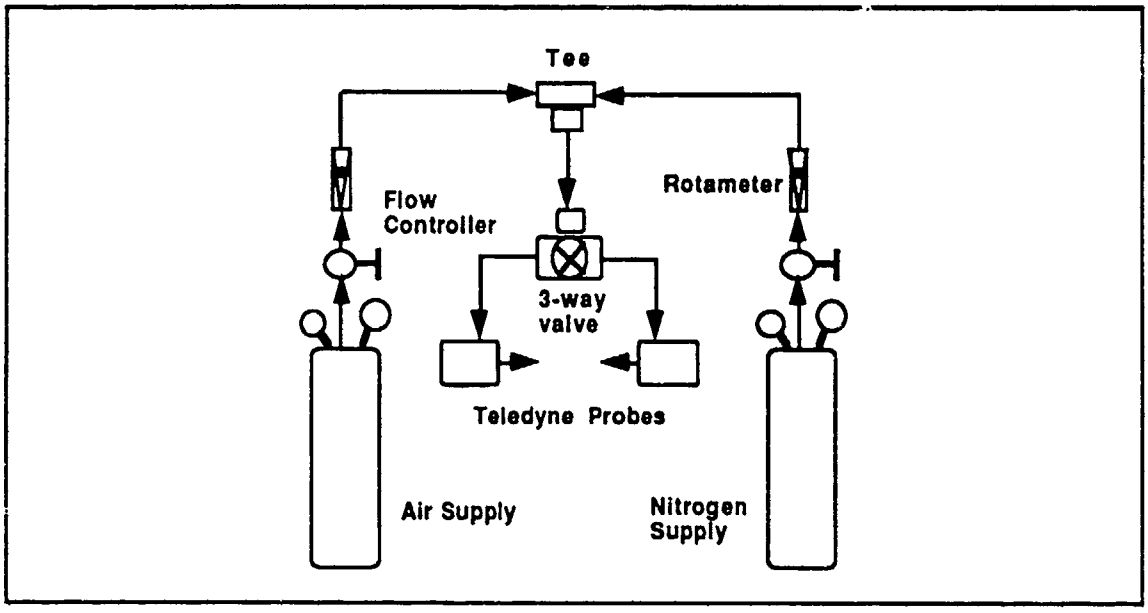

FIGURE 16
Schematic for Teledyne Probe Calibration Setup

Before the various components of the experiment were connected into the system, all the probes were calibrated. The Teledyne probes were calibrated by flowing different mixtures of air and nitrogen through them. The apparatus to do this is depicted in Figure 16. The calibration was performed to identify the gain setting on the Teledyne probe signal conditioner that would give the best accuracy in the measurement of the oxygen content at the air and nitrogen stream exits. The flowmeter was calibrated by connecting it directly to the source of air or nitrogen through a rotameter and using the rotameter as the device for comparison. Teledyne probe accuracy was found to be within 3%.

Flat Sheet Membrane Testing Procedure

All components were assembled as per the details in Figure 15, and power switched on to all instruments. The data acquisition program in the computer was executed to start the acquisition of data and its entry into an appropriately designated file on disk. The zero readings for all the instruments were taken at the outset for use as offsets in data analysis. Nitrogen and air flow were then turned on at their smallest respective values namely 50 ml/min and the system allowed to come to equilibrium. Data was recorded for five consecutive data points after steady state was attained thus corresponding to approximately 7.5 minutes of steady state behavior. The nitrogen flow rate was then increased in steps to values of 100, 200, 300, and 400 ml/min and five consecutive data points recorded for each step at steady state.

The steps described above were then repeated for different air flows (50, 100, 200, and 400 ml/min). Each combination of air and nitrogen flow rate was evaluated for roughly a period of 7.5 to 10 minutes and notations made in the laboratory notebook corresponding

to these sets of data. Readings from the displays of the two Teledyne probes were also noted down in the notebook.

Hollow Fiber Solid Membrane Cartridge Testing Procedure

In the case of the prototype hollow fiber solid membrane cartridge, an effort was made to keep the Reynolds Number unchanged from the flat sheet experiments. Based on this, flow rates were calculated for the hollow fiber geometry, where the air was flowed on the outside of the fibers and the nitrogen through the lumen. Nitrogen flow rates used for this cartridge were 285, 570, 855, 1140, and 1400 ml/min. The air flow rates used were 650, 1300, 2600, and 5250 ml/min. In view of the increased gas flow rates for the hollow fiber prototype, a different set of rotameters and gas flowmeter had to be used. The gas flowmeter was a 0 to 5 l/min full scale model and was calibrated prior to the experiment with the help of a rotameter.

Experiment Designation

The experiment on the SciMed membrane sample was repeated once because in the first experiment the Nitrogen exit Teledyne probe was used in its highest range setting (0 - 100%) and was therefore measuring in the extreme low end of its range. This was expected to lead to large measurement errors and the experiment with the SciMed membrane was repeated with the nitrogen exit probe set at 0 to 5% scale. These two experiments were denoted 1KS49 and 1KS50 respectively. The experiment with the MTR composite membrane was performed with both Teledyne probes in their 0 to 25% scale settings and was denoted 1KS54. The experiment with the hollow fiber prototype was performed with settings similar to the MTR composite, and was denoted 1KS51.

RESULTS

Presentation of Results

Two graphs are presented for each experiment. The first graph plots oxygen flux as a function of the nitrogen flow rate for different air flow rates. The second graph plots the overall mass transfer coefficient as a function of the nitrogen flow rate for different air flow rates.

Figures 17 and 18 correspond to data taken with the SciMed membrane in experiment 1KS49, while Figures 19 and 20 show data acquired using the same membrane but with the more advantageous Teledyne probe settings (laboratory notebook reference 1KS50). Figures 21 and 22 refer to data taken with the MTR composite membrane in experiment 1KS54. Figures 23 and 24 depict data from the hollow fiber solid membrane prototype and experiment 1KS51. Data from each experiment is therefore represented by two graphs as described above, namely one graph showing oxygen flux and the other showing the overall mass transfer coefficient.

Calculation Procedure

The oxygen flux and overall mass transfer coefficient were calculated in a spreadsheet from the data acquired from the instruments. The data from the nitrogen stream exit Teledyne probe and the Omega flowmeter were converted into oxygen content and flow rate respectively and the oxygen flux arrived at by simply multiplying the fractional oxygen content by the total flow rate. The concentration difference was calculated by using a log mean difference formulation shown in Equation 6.

FIGURE 17

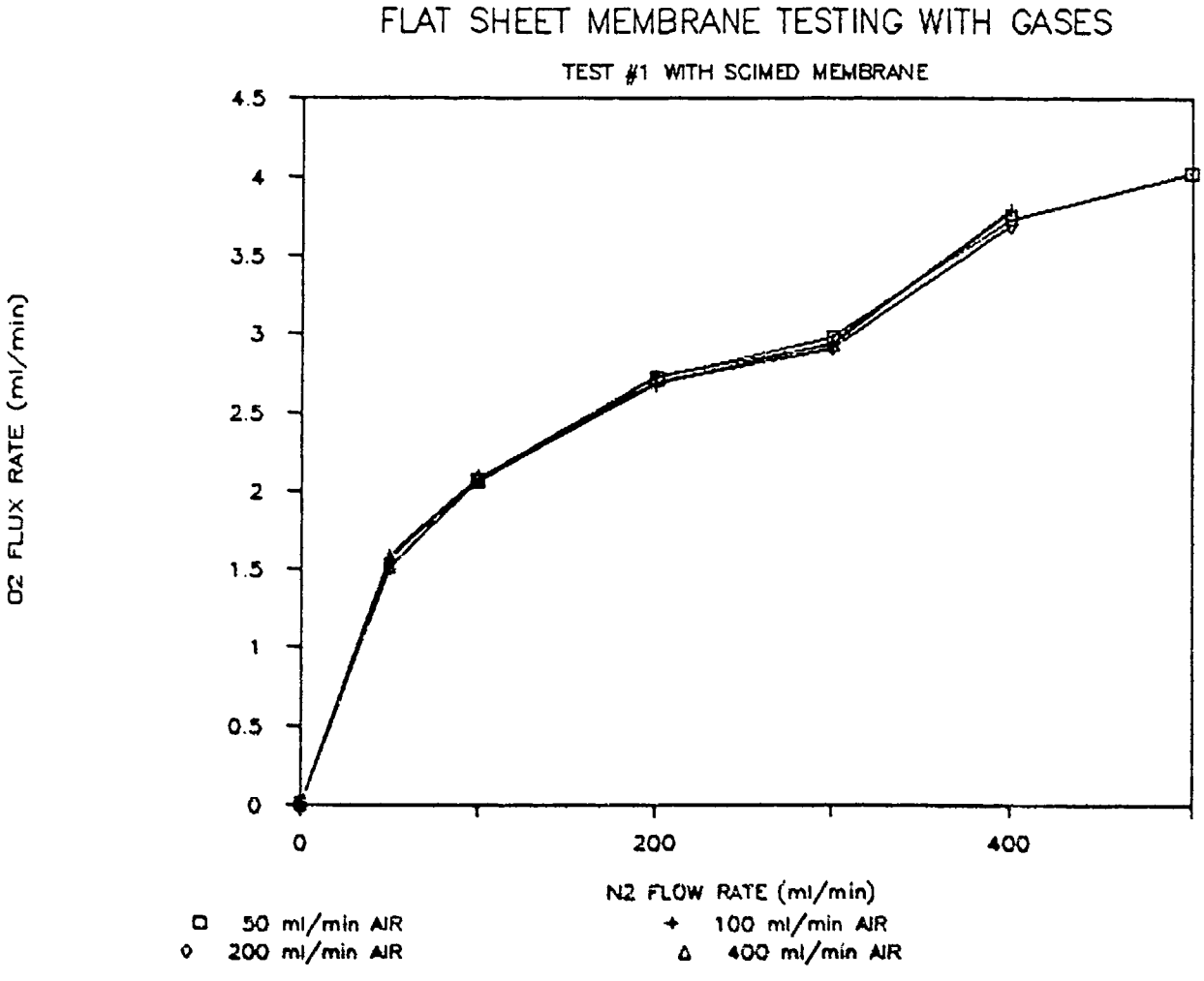
FLAT SHEET MEMBRANE TESTING WITH GASES
TEST #1 WITH SCIMED MEMBRANE
O2 FLUX RATE (ml/min)
4.5
4
3.5
3
2.5
2
1.5
1
0.5
0
0
200
400
N2 FLOW RATE (ml/min)
□ 50 ml/min AIR
+ 100 ml/min AIR
◊ 200 ml/min AIR
Δ 400 ml/min AIR

FIGURE 18

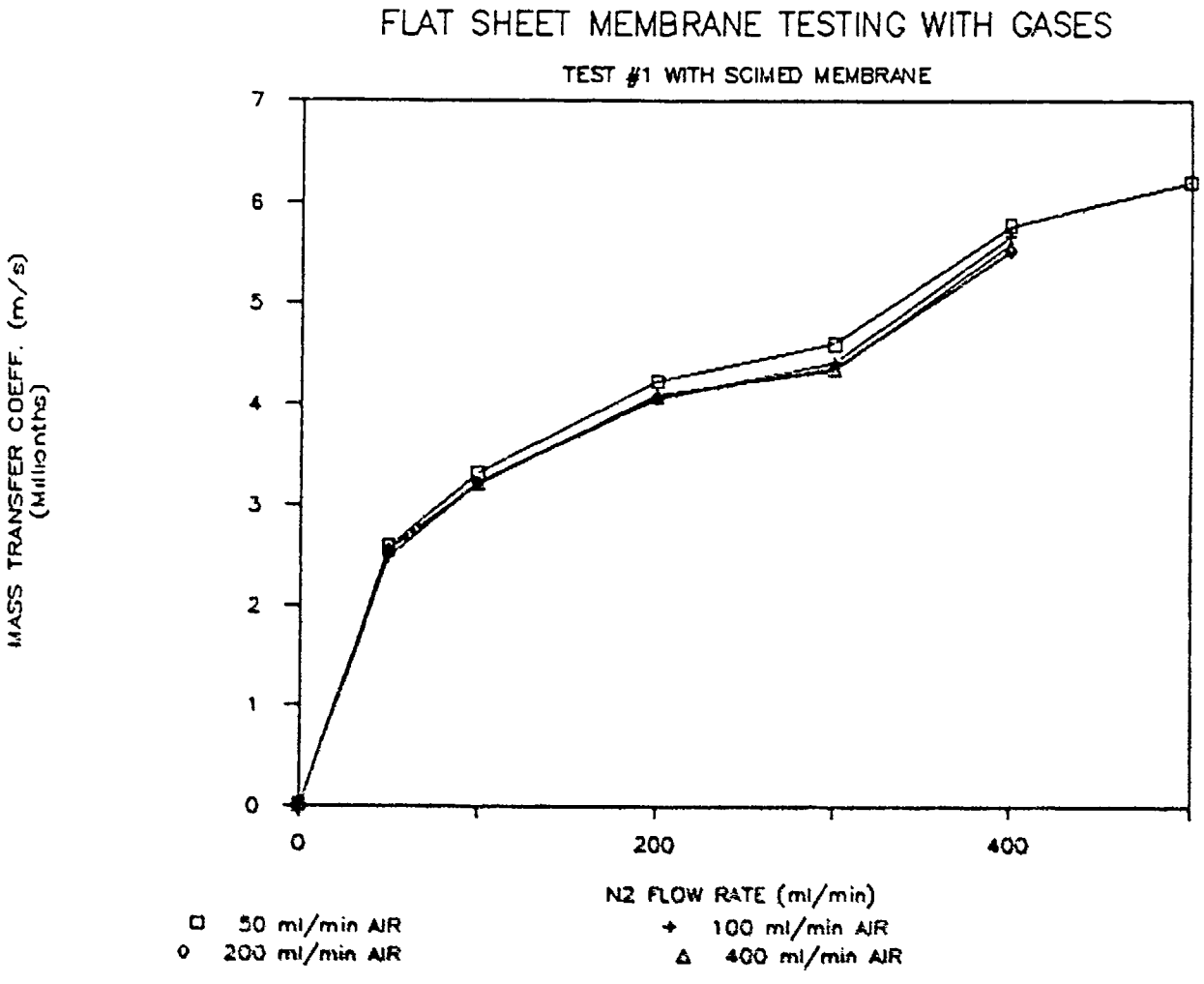
FLAT SHEET MEMBRANE TESTING WITH GASES
TEST #1 WITH SCIMED MEMBRANE
MASS TRANSFER COEFF. (m/s)
(Millionths)
7
6
5
4
3
2
1
0
0
200
400
N2 FLOW RATE (ml/min)
□ 50 ml/min AIR
+ 100 ml/min AIR
o 200 ml/min AIR
Δ 400 ml/min AIR

FIGURE 19

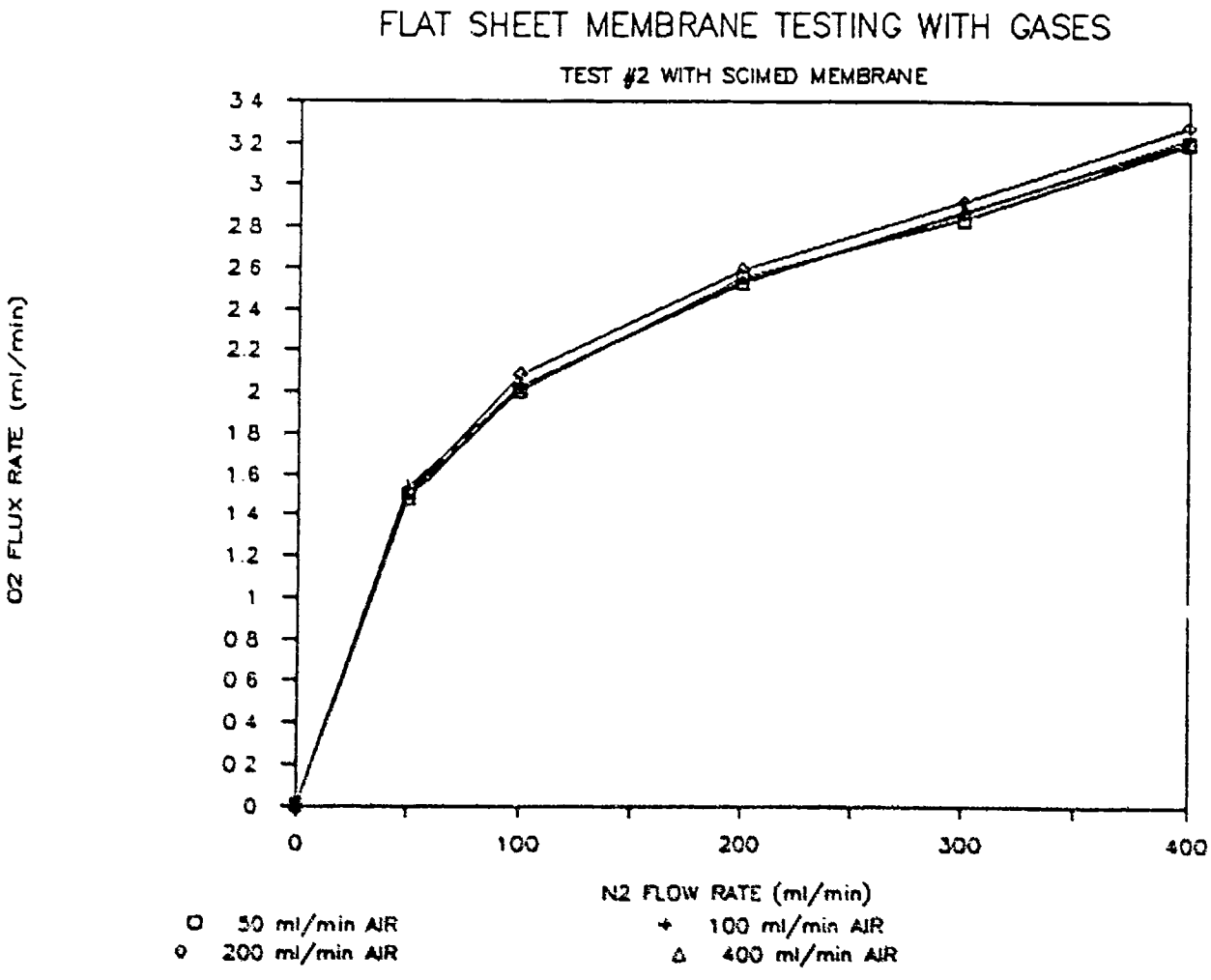
FLAT SHEET MEMBRANE TESTING WITH GASES
TEST #2 WITH SCIMED MEMBRANE
O2 FLUX RATE (ml/min)
3.4
3.2
3
2.8
2.6
2.4
2.2
2
1.8
1.6
1.4
1.2
1
0.8
0.6
0.4
0.2
0
0
100
200
300
400
N2 FLOW RATE (ml/min)
O 50 ml/min AIR
+ 100 ml/min AIR
9 200 ml/min AIR
Δ 400 ml/min AIR

FIGURE 20

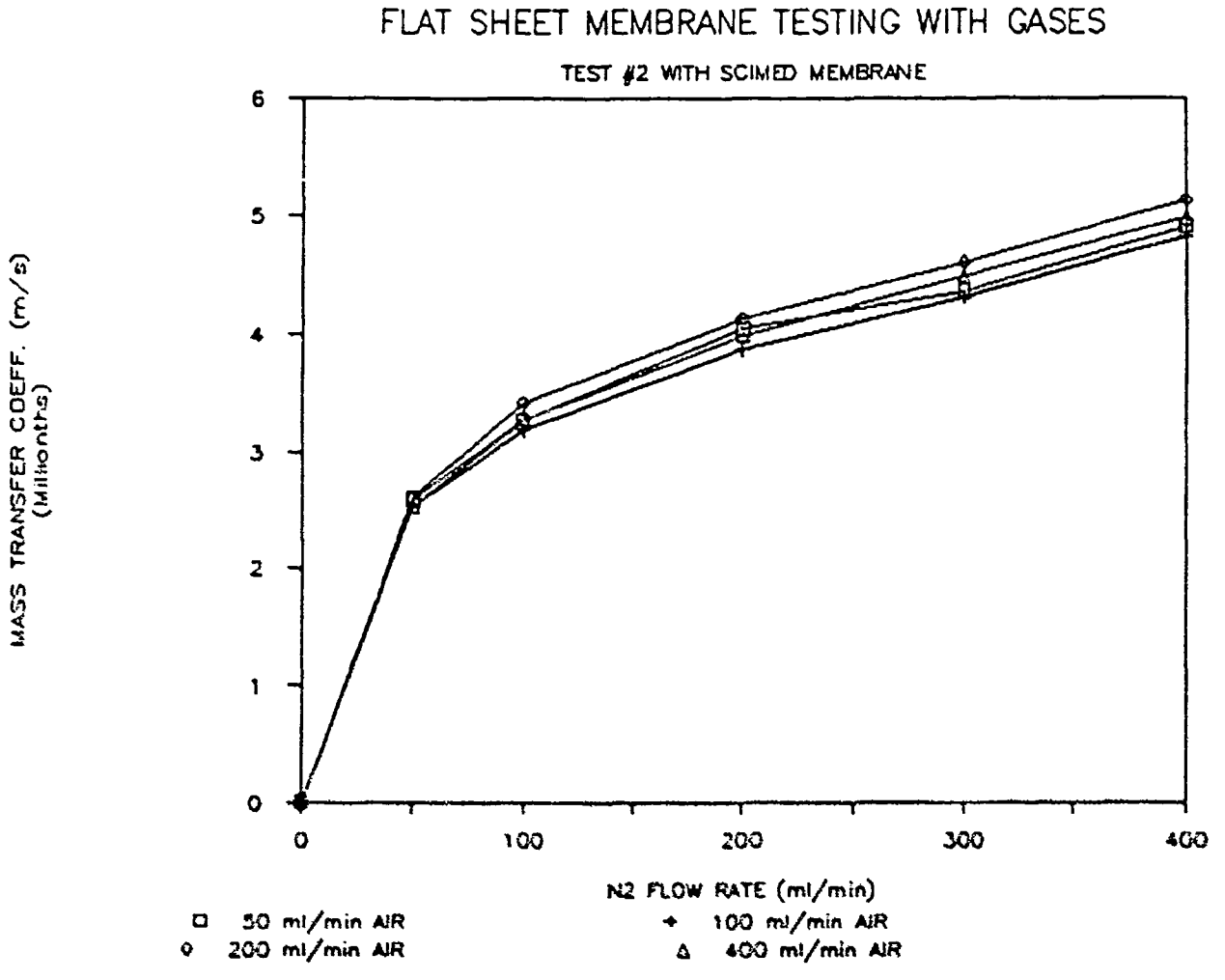
FLAT SHEET MEMBRANE TESTING WITH GASES
TEST #2 WITH SCIMED MEMBRANE
MASS TRANSFER COEFF. (m/s)
(Millionths)
0
1
2
3
4
5
6
0
100
200
300
400
N2 FLOW RATE (ml/min)
50 ml/min AIR
100 ml/min AIR
200 ml/min AIR
400 ml/min AIR

FIGURE 21

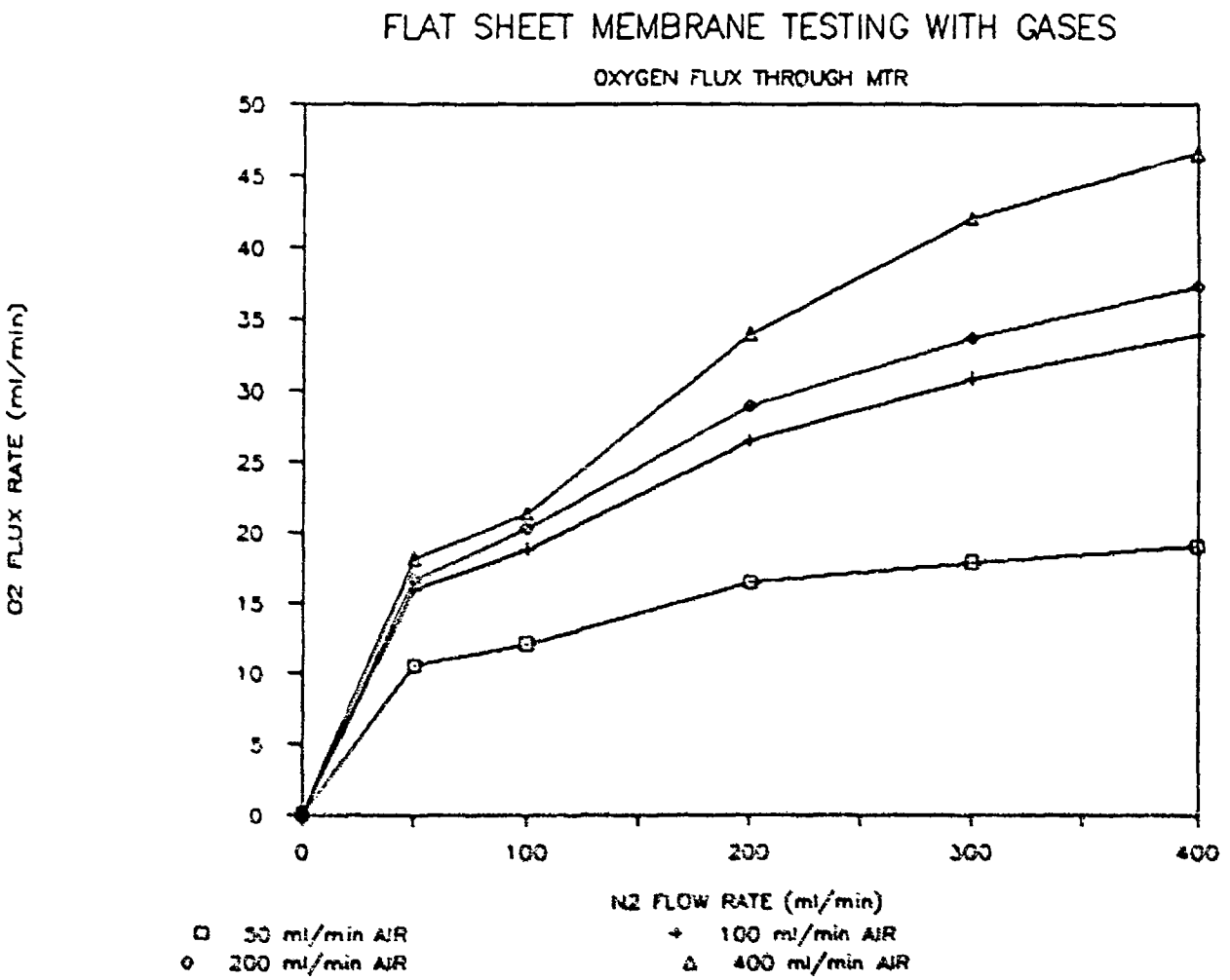
FLAT SHEET MEMBRANE TESTING WITH GASES
OXYGEN FLUX THROUGH MTR
O2 FLUX RATE (ml/min)
50
45
40
35
30
25
20
15
10
5
0
0
100
200
300
400
N2 FLOW RATE (ml/min)
50 ml/min AIR
100 ml/min AIR
200 ml/min AIR
400 ml/min AIR

FIGURE 22

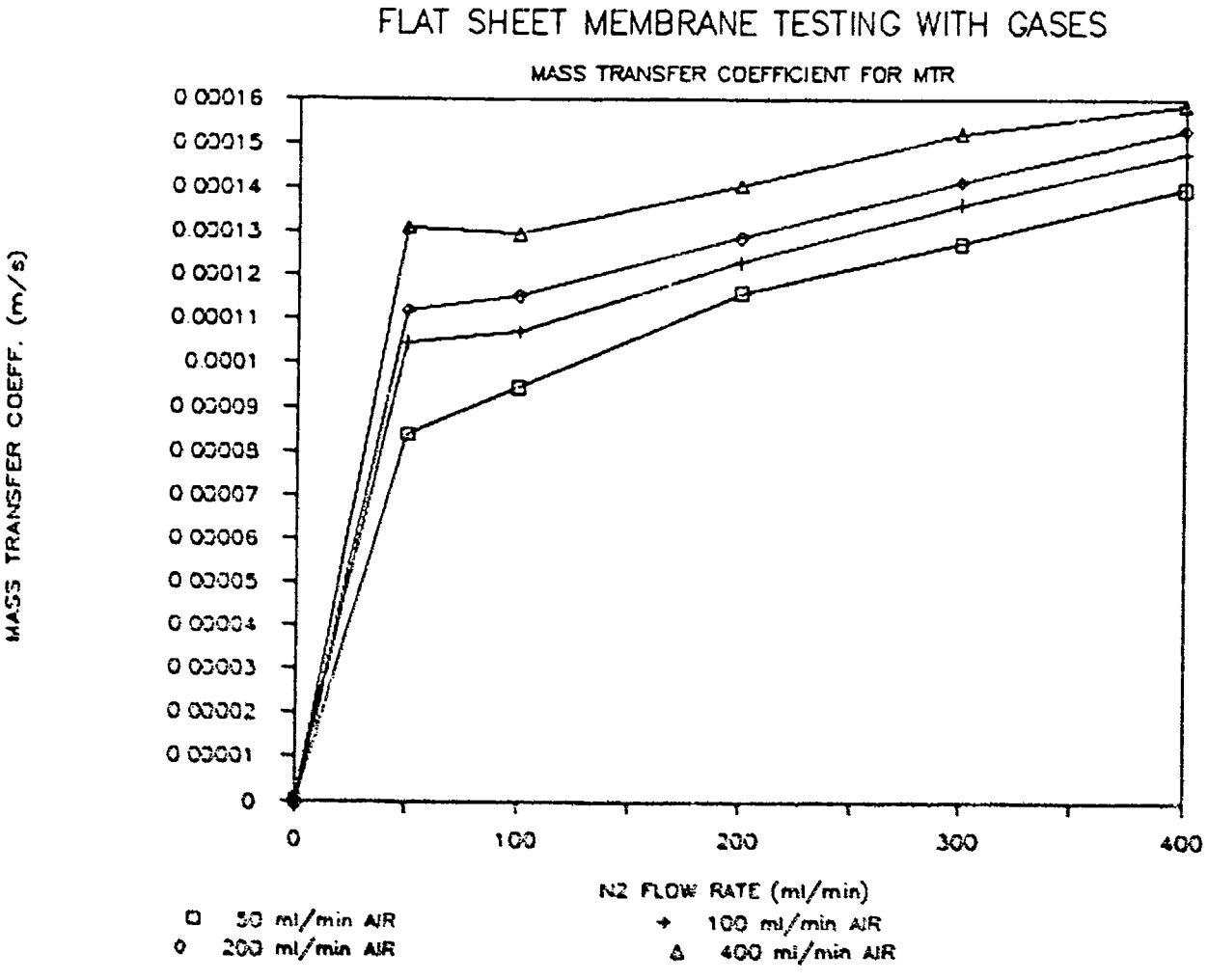
FLAT SHEET MEMBRANE TESTING WITH GASES
MASS TRANSFER COEFFICIENT FOR MTR
MASS TRANSFER COEFF. (m/s)
0.00016
0.00015
0.00014
0.00013
0.00012
0.00011
0.0001
0.00009
0.00008
0.00007
0.00006
0.00005
0.00004
0.00003
0.00002
0.00001
0
0
100
200
300
400
N2 FLOW RATE (ml/min)
50 ml/min AIR
100 ml/min AIR
200 ml/min AIR
400 ml/min AIR

FIGURE 23

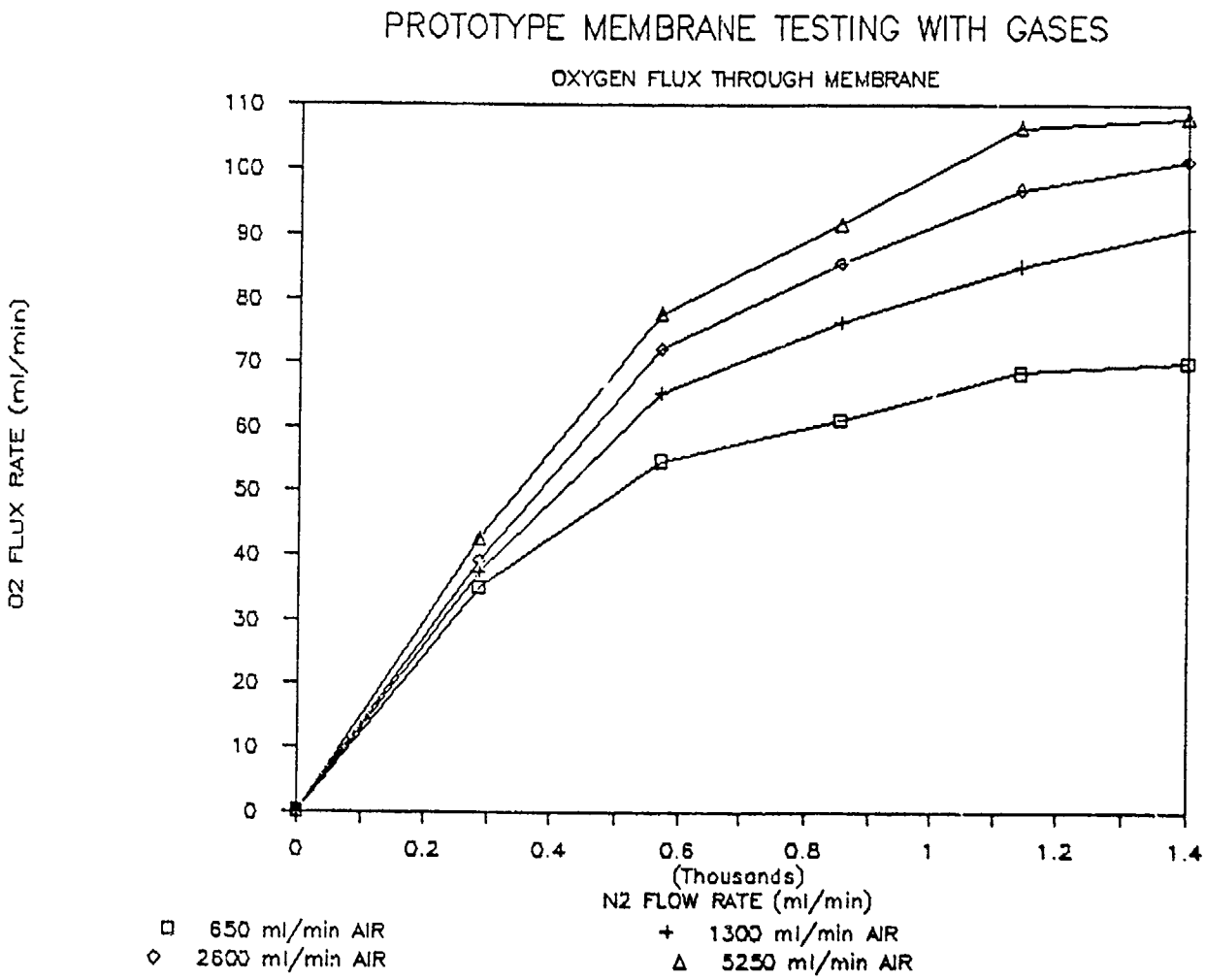
PROTOTYPE MEMBRANE TESTING WITH GASES
OXYGEN FLUX THROUGH MEMBRANE
O2 FLUX RATE (ml/min)
110
100
90
80
70
60
50
40
30
20
10
0
0
0.2
0.4
0.6
0.8
1
1.2
1.4
(Thousands)
N2 FLOW RATE (ml/min)
650 ml/min AIR
2600 ml/min AIR
1300 ml/min AIR
5250 ml/min AIR

FIGURE 24

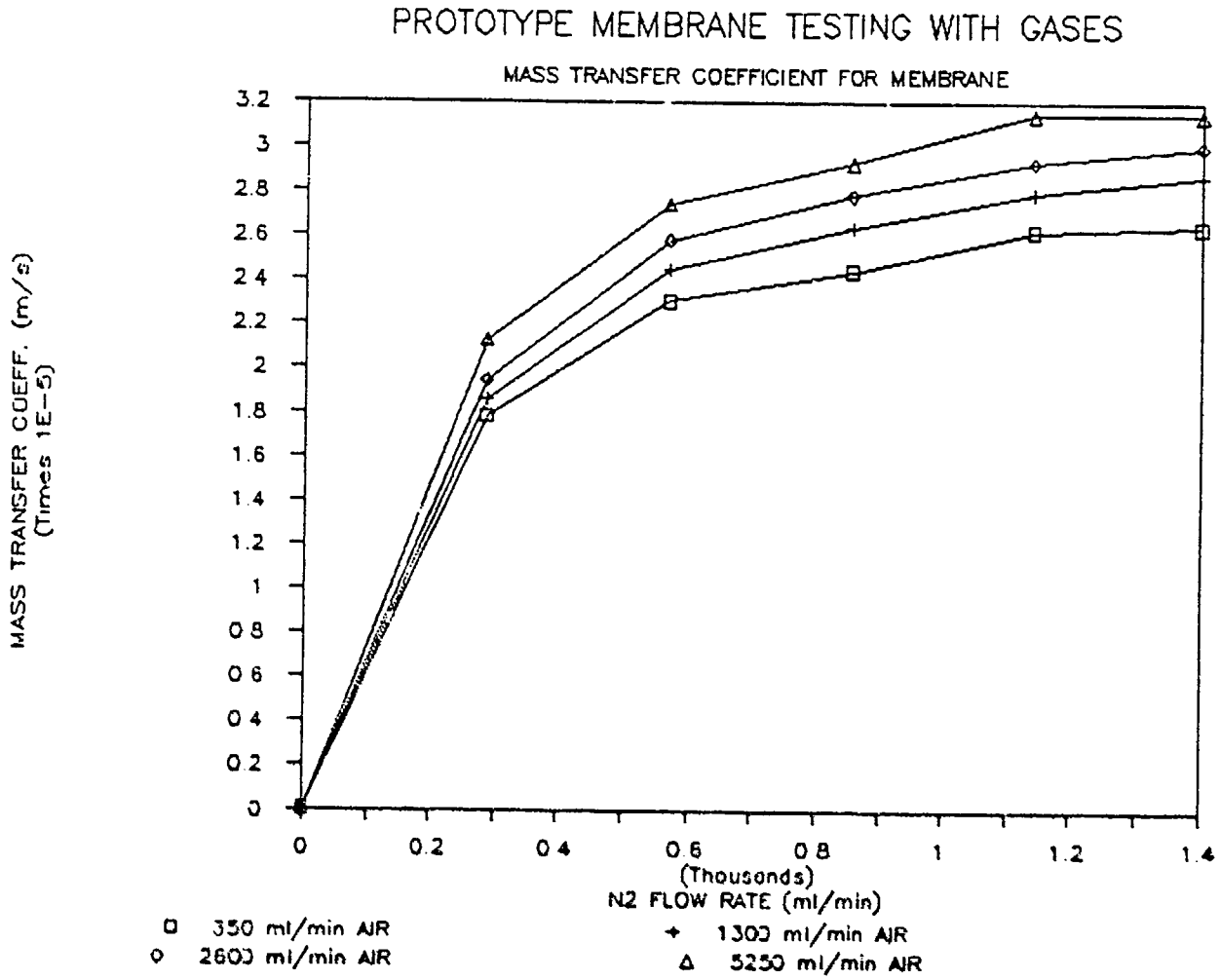
PROTOTYPE MEMBRANE TESTING WITH GASES
MASS TRANSFER COEFFICIENT FOR MEMBRANE
MASS TRANSFER COEFF. (m/s)
(Times 1E-5)
3.2
3
2.8
2.6
2.4
2.2
2
1.8
1.6
1.4
1.2
1
0.8
0.6
0.4
0.2
0
0
0.2
0.4
0.6
0.8
1
1.2
1.4
(Thousands)
N2 FLOW RATE (ml/min)
□ 350 ml/min AIR
◇ 2600 ml/min AIR
+ 1300 ml/min AIR
△ 5250 ml/min AIR

$$\Delta C = \frac{(C_{ai} - C_{no}) - (C_{ao} - C_{ni})}{\ln\left\{\frac{C_{ai} - C_{no}}{C_{ao} - C_{ni}}\right\}} \quad (6)$$

where, C_{ni} is the oxygen conc. in the nitrogen stream at the inlet,
C_{no} is the oxygen conc. in the nitrogen stream at the outlet,
C_{ai} is the oxygen conc. in the air stream at the inlet, and
C_{ao} is the oxygen conc. in the air stream at the outlet.

All the concentrations are expressed in terms of standard cubic meter of oxygen per cubic meter of total volume. The nitrogen side concentrations were corrected by using the differential pressure of the nitrogen side when compared to the air side. In reality this did not make a difference because both sides were shown to be at a relatively equal total pressure.

The overall mass transfer coefficient was computed by using Equation 7,

$$k_o = \frac{Q_{ox}}{A\,\Delta C} \quad (7)$$

where, k_o is the overall mass transfer coefficient in units of m/s,
Q_{ox} is the oxygen flux calculated as described above,
A is the interfacial area of the membrane, and
ΔC is the log mean concentration difference calculated as per Equation 6.1.

The oxygen flux and mass transfer coefficient for the various combination of nitrogen and air flow rates were then determined in the spreadsheet by averaging the five steady state data points that were recorded as described in the preceding section entitled "Procedure".

DISCUSSION OF RESULTS

Flat Sheet Samples

The testing of the SciMed sample was repeated due to improper setting of the nitrogen exit Teledyne probe during the first experiment. The data taken in both experiments yielded results that were roughly comparable. The oxygen flux in the first experiment was consistently higher than in the second more reliable experiment. This can be attributed to the loss in resolution of the Teledyne probe in its 0 to 100% setting in the first experiment. The difference between the two experiments was most pronounced at high flow rates of nitrogen and amounted to a 15 to 20% larger oxygen flux in the first and suspect experiment.

Overall the oxygen flux through the SciMed membrane as shown in Figures 17 and 19 reveal a consistent increase in the rate of oxygen flux as the nitrogen flow rate is increased. The air flow rate, on the other hand, seems to have a negligible impact on the rate of oxygen transport. This is surprising in view of the fact that the diffusion characteristics of oxygen through nitrogen and air are similar as are the viscosities of air and nitrogen. The other important piece of information culled from this experiment is derived from Figures 18 and 20 which depict overall mass transfer coefficients plotted as a function of the nitrogen flow rate. While these plots once again demonstrate insensitivity to air flow rates, it is also

obvious that the coefficients are two orders of magnitude lower than expected based on calculations of the air and nitrogen side mass transfer coefficients using published correlations.[4] This leads to the conclusion that the membrane is offering a predominant portion of the resistance to oxygen flux. The membrane, in other words, is not very permeable to oxygen when compared to traditional microporous membranes. The overall permeability also does not change with air flow rates and this may be due to the difference in the two sides of the membrane. One side of the membrane is not very smooth due to the presence of the nylon mesh substructure. This side was exposed to the nitrogen, while the smooth side, corresponding to the deposited membrane material, was used on the air stream side.

The results from the MTR membrane that are presented in Figures 21 and 22 show that the MTR membrane permits up to 15 times more oxygen flux than the SciMed membrane does. Moreover, the MTR is sensitive to both air and nitrogen flow rate variations. At a low air flow rate (50 ml/min) the oxygen flux reaches an asymptotic maximum at nitrogen flow rates of 300 to 400 ml/min. Flux rates at higher air flow rates (100, 200 and 400 ml/min) do not attain an asymptotic value within the range of experimental observations.

An incongruous observation made in this experiment is the quantity of oxygen that is sensed at the nitrogen exit. For air flow rates of 50 and 100 ml/min, it was noticed that the amount of oxygen that was transported across the membrane exceeded the amount present in the supply air, especially at high nitrogen flow rates. For example at a nitrogen flow rate of 400 ml/min and air flow rate of 50 ml/min, the oxygen flux was measured to be approximately 17 ml/min. This is patently absurd given the immutable fact that 50 ml/min of air flow can only supply approximately 10.5 ml/min of oxygen. Initial conjecture points to the rotameters as the source of error. In the experimental setup the rotameters were used to set flow rates and the data taken was assumed to have been for flow rates indicated by these rotameters. The nitrogen side had a digital flowmeter after the membrane, but this flowmeter indicated total nitrogen side exit flow rate, which included the oxygen that was transported across the membrane from the air side. Therefore, apart from the rotameters, there were no other definite or reliable measurements of air flow rates as well as nitrogen flow rates prior to the membrane. The rotameters in this experiment had a full scale reading of 5 l/min and are known to exhibit erroneous behavior at the lower end of their measurement range. It could be assumed, therefore, that the air flow rate indicated by the rotameters, especially at the lower end of the experimental observation, was less than that in reality.

The overall mass transfer coefficients observed for this membrane was also much higher than that for the SciMed membrane. Figure 22 shows a peak coefficient of 1.6E-04 m/s which is two orders of magnitude larger than that for the SciMed membrane and well within the expected range of behavior based on the models that were worked out for the transport phenomenon.

Hollow Fiber Solid Membrane Prototype

The results obtained from the hollow fiber module tested are presented in Figures 23 and 24 and show that the oxygen flux through the membrane is quite substantial. Up to 108 ml/min of oxygen was transported at high air and nitrogen flow rates. Most of the curves in Figure 23 show that the flux is reaching an asymptotic maximum when the nitrogen flow rate approaches 1.4 l/min. Moreover, the membrane shows a definite sensitivity to air flow

[4]Yang, M.C., and Cussler, E.C., "Designing Hollow Fiber Contactors," *AIChE J.*, **32**, 11 (1986).

rates unlike the SciMed membrane. Permeability values approach a maximum of 3.2E-05 m/s which falls somewhere in between the SciMed membrane and the MTR membrane tested with the flat sheet device. Comparisons of the hollow fiber and flat sheets are not valid at this point because the oxygen flux is affected by both the membranes as well as the flow geometries, and the hollow fiber cartridge presents a different flow geometry than the flat sheet membranes.

CONCLUSIONS

It is apparent from those experiments that the SciMed membrane does not offer a good solution to the membrane selection problem. The MTR membrane exhibited very good oxygen permeability and the material in the prototype hollow fiber cartridge also showed low resistance to oxygen flux. The actual membrane permeability can only be calculated by using the models presented in the paper by Yang and Cussler[5]. Once these models are incorporated into the data analysis procedure, it should be easy to account for the contribution of the air and nitrogen side diffusion boundary layers to the mass transfer coefficient. This would enable determination of the membrane permeability from the overall mass transfer coefficient that is calculated from experimental data. The work towards this analysis procedure will only proceed if membrane permeability becomes a predominant issue in the transfer of oxygen from seawater to carrier. This is not likely given the fact that oxygen diffusion through seawater - the controlling phenomenon in the actual application of the gill to power generation undersea - is slow enough to negate any influence the membrane might have on the process. The SciMed membrane is ruled out from use underwater because, even allowing for slow diffusion rates through seawater, it is likely to adversely affect oxygen transport because of its low permeability.

Another important contribution made by this process is the setting up of a data base as well as experimental protocol by which initial evaluation of other membrane samples and hollow fiber cartridges can be accomplished. The experimental apparatus for this study can be easily modified or adapted to accommodate any new samples that may arrive and initial estimates of its efficacy established within one day and without the expense of making a batch of carrier solution to study seawater to carrier transport. Moreover the efficiency of the experiment would allow pre-screening of prospective membranes prior to the long and expensive process of testing with carrier and seawater at lowered temperatures.

5.2 Packaged Gill Membrane Testing

OBJECTIVE

The gill membrane of the deep sea oxygen extraction system has three major performance requirements. The first objective dictates that the membrane withstand operating conditions of up to 6,000 meters of ocean depth. The second objective requires that the total volume of the gill be no larger than 80 liters per liter per minute of delivered oxygen. The third objective stipulates that the power required to pump seawater across the gill surface not exceed 24 watts per liter of delivered oxygen.

Experimentation on different types of solid, gas permeable membranes has been carried out. Both flat sheet and hollow fiber membranes have been studied for their oxygen flux characteristics. The purpose of this experimentation was to determine the best gill membrane material and the best packaging arrangement for the gill membrane.

[5]Yang, and Cussler, op cit.

BACKGROUND

The Aquanautics gill system must be able to withstand the rigors of ocean depth. The system requires that the membrane be constructed of a solid nonporous oxygen permeable material. Prior to the work on the deep sea applications, all the gill membrane studies were undertaken with microporous membrane materials. A search was undertaken to identify membranes which had both good oxygen flux characteristics and provided a good liquid barrier. Comparisons were first made between the solid flat sheet membranes obtained from Membrane Technology Research and SciMed Life Systems and a flat sheet microporous control. Studies were also carried out comparing a prototype solid hollow fiber membrane to a microporous hollow fiber membrane.

EXPERIMENTAL SET-UP

The experimental setup is shown in Figure 25. The electrochemical cell was a two cell stack of the Aquanautics ABC 250 cell with titanium current collectors. The total area of the electrochemical cell was 0.050 m^2. The air loader was a Hoechst-Celanese 50101040 microporous membrane module containing 1.9 m^2 of surface area. The seawater loader was different types of flat sheet and hollow fiber solid membranes. These membranes included samples from SciMed Life Systems, Membrane Technology Research and a control of Hoechst-Celanese Celgard 2400 microporous hydrophobic flat sheet. The flat sheet samples measured 0.1 m x .5 m and the hollow fiber solid prototype membrane contained 0.37 m^2 of surface area. A Minntech microporous hollow fiber blood oxygenator measuring 3.8 m^2 in surface area was used as a control for oxygen flux measurements which used carrier. A Hoechst-Celanese 50101010 microporous shell and tube hollow fiber membrane module was used as the control in the seawater to nitrogen experiments. Two flat sheet blood oxygenators manufactured by SciMed Life Systems were also examined. These are designated 1500 A (1.5 square meter) and SM-35 (3.5 square meter) and are sold as commercial blood oxygenating modules. The unloader was a sparging tower using 50 ml per minute of nitrogen for the sparge gas. Compound 64 freebase mixed to a concentration of 0.43 molar was used as the oxygen carrier. Seawater was Instant Ocean mixed to a refractive index corresponding to 33 parts per thousand and chilled to 3 degrees Celsius. The oxygen concentrations in the seawater were measured with Yellow Springs Instrument 5331 Clarke type oxygen probes. A gear type Micropump was used to circulate the carrier. Needle valves were used to control the volume of flow from the electrochemical cell to the seawater loading membrane.

PROCEDURE

The examination of the oxygen flux from seawater to nitrogen gas took place on the same test set-up used for carrier testing. The nitrogen gas was flowed through the test module at 0.135 liters per minute per square meter of membrane area. Transfer of dissolved oxygen from seawater to nitrogen was measured while flowing nitrogen both inside and outside the prototype membrane fibers with seawater flowing on the other side. This was compared to a control using a microporous hollow fiber Hoechst-Celanese membrane module measuring 1.2 m^2 in surface area. In the control test, data was acquired only for seawater flow inside the lumen.

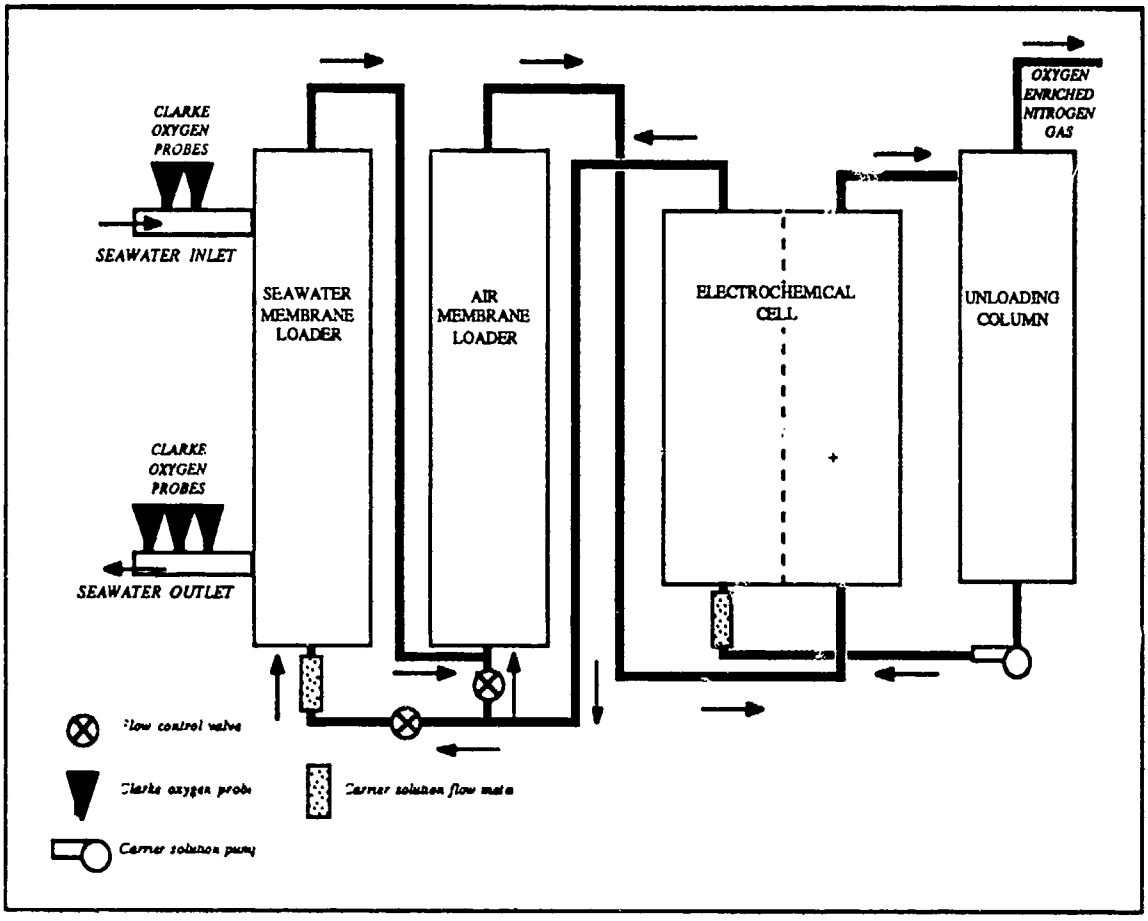

FIGURE 25
Seawater Loading Experimental Set-Up

Seawater to carrier experiments were run using the experimental set-up described in the previous section. Carrier solution was mixed according to the standard procedure for freebase solutions of low conductivity. The carrier solution was then introduced into the experimental set-up and allowed to fully load with oxygen. After running the system at high seawater and carrier flow rates to allow the seawater oxygen probes to equilibrate with the loading of the carrier, the carrier and seawater flow through the seawater loader were set to the desired experimental flow rates. Due to the temperature and flow sensitivity of the YSI oxygen probes, the background or air saturated value for the probes were taken prior to each sampling of the seawater oxygen partial pressure. This was accomplished by running the seawater and carrier at the desired flow rates with the electrochemical cell turned off so that no deoxygenated carrier was presented to the seawater loader. Once the oxygen probes stabilized at each flow rate, the electrochemical cell was turned on and oxygen flux measurements were recorded. YSI probe air background values were taken at each combination of seawater and carrier flow rates.

Carrier was run through the electrochemical cell at approximately the same flow rate throughout the experiments to ensure reasonable fractional conversion. The addition of an air loader ensured that the carrier was fully loaded as it returned to the electrochemical cell, thus not presenting the seawater loader with an abnormally high amount of deoxygenated

carrier. The carrier pump ran at a constant speed corresponding to a flow rate of about 7 liters per minute per square meter of cell area. Flow rates of carrier through the seawater loader were 0.134, 0.067 and 0.027 liters per minute per square meter of membrane. Seawater flow ran at 0.54, 0.81, 1.08 and 1.35 liters per minute per square meter of membrane. Carrier flow was inside the lumen while seawater flow was outside the lumen.

Measurement of oxygen transfer from seawater to nitrogen through flat sheet membranes was also carried out. In these experiments a testing jig of area .05 m^2 was run with seawater on one side of the membrane and nitrogen on the other side. Determination of seawater flow rates was done by matching the Reynolds Numbers of a flat sheet jig with that of a bundle of hollow fiber tubes. Again the Clarke probes were equilibrated for a background value but only at the highest seawater flow rate. No precautions were taken to keep the seawater temperature from rising even though heat transfer to the room at slow flow rates was significant.

RESULTS

Flat sheet testing of the SciMed, MTR and Celgard membranes gave such a small flux of oxygen that it was both non quantifiable and not useful for gill design. Due to temperature and flow rate sensitivity of the Clarke oxygen probes, it was found that the background or air value of the Clarke probes had to be taken for each experimental regime. This also made the flat sheet testing hard to interpret and showed the need to take more background values in further testing.

Testing of the SciMed Life Systems membrane cartridges proved impossible due to leaks observed during system water testing. The SciMed blood oxygenators are intended for use in facilitating gas to liquid transport rather than liquid to liquid transport. Flowing the carrier solution through the gas side of the membrane caused leaks in the membrane making them difficult to use.

Figure 26 shows oxygen flux from seawater to nitrogen with both seawater flowing through the lumen and outside the lumen of the prototype membrane module. In a liquid to gas configuration, seawater flow through the lumen gives the best oxygen transfer at low flow rates with the rate of transfer equalizing as flow rates rise. Figure 27 is a comparison of a microporous membrane to a solid membrane. In both cases the seawater flow is through the lumen and nitrogen flow outside the membrane fibers. All seawater and nitrogen flow rates are normalized by the membrane area.

The oxygen flux in the prototype solid hollow fiber membrane module is shown in Figure 28. Three different carrier flow rates were examined and the oxygen flux characterized at four different seawater flow rates as shown in Figure 28. The flow rate of the seawater is shown next to each curve on the right side of the graph.

Figure 29 compares oxygen flux through a microporous cartridge with that in the prototype solid membrane. Initial results show about twice the oxygen flux through a microporous hollow fiber cartridge when compared to the prototype solid hollow fiber membrane. The microporous cartridge employed here was the Minntech blood oxygenator.

FIGURE 26

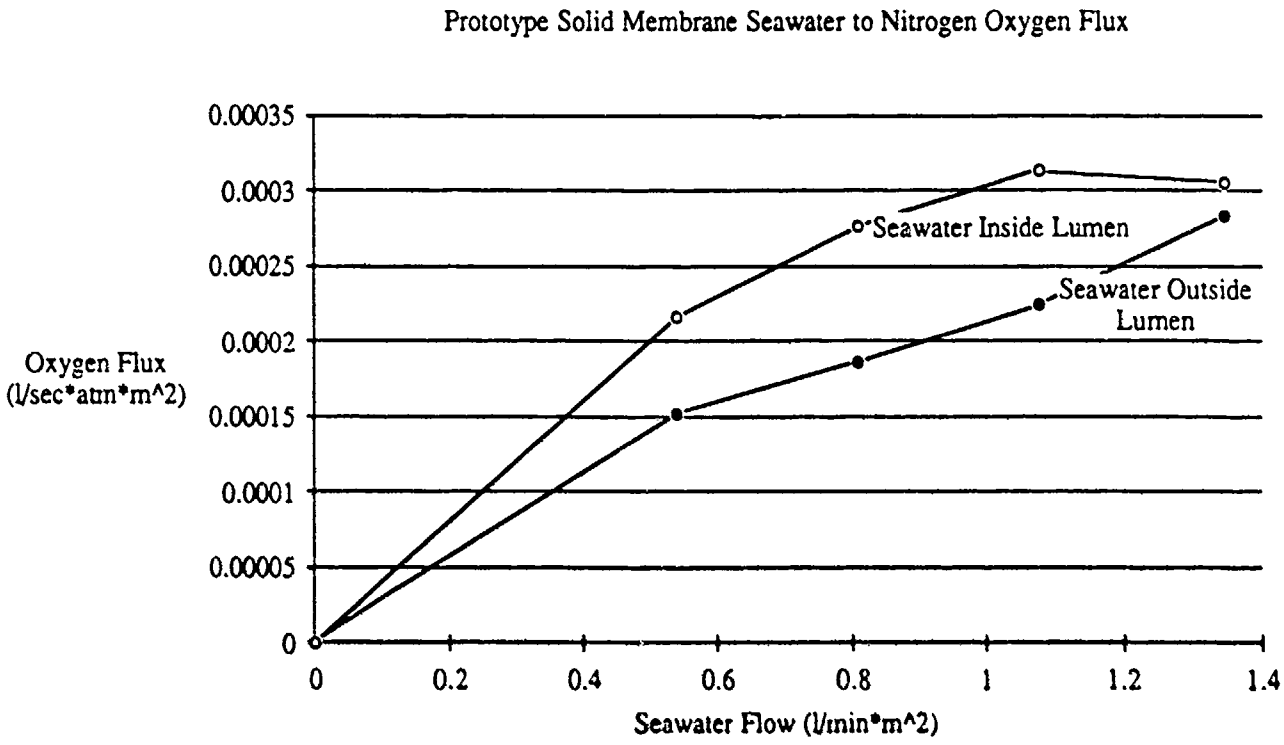
Prototype Solid Membrane Seawater to Nitrogen Oxygen Flux
Oxygen Flux
(l/sec*atm*m^2)
0.00035
0.0003
0.00025
0.0002
0.00015
0.0001
0.00005
0
0
0.2
0.4
0.6
0.8
1
1.2
1.4
Seawater Flow (l/min*m^2)
Seawater Inside Lumen
Seawater Outside
Lumen

FIGURE 27

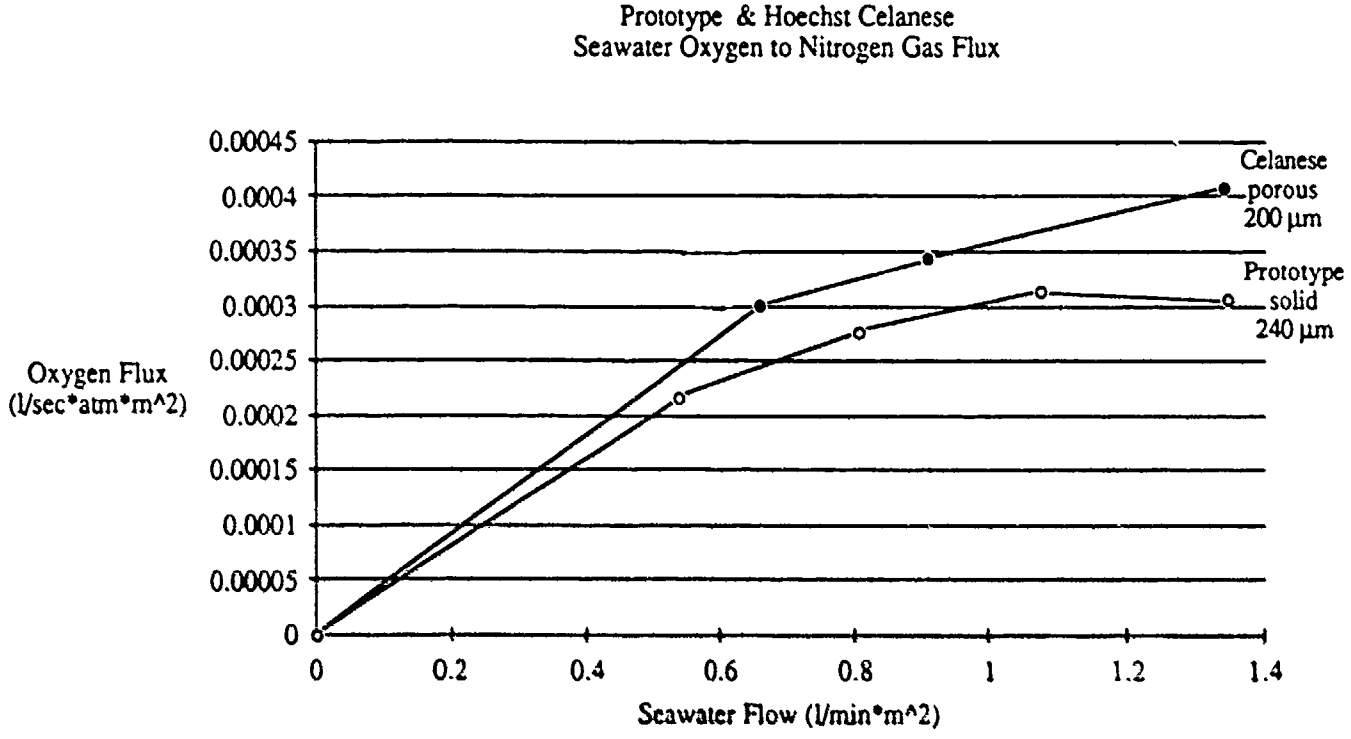
Prototype & Hoechst Celanese
Seawater Oxygen to Nitrogen Gas Flux
Oxygen Flux
(l/sec*atm*m^2)
0.00045
0.0004
0.00035
0.0003
0.00025
0.0002
0.00015
0.0001
0.00005
0
0
0.2
0.4
0.6
0.8
1
1.2
1.4
Seawater Flow (l/min*m^2)
Celanese
porous
200 µm
Prototype
solid
240 µm

FIGURE 28

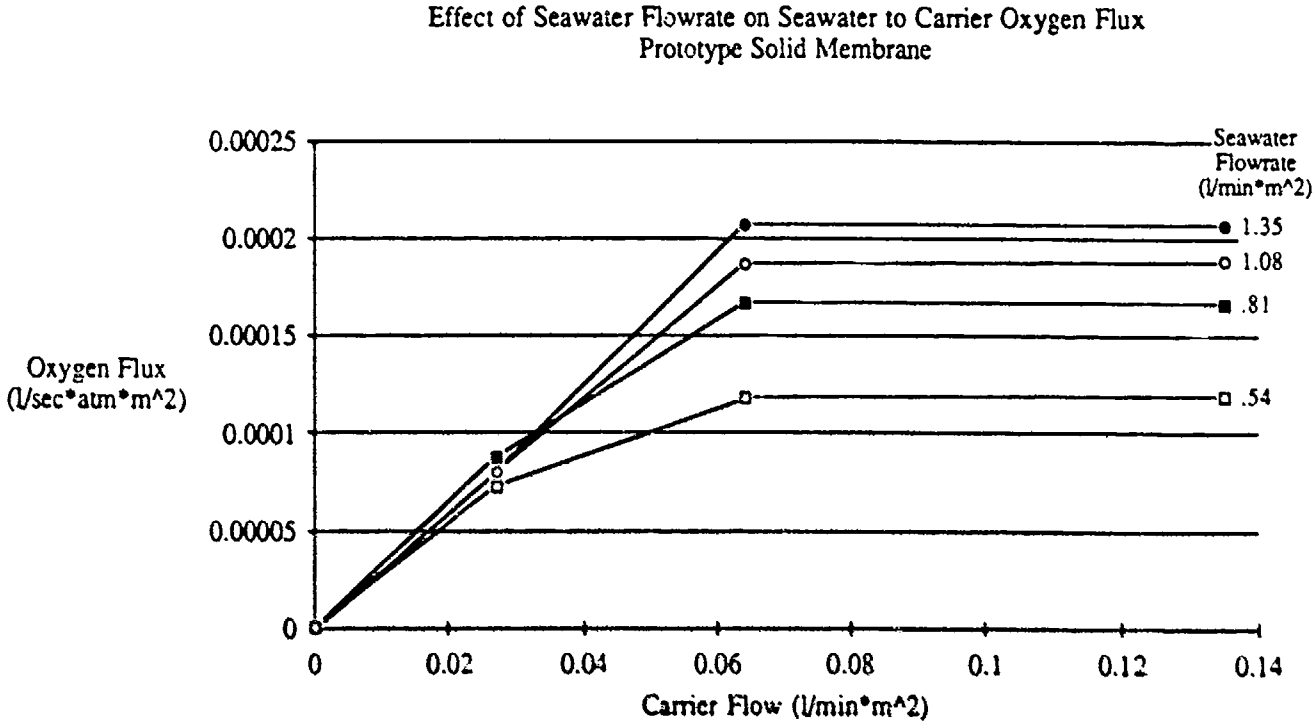
Effect of Seawater Flowrate on Seawater to Carrier Oxygen Flux
Prototype Solid Membrane
Oxygen Flux
(l/sec*atm*m^2)
0.00025
0.0002
0.00015
0.0001
0.00005
0
0
0.02
0.04
0.06
0.08
0.1
0.12
0.14
Carrier Flow (l/min*m^2)
Seawater
Flowrate
(l/min*m^2)
1.35
1.08
.81
.54

FIGURE 29

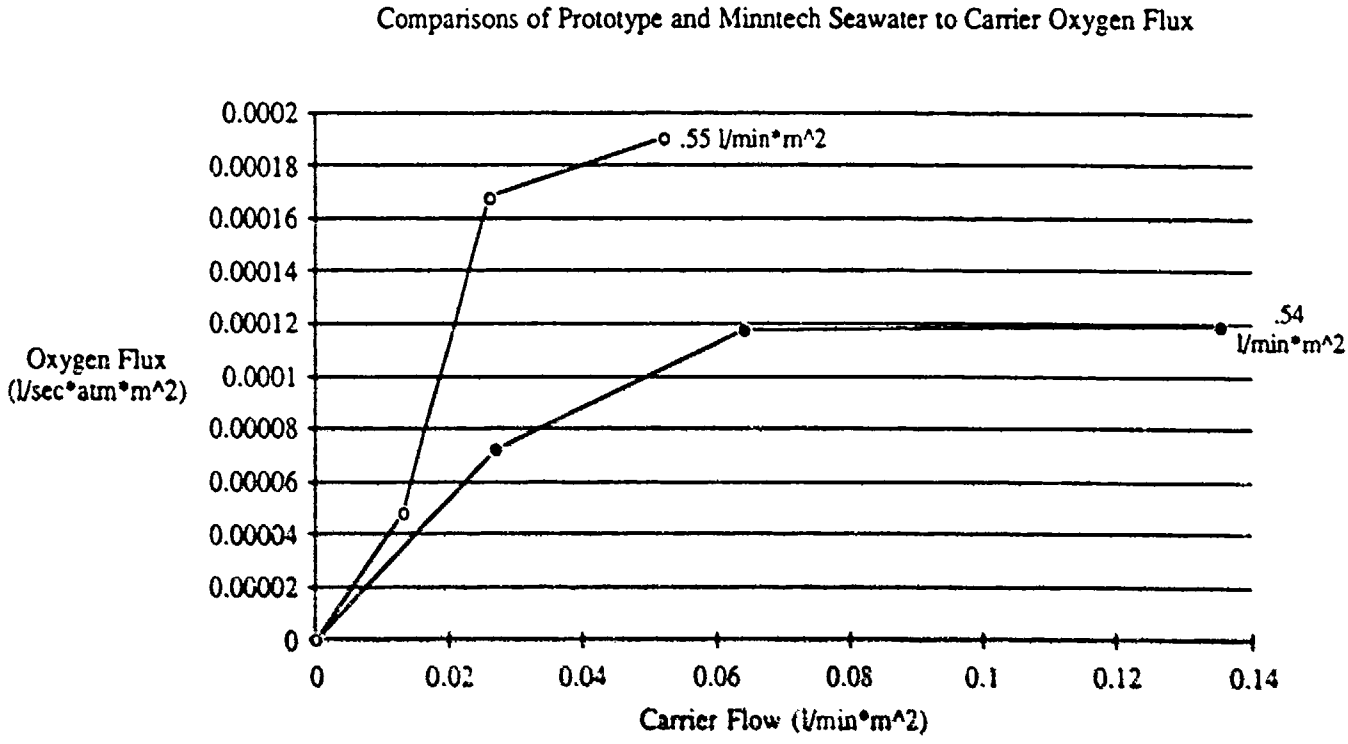
Comparisons of Prototype and Minntech Seawater to Carrier Oxygen Flux
Oxygen Flux
(l/sec*atm*m^2)
0.0002
0.00018
0.00016
0.00014
0.00012
0.0001
0.00008
0.00006
0.00004
0.00002
0
.55 l/min*m^2
.54
l/min*m^2
0
0.02
0.04
0.06
0.08
0.1
0.12
0.14
Carrier Flow (l/min*m^2)

Table 4 is a tabulation of experimental results of oxygen transfer from seawater to carrier and nitrogen. The membrane modules used for seawater to nitrogen flux studies included the prototype membrane and the Celanese 50101010 modules. Experimentation of seawater to carrier flux used the prototype and Minntech modules. Experiments characterizing seawater to carrier flux of oxygen were repeated with the prototype solid membrane cartridge at the maximum seawater flow rate used previously, i.e. 1.35 l/min/m^2. A different batch of carrier chemically identical to the previous batch was employed and flow rates of 0.064 and 0.135 l/min/m^2 used. The oxygen flux was again seen to remain constant over this range of carrier flow rates indicating that the seawater side limited the transport. The actual oxygen flux was, however, measured to be about 20% higher than that measured in the initial experiments that are depicted in Figure 28.

DISCUSSION

The small amounts of oxygen recovered from the seawater flat sheet testing made it hard to interpret the results. It is evident from these results that oxygen flux from such a membrane even when it is scaled up in size will not be sufficient for the purpose at hand. For a flat sheet to give enough oxygen transfer, the amount of seawater that would need to flow across the membrane would make the power costs prohibitive. This is caused by inefficient packaging, thus making the gill volume too large.

The prototype cartridge was initially tested to evaluate the flux of oxygen from seawater to a nitrogen gas stream. The first evaluation of this was carried out with the seawater outside the lumen. This is the configuration which would be used in a gill setup. Because an experimental control against a microporous module seemed prudent, testing was also done with a Hoechst-Celanese module. The design of the Hoechst-Celanese 50101010 microporous membrane module, used as the control, is similar to the prototype module except that the Celanese module has big voids in the space outside the lumen, making fluid channeling a major problem. By running the seawater in the insides of both types of fibers, however, Aquanautics was able to compare membrane affects rather than hydrodynamic affects.

The comparison of the two regimes of flow shown in Figure 26 reveals that the diffusion of oxygen in seawater is slowed when the seawater flow is outside the lumen. When the flow rate of seawater rises the oxygen transfer becomes more equal as more mixing occurs outside the fibers. Seawater to nitrogen testing of the modules showed that the prototype solid membrane permits about eighty percent of the oxygen flux allowed by the microporous membrane in the control experiment. This data is depicted in Figure 27. In both cases, this is for seawater flow inside the lumen. The difference was determined to be due to the hydrodynamic effects, primarily the effect of the inside diameter of the fiber itself. The membrane thus seems to not affect oxygen transport.

Seawater to carrier oxygen flux results shown in Figure 28 show that the flux is independent of carrier flow above 0.062 l/min/m^2. Oxygen flux is dependent only on seawater flow once carrier flow reaches its limiting conditions.

TABLE 4

OXYGEN FLUX: SEAWATER TO CARRIER EXPERIMENTAL RESULTS: 3-14-89

PROTOTYPE MEMBRANE MODULE; SHELL AND TUBE COUNTER CURRENT FLOW:
Fluid distribution is carrier inside the lumen and seawater outside the lumen.

Carrier flow l/min*m^2	O2 Flux Seawater flow = 1.35	O2 Flux Seawater flow = 1.08	O2 Flux Seawater flow = 0.81	O2 Flux - (l/min*m^2) Seawater - (l/min*m^2) flow = 0.54
0.135	2.07E-04	1.89E-04	1.67E-04	1.19E-04
0.064	2.07E-04	1.87E-04	1.67E-04	1.18E-04
0.027	7.96E-05	7.96E-05	8.76E-05	7.24E-05
0	0	0	0	0

MINNTECH OXYGEN FLUX: SEAWATER TO CARRIER EXPERIMENTAL RESULTS

Carrier Flow l/min*m^2	O2 Flux - (l/sec*atm*m^2) Seawater - (l/min*m^2) flow = 0.55
0.052	1.90E-04
0.026	1.68E-04
0.013	4.78E-05
0	0

PROTOTYPE OXYGEN FLUX: SEAWATER TO NITROGEN EXPERIMENTAL RESULTS:
Nitrogen flow is 50 ml/min (.134 l/min*m^2)
Nitrogen flow is inside the lumen, seawater is outside.

SW Flow l/min*m^2	O2 Flux l/sec*atm*m^2
1.345	2.84E-04
1.076	2.24E-04
0.807	1.86E-04
0.538	1.52E-04
0	0

PROTOTYPE GDS-GL-5-001
Nitrogen flow is .134 l/min*m2 (50 ml/min prototype & 162 ml/min Hoechst Celanese 50101010)
Nitrogen flow is outside the lumen, seawater is inside.

SW Flow l/min*m^2	O2 Flux l/sec*atm*m^2
1.345	3.06E-04
1.076	3.14E-04
0.807	2.76E-04
0.538	2.16E-04
0	0

HOECHST CELANESE 50101010

SW Flow l/min*m^2	O2 Flux l/sec*atm*m^2
1.34	4.08E-04
0.91	3.43E-04
0.66	3.01E-04
0	0

The Minntech module shows about twice the oxygen flux when compared to the prototype solid membrane module on a unit area basis. This increased oxygen flux is most likely due to hydrodynamic affects rather than membrane effects. On the Minntech module the seawater flow is perpendicular to the direction of carrier flow and the direction of the fibers themselves. This cross flow configuration is inherently more advantageous with respect to mass transport than the co-flow configuration of the prototype solid membrane cartridge. In the co-flow configuration the seawater flow is parallel to the fibers and hence the carrier flow direction. Previous experiments and published results have shown that using crossflow should yield a five-fold to twenty-fold improvement in mass transport when compared to co-flow results. The two-fold improvement shown in Figure 29 is therefore not unexpected and is not a result of using the solid membrane.

More experimentation has to be carried out with the prototype membrane using different carrier compounds and lower oxygen concentrations in the seawater. All the seawater testing was carried out at saturated conditions. The experimental error in this data was found to be ±20% within a confidence interval of ninety five percent. To better evaluate the true size needed for the gill membrane and the gill system, more carrier experimentation is needed.

CONCLUSIONS

- The prototype solid hollow fiber membrane has the same seawater to nitrogen flux characteristics as a microporous hollow fiber membrane.
- The gill membrane must be a solid hollow fiber array to permit efficient packaging of the required membrane area as well as to withstand high pressures.
- Experimentation should to be carried out at oxygen concentrations found at the proposed depth of operation.
- The most important aspect of gill design seems to be the flow characteristics on the seawater side of the membrane.
- Repeats of experiments with the final gill configuration should be undertaken, to give a better level of confidence in the error calculations.

5.3 Theoretical Analysis of Experimental Results

INTRODUCTION

This section describes the model used to simulate transport of oxygen from seawater to carrier through a hollow fiber membrane cartridge The experiments that the model was intended to simulate were performed with the prototype hollow fiber solid membrane cartridge that was procured from Applied Membrane Technology, Inc. as described in previous sections. The experiments that provided the data for comparison with the results of the modelling work were performed by Mr. Charles Benedict in March 1989 and are described in the previous sub-section. The prototype cartridge was also characterized with gases prior to its use in determining oxygen transport from seawater to carrier. The results of this experiment have been described prior to this section.

BACKGROUND

The background for this work is the DARPA Phase V contract which seeks to establish the feasibility of using the Aquanautics oxygen separation technology for the purpose of generating electrical power undersea by extracting dissolved oxygen from seawater. The system proposed for this would include a gill or loader where the oxygen transport would take place. The design of such a gill would have to allow for the high pressures present at great depths and therefore solid membranes were preferred to the microporous membranes that have been used at Aquanautics extensively to this point. In view of this fact, Mr. Benedict of Aquanautics instituted a membrane product review seeking to obtain samples of solid membranes for evaluation and comparison with conventional microporous membranes. Of the samples obtained, one supplier, namely, Applied Membrane Technology, Inc. sent a hollow fiber solid membrane cartridge which was constructed by the ultra-deposition of a proprietary layer on top of a commercially available microporous hollow fibers from Hoechst-Celanese. Evaluation of this cartridge formed the bulk of the effort expended this quarter towards gill membrane selection and qualification.

OBJECTIVE

The objective of this study was to model the process of oxygen transport through the solid membrane and compare the results of this simulation with the experimental data obtained from membrane testing performed in the laboratory. The testing involved measurement of oxygen flux through the membrane from seawater to both nitrogen and carrier. Measurements were made in three stages using the prototype membrane. The three stages are described below.

1) Oxygen flux from seawater to nitrogen with seawater on the outside of the hollow fibers and nitrogen on the inside.
2) Oxygen flux from seawater to nitrogen with seawater on the inside of the hollow fibers and nitrogen on the outside.
3) Oxygen flux from seawater to carrier with seawater on the outside of the fibers and carrier on the inside.

In addition to the above-mentioned experiments performed with the prototype membrane cartridge, step #1 was repeated with a conventional microporous hollow fiber cartridge made by Hoechst-Celanese, and step #3 repeated with a Minntech blood oxygenator as described previously.

The objective of this work is to establish a model for the oxygen transport that can then be introduced into the model for optimizing gill volume and power. The gill power and volume relationship[6] that is currently used for gill design is open-ended in the sense that the model has to be supplied with information regarding the oxygen concentration difference between the seawater and the carrier. Ideally the model should be capable of determining this implicitly. This improvement in gill model is expected to allow a more accurate and complete gill design.

[6]Cussler, E.L., "Designing an Artificial Gill," Personal Communication, dated July 26, 1988, amended January 27, 1989.

MODEL DESCRIPTION

Basic Equations

Oxygen transport through a membrane can generally be described using Equation 8 shown below.

$$Q_{ox} = k_o A \Delta C \tag{8}$$

where, Q_{ox} is the flux rate of oxygen through the membrane (m^3 @ STP /s),
k_o is the overall mass transfer coefficient in the membrane cartridge (m/s),
A is the total surface area of the membrane (m^2), and
ΔC is the concentration difference that drives the oxygen flux (m^3 @ STP /m^3).

It is useful to note here that this equation is general, not only in the sense that it can be applied no matter what the feed and sweep fluids but also for all types of membranes. The flux and concentration difference units chosen here describe the oxygen transport in terms of volumes of oxygen referred to Standard Temperature and Pressure. Measurements in terms of mols or weight units are also valid and the above equation can be converted to mols or weight units by applying the well known conversion factor, 0.0224 m^3 @ STP = one mol.

The concentration difference in a membrane cartridge is usually calculated by using a log mean difference expression such as that shown in Equation 9.

$$\Delta C = \frac{(C_{fi} - C_{so}) - (C_{fo} - C_{si})}{\ln\left\{\frac{C_{fi} - C_{so}}{C_{fo} - C_{si}}\right\}} \tag{9}$$

where, C_{fi} is the oxygen concentration in the feed stream at its inlet,
C_{fo} is the oxygen concentration in the feed stream at its outlet,
C_{si} is the oxygen concentration in the sweep at its inlet, and
C_{so} is the oxygen concentration in the sweep at its outlet.

The concentration terms can be in any of three forms, namely m^3 @ STP, mols or kg of oxygen per m^3 of the feed or sweep fluid. The expression for the log mean concentration difference in Equation 9 holds good only for counterflow configurations, where the feed stream and the sweep stream inlets are at opposite ends of the cartridge. The feed stream in the experiments described before consists of seawater and the sweep consists of either nitrogen or the carrier.

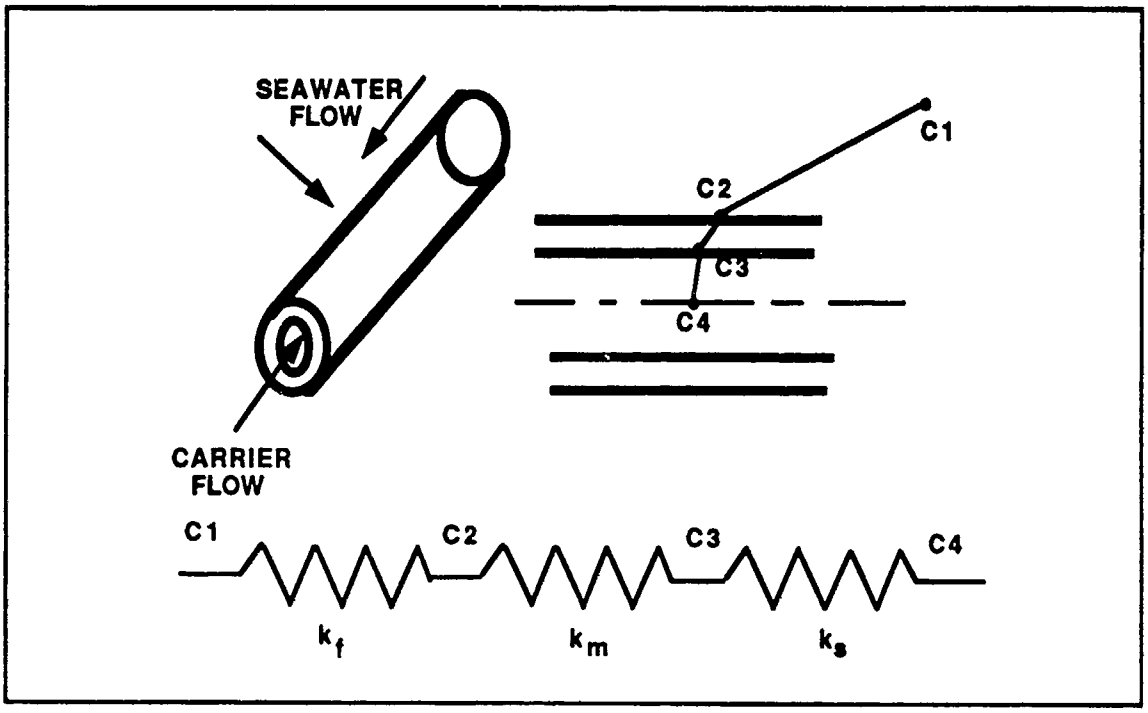

FIGURE 30
Representation of membrane resistance to oxygen flux

The overall mass transfer coefficient k_O typically encompasses three constituents, as shown in Figure 30. The three components to the resistance to oxygen flux are diffusion in the carrier, diffusion through the membrane and diffusion in the seawater. Since the resistances to oxygen flux are in series, an electrical analog would yield that the overall resistance is equal to the sum of the individual or component resistances. The resistance to oxygen flux could be defined, using the electrical analogy, as the concentration difference divided by the oxygen flux. The effective or overall mass transfer coefficient could therefore be expressed as shown in Equation 10.

$$\frac{1}{k_O} = \frac{1}{k_f} + \frac{1}{k_m} + \frac{A_O}{A_i\, k_S} \qquad (10)$$

where, k_O is the overall mass transfer coefficient (m/s),
k_f is the feed stream mass transfer coefficient (m/s),
k_S is the sweep stream mass transfer coefficient (m/s),
k_m is the membrane permeability (m/s),
A_i is the total surface area presented by the insides of the hollow fiber membranes (m^2), and
A_O is the total surface area presented by the outsides of the hollow fiber membranes (m^2)

The area A in Equation 8 is usually the membrane area calculated on the basis of the outer diameter of the hollow fibers and is therefore the same as the parameter A_O in Equation 10. This is the reason that all the mass transfer coefficients in Equation 10 are referred to the outer diameter or the outer surface area of the fibers. It may also be noted here that manufacturers usually present membrane permeabilities in terms of m^3 @ STP/(s m^2 atm),

where the pressure term in the denominator indicates a concentration difference or more specifically partial pressure difference. When dealing with liquids and dissolved gas transport, it is more instructive to convert partial pressures into corresponding concentration terms like m^3 @ STP/m^3. Upon utilization of Henry's Law to make this conversion, the units for membrane permeability changes to m/s as in the case of the feed stream and sweep stream mass transfer coefficients.

To evaluate the different mass transfer coefficients the flow geometries and flow rates of the feed and sweep have to be taken into account. There is a wide body of literature that describes mass transfer in a variety of different flow configurations. All these correlations are expressed in terms of non-dimensional numbers. These expressions take on the form

$$Sh = a\,(Re)^b\,(Sc)^c, \qquad (11)$$

where, Sh is the Sherwood number ($k_o\,d/D$),
Re is the Reynolds number ($v\,d/\upsilon$), and
Sc is the Schmidt number (υ/D).

The constants "a", "b", and "c" are dependent on both the flow regime - laminar or turbulent - as well as on the geometry of the cartridge under analysis. The correlation shown in Equation 11 above has been reported for a variety of cartridge configurations[7] and modelling work was started with the use of some of these published correlations. The aim of modelling is to determine the theoretical value of the overall mass transfer coefficient and compare that with the value obtained from experiments using the formulations reported in Equation 8 and 9. Typically experiments involve measurement of the oxygen flux Q_{ox} and the concentration difference on the seawater side to yield a value for the term k_o. The correlation shown in Equation 11 is used to determine the theoretical value for k_o given the flow conditions (denoted by Re) and the fluid properties (implied in Sc). Table 5 shows the various values of "a", "b", and "c" for the different flow geometries considered in the modelling work performed to simulate mass transport through membranes.

TABLE 5
Constants for Equation 11 in Laminar Flow

Description of Flow	a	b	c
Inside Hollow Fibers	$1.62\,(d_h/l)^{0.33}$	0.33	0.33
Flow outside parallel to fibers	0.022	0.60	0.33
Flow outside perpend. to fibers	0.39	0.59	0.33

In the table shown above, d_h represents the hydraulic diameter for flow inside the fibers, and in the case of cylindrical hollow fibers is equal to the inner diameter of the fibers themselves. The term l represents the path length for flow inside the fibers and is equal to the length of the fibers themselves.

[7]Yang, and Cussl , op cit.

Application of Equations to Modelling

Equation 10 defines the contribution made by the three constituents to the overall mass transport of oxygen in a membrane cartridge. In the actual application, it was assumed that the resistance offered by the sweep stream diffusion layer is negligible in comparison to the feed side diffusion layer and can thus be ignored. In the case where nitrogen gas is the sweep medium, the rationale for this assumption is immediately apparent. Diffusion of oxygen through nitrogen gas is exactly four orders of magnitude faster than the diffusion of oxygen through seawater. It is therefore safe to assume that the resistance of the nitrogen sweep stream is not the controlling factor.

In the case where the carrier is employed to absorb dissolved oxygen from seawater, the same statement may be proved given one condition, namely that the concentration of dissolved oxygen in the carrier is always zero. This is the case when a stoichiometric excess of deoxygenated or unbound carrier molecules are supplied to the membrane. Since the experiments that are being simulated here consistently involved excessive flow rates of carrier, this assumption was held to be valid. Given this condition, the factor limiting oxygen transport was determined to be the diffusion of oxygen through seawater. Therefore, the sweep side mass transport coefficient was ignored.

Equation 10 was then modified to include only k_f and k_m. The expression for the concentration difference (given in Equation 9) was also modified to account for the fact that the values of C_{si} and C_{so} were always zero. In the case of nitrogen, this was a simplification because the oxygen that was transported across the membrane was not bound chemically as in the case of the carrier. But given the low transport rates and hence the low oxygen concentrations on the nitrogen side, the error introduced by this assumption was not large.

The application of the model proceeds with the experimental data which yielded values for Q_{ox} and ΔC. Q_{ox} was determined by measuring the dissolved oxygen content of the seawater prior to and after the membrane cartridge and by multiplying the difference into the flow rate of seawater as per Equation 12.

$$Q_{ox} = Q_{sw} (C_{fi} - C_{fo}), \tag{12}$$

where, Q_{sw} is the seawater flow rate in m^3/s, and
Q_{ox}, C_{fi}, and C_{fo} are as defined before.

ΔC was determined by using Equation 9 modified to account for the fact that C_{si} and C_{so} are both zero. This modified expression for ΔC is shown in Equation 13.

$$\Delta C = \frac{C_{fi} - C_{fo}}{\ln\left\{\frac{C_{fi}}{C_{fo}}\right\}} \tag{13}$$

Using the values of Q_{ox} and ΔC thus determined, the value of k_o was calculated using Equation 8. The next step involved using the expression shown in Equation 11 to calculate a theoretical value for the overall mass transport coefficient k_o. The feed side coefficient k_f was determined from the feed side Sherwood Number, which was in turn calculated by evaluating the feed side Reynolds number and Schmidt number and then using the

appropriate form of Equation 11 (by substituting the appropriate values of "a", "b", and "c" from Table 3). This value of k_f was then substituted into the modified form of Equation 10 (using the assumption that ks is always large enough to ignore) shown below as Equation 14, and the theoretical value of k_o determined.

$$\frac{1}{k_o} = \frac{1}{k_f} + \frac{1}{k_m} \qquad (14)$$

Using the same set of equations, it was also possible to determine the experimental Sherwood number on the seawater side. This was done by substituting in Equation 14 the experimentally determined value for k_o and the membrane permeability k_m,to evaluate k_f. This value of kf was then converted into a Sherwood Number and plotted against the seawater side Reynolds Number.

RESULTS

The results of the modelling exercise are presented in the form of two graphs, for each experiment type. Both the graphs involve plots of Sherwood Number on the feed side with the Reynolds Number for the feed stream flow. The first graph is a comparison of the model prediction with the experimental data, while the second plot involves a plot of the experimental data with a best-fit modification to the model. In the second plot, the value of the multiplier "a" in Equation 11 was varied until the model yielded results comparable to the experimental data. This exercise was carried out to examine the difference between the correlations reported in literature and the corresponding correlations obtained from analyzing the experimental data.

Figures 31 and 32 describe the results obtained from analyzing the data taken with the prototype cartridge using nitrogen inside the fibers and seawater on the outside. Figures 33 and 34 correspond to the experiments conducted with nitrogen outside and seawater inside the fibers. Figures 35 and 36 correspond to experiments conducted with seawater as the feed and carrier as the sweep.

DISCUSSION

Seawater to Nitrogen Transport

The experiments for oxygen transport from seawater to nitrogen have been modelled for the prototype solid hollow fiber cartridge and are presented in Figures 31 through 34. It can be seen from Figure 31 that when simulating seawater flow on the outside of the fiber, the model under-predicts the Sherwood Number and therefore the oxygen flux. The data was better fitted by a modified correlation with a value of 0.0675 for the constant "a" (compared to 0.022) as shown in Figure 32. The data points were all taken with a nitrogen flow rate of 50 ml/min. Figure 33 shows the comparison made between model and experimental data for seawater flow inside the fibers. It can be seen that in this case the model slightly over-predicts the Sherwood Number or the oxygen flux. The multiplier 1.62 in the value for the constant "a" had to be reduced to 1.4 to make the model match the data better. The nitrogen flow rate used in this experiment was also 50 ml/min.

FIGURE 31

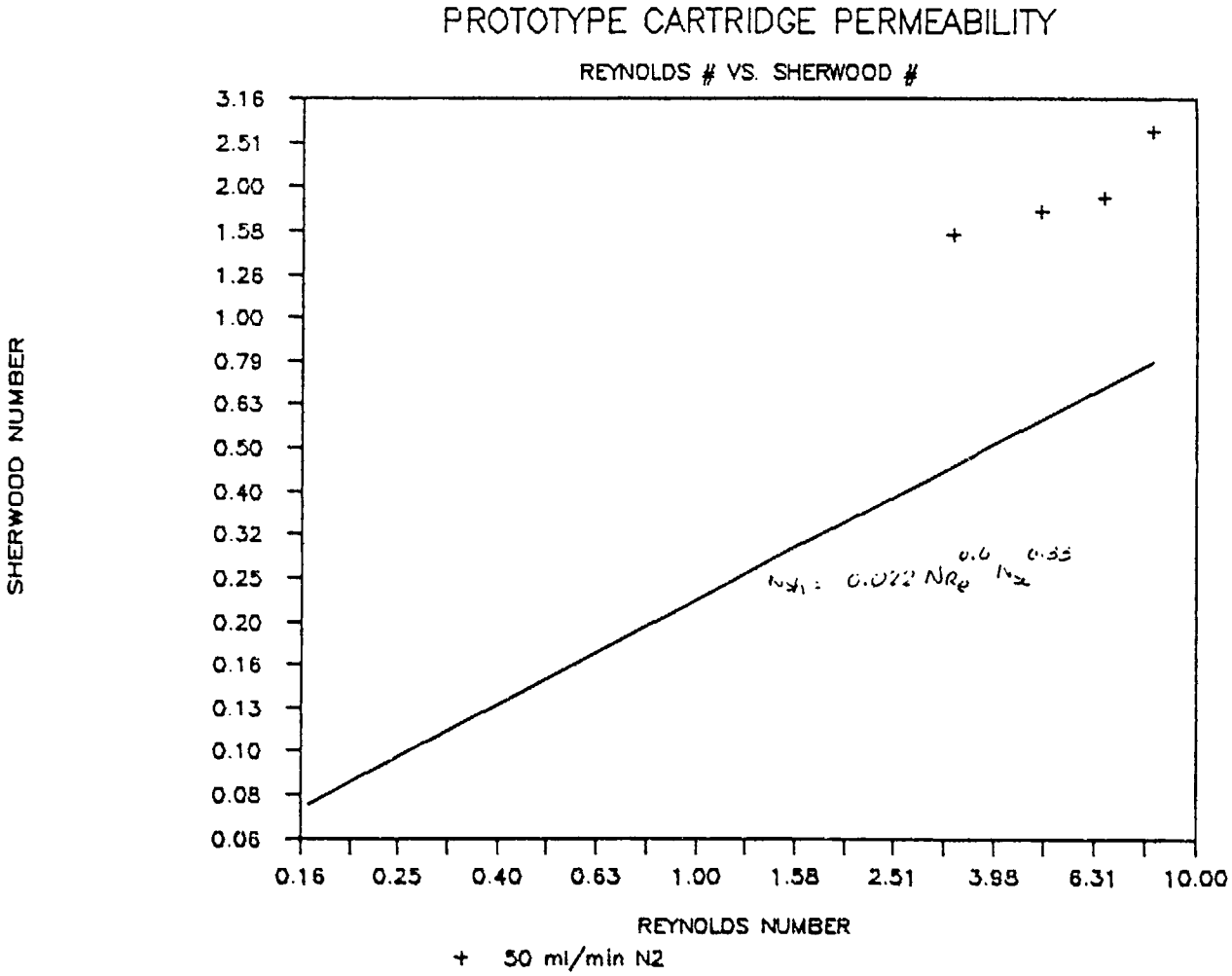
PROTOTYPE CARTRIDGE PERMEABILITY
REYNOLDS # VS. SHERWOOD #
SHERWOOD NUMBER
3.16
2.51
2.00
1.58
1.26
1.00
0.79
0.63
0.50
0.40
0.32
0.25
0.20
0.16
0.13
0.10
0.08
0.06
0.16
0.25
0.40
0.63
1.00
1.58
2.51
3.98
6.31
10.00
REYNOLDS NUMBER
+ 50 ml/min N2

FIGURE 32

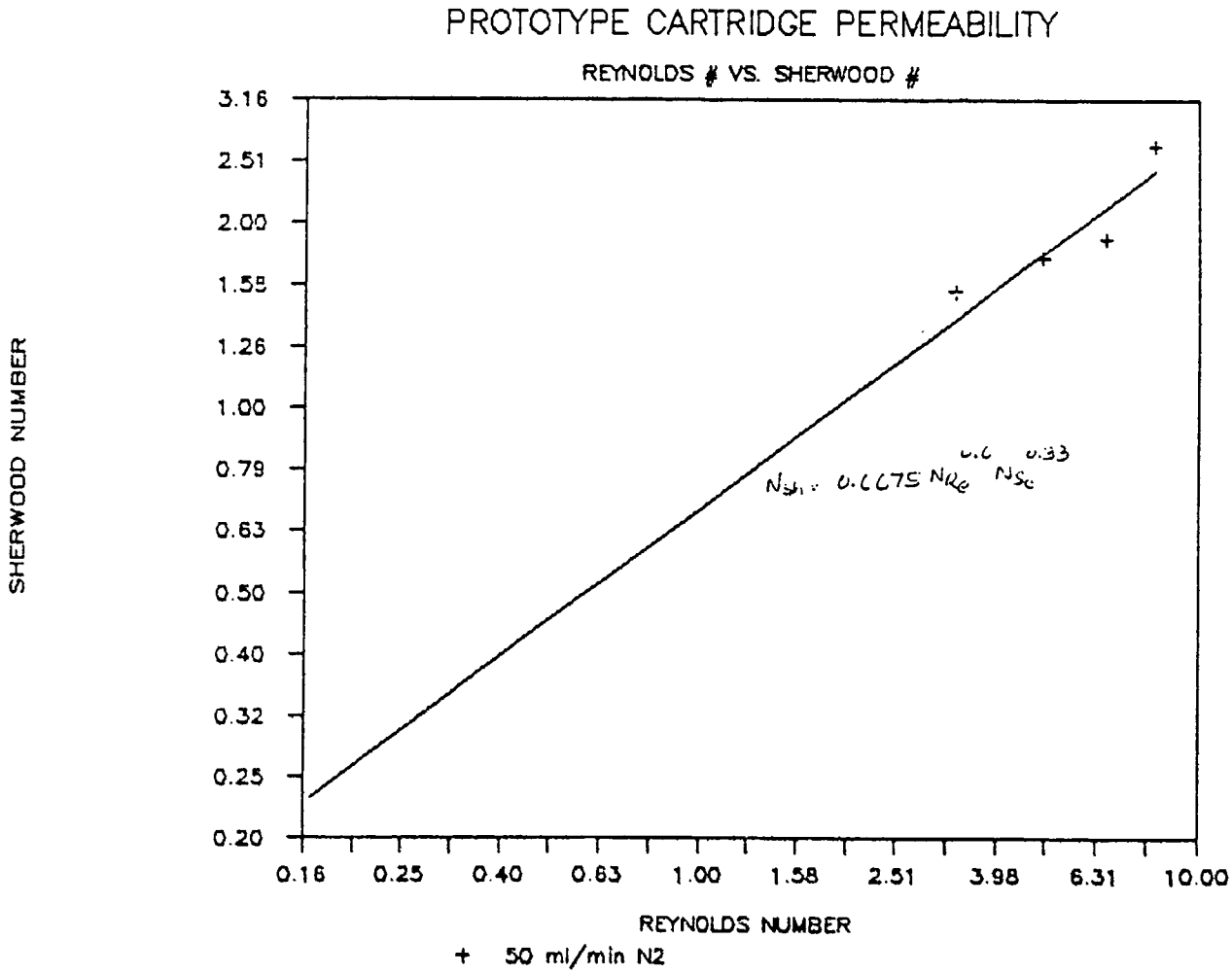
PROTOTYPE CARTRIDGE PERMEABILITY
REYNOLDS # VS. SHERWOOD #
SHERWOOD NUMBER
3.16
2.51
2.00
1.58
1.26
1.00
0.79
0.63
0.50
0.40
0.32
0.25
0.20
0.16
0.25
0.40
0.63
1.00
1.58
2.51
3.98
6.31
10.00
REYNOLDS NUMBER
+ 50 ml/min N2

FIGURE 33

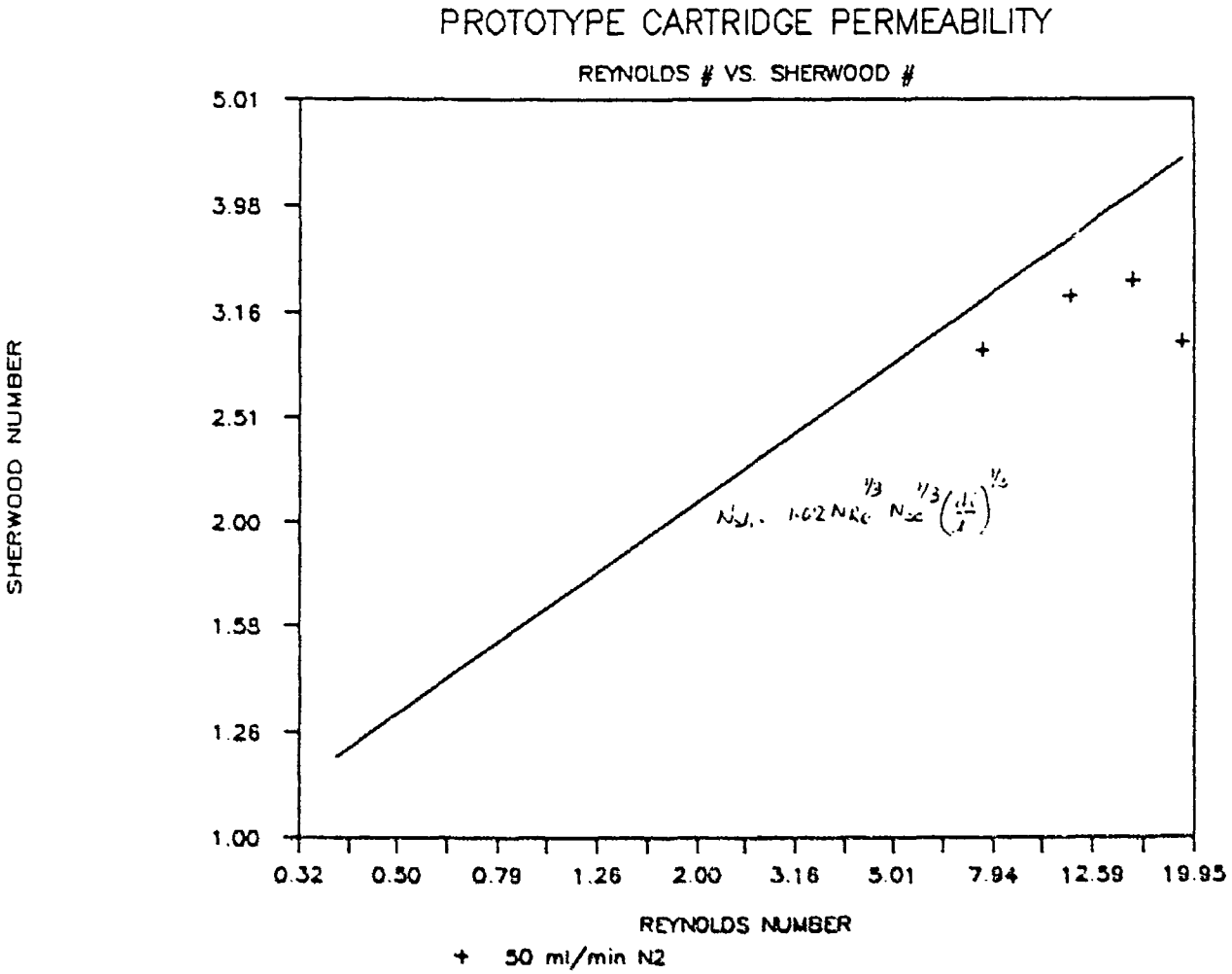
PROTOTYPE CARTRIDGE PERMEABILITY
REYNOLDS # VS. SHERWOOD #
SHERWOOD NUMBER
5.01
3.98
3.16
2.51
2.00
1.58
1.26
1.00
0.32
0.50
0.79
1.26
2.00
3.16
5.01
7.94
12.59
19.95
REYNOLDS NUMBER
+ 50 ml/min N2

FIGURE 34

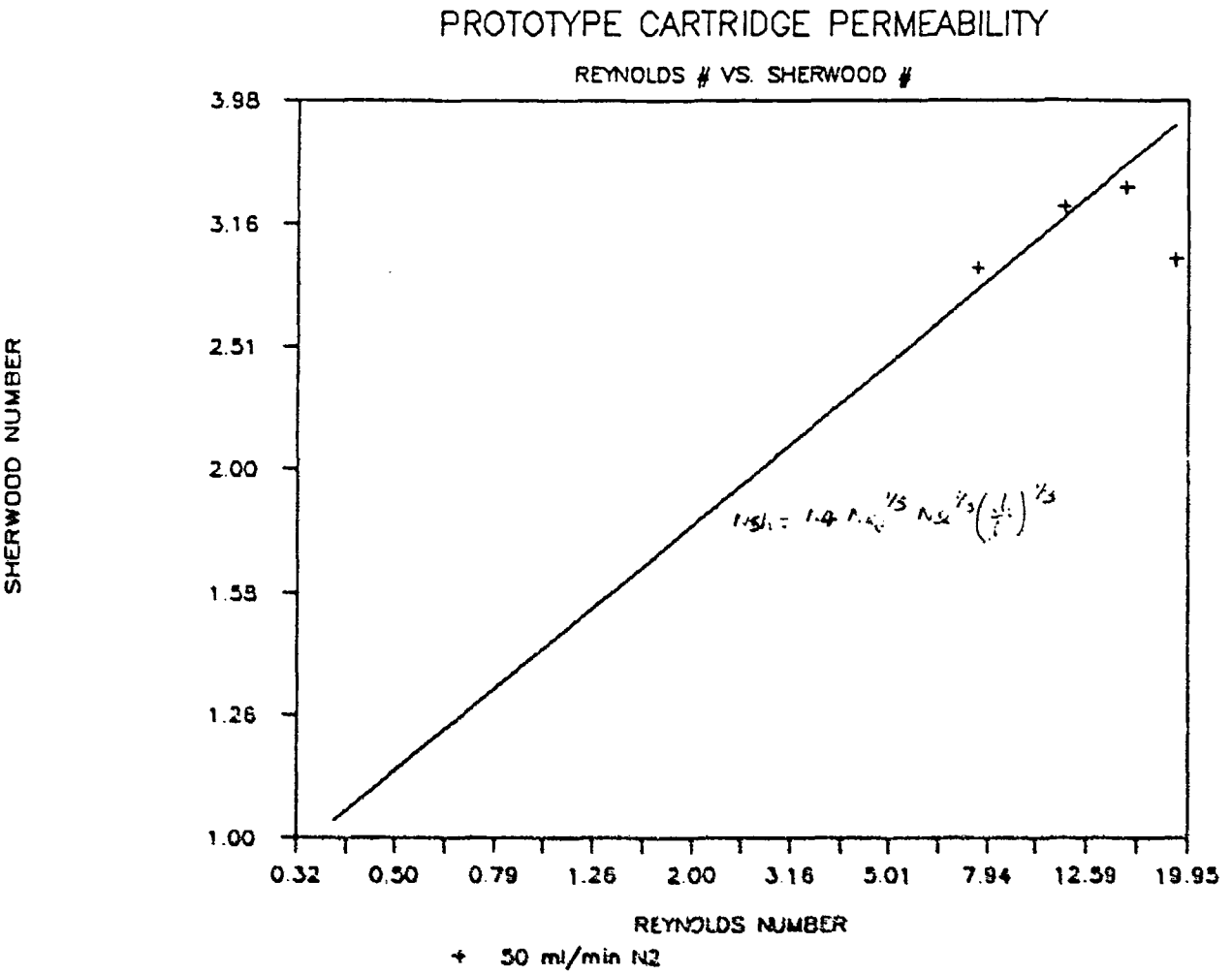
PROTOTYPE CARTRIDGE PERMEABILITY
REYNOLDS # VS. SHERWOOD #
SHERWOOD NUMBER
3.98
3.16
2.51
2.00
1.58
1.26
1.00
0.32
0.50
0.79
1.26
2.00
3.16
5.01
7.94
12.59
19.95
REYNOLDS NUMBER
+ 50 ml/min N2

FIGURE 35

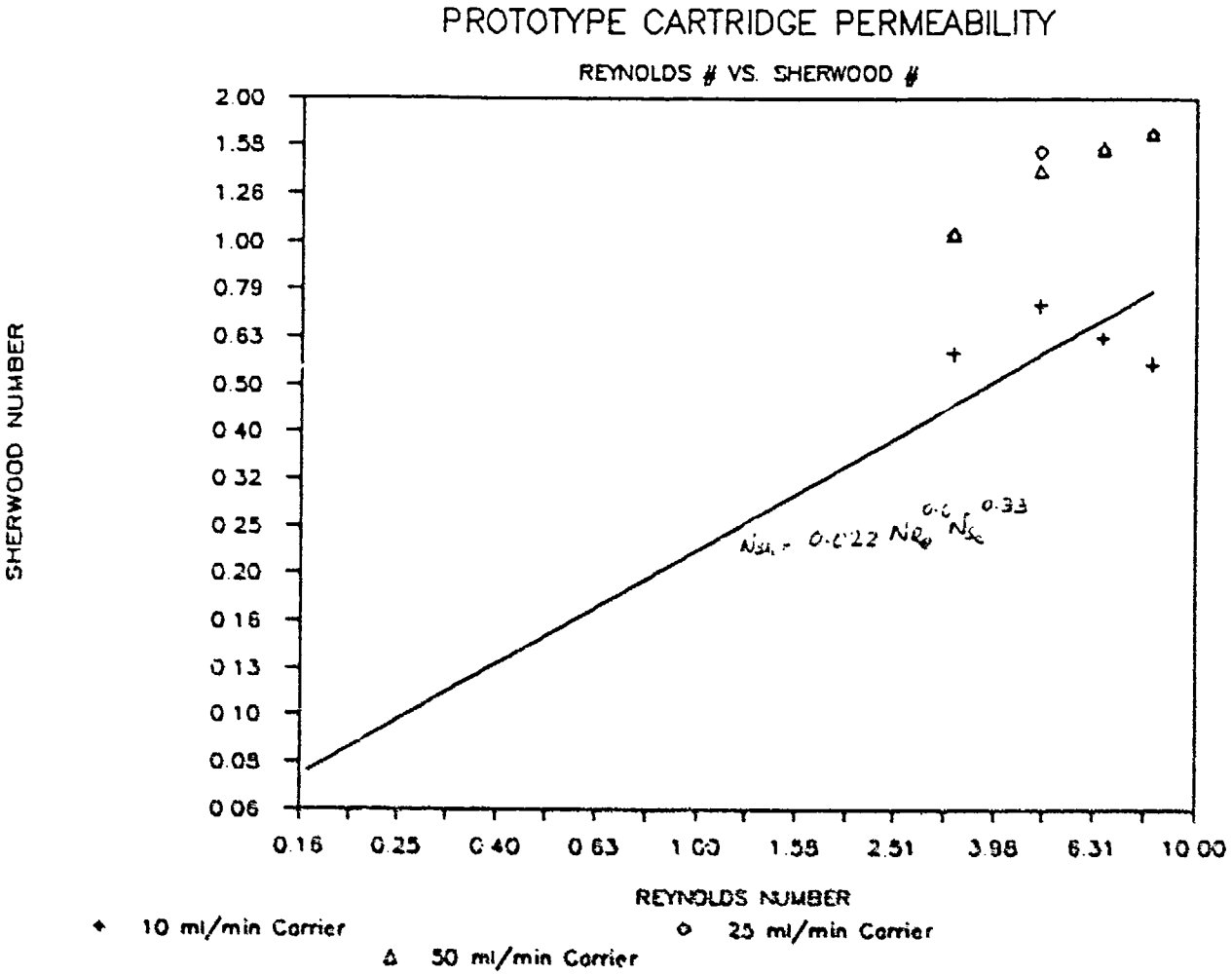
PROTOTYPE CARTRIDGE PERMEABILITY
REYNOLDS # VS. SHERWOOD #
SHERWOOD NUMBER
2.00
1.58
1.26
1.00
0.79
0.63
0.50
0.40
0.32
0.25
0.20
0.16
0.13
0.10
0.08
0.06
0.16
0.25
0.40
0.63
1.00
1.58
2.51
3.98
6.31
10.00
REYNOLDS NUMBER
10 ml/min Carrier
25 ml/min Carrier
50 ml/min Carrier

FIGURE 36

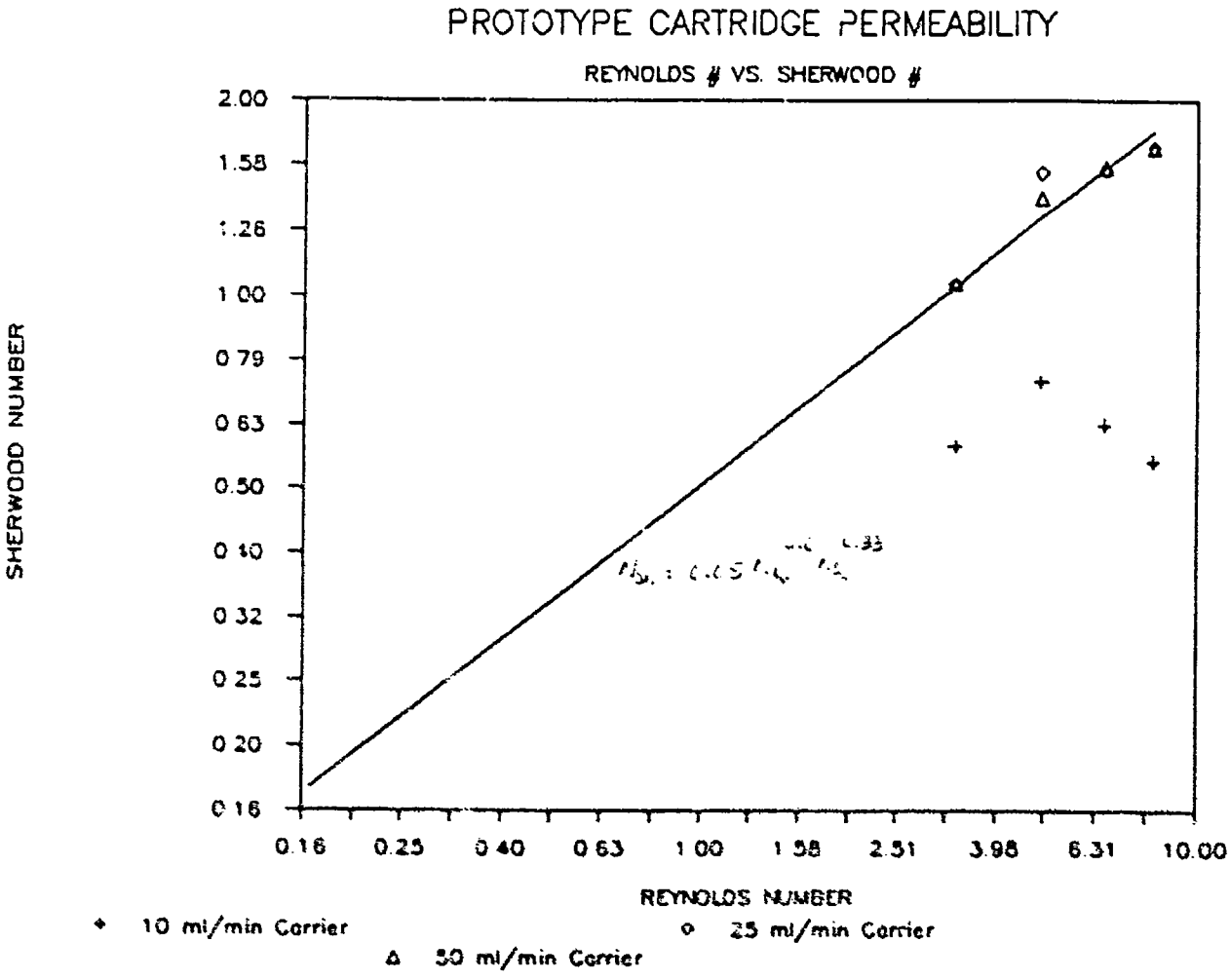
PROTOTYPE CARTRIDGE PERMEABILITY
REYNOLDS # VS. SHERWOOD #
SHERWOOD NUMBER
2.00
1.58
1.26
1.00
0.79
0.63
0.50
0.40
0.32
0.25
0.20
0.16
0.16
0.25
0.40
0.63
1.00
1.58
2.51
3.98
6.31
10.00
REYNOLDS NUMBER
10 ml/min Carrier
25 ml/min Carrier
50 ml/min Carrier

Seawater to Carrier Transport

The results of modelling seawater to carrier transport of oxygen are shown in Figure 35 and 36. In Figure 35 the data taken with the prototype solid membrane hollow fiber cartridge is compared with predictions made using the original constants as per Table 3. It is obvious that the model matches the data taken at a carrier flow rate of 10 ml/min. A flow rate of 10 ml/min of carrier represents an unbound cobalt excess of 50%. The assumption that the carrier side diffusion of oxygen can be ignored is least applicable to this case and therefore the model had to be adjusted to match data taken at carrier flow rates of 25 and 50 ml/min. It was found that by changing the value of "a" from 0.022 to 0.05 the model could predict the oxygen flux at the larger carrier flow rates better. It is also important to note that the oxygen flux does not appreciably change when the carrier flow rate is increased from 25 ml/min to 50 ml/min thus affirming the assumption that oxygen transport is limited by the flow rate of seawater and that the elimination of k_S in the equation for k_O is valid.

CONCLUSIONS

It can be concluded from this exercise that the use of published correlations does not accurately predict oxygen flux in the hollow fiber cartridge that was tested, but provides a good starting point from which better models can be derived. At this stage the data used for comparison purposes is insufficient and the experiments that have been conducted so far need to be repeated and expanded in scope to encompass more carrier and seawater flow rates. Once more experimental data has been accumulated, it should be possible to put a bound on the error to be expected by relying on theoretical models and to proceed to incorporate such models into gill design equations.

Another shortcoming of the modelling procedure outlined above is its inability to solve the equations for the carrier side diffusion at lower carrier flow rates. It is obvious that at lower carrier flow rates, the carrier side mass transfer coefficient can no longer be ignored. Hence to make the model more complete, it may become imperative that a model be constructed for the transport of oxygen through the carrier. This would have to include description of a dual process wherein diffusion of oxygen and the oxygenated species combine to contribute to oxygen transport. To complete such a model the kinetics of the reaction between oxygen and unbound carrier would also have to be described and accounted for in the rate of oxygen transfer.

Further work on incorporating the mass transport equations into the gill power-volume relationship is needed. This work would make the model for a gill less open-ended and would allow better gill design.

5.4 Gill Fouling

INTRODUCTION

The Aquanautics gill system consists of a solid gas permeable membrane which separates the oxygen carrier solution from the seawater. The mechanism for oxygen transfer across the membrane is passive diffusion. Biological and geological deposits may form on the membrane, inhibiting the flux of oxygen gas across the membrane and obstructing the flow of seawater around the membrane. Both these fouling processes would increase the power cost of pumping seawater across the membrane surface.

The ocean is filled with microbial life. Through various types of interactions, these plankton and bacteria can colonize any surface compatible with microbes. Underwater power source design considerations stipulate that this colonization, or fouling, must occur in small enough amounts that oxygen flux across the membrane does not drop by more than twenty percent and the power to pump seawater over the membrane does not rise by more than ten percent over a two year period.

BACKGROUND

The ocean environment provides an environment rich in nutrients which supports life from the smallest phytoplankton and bacterioplankton to the largest nekton such as squid and whales. The introduction of a foreign surface into the ocean is seen by its inhabitants as the perfect place to create a carpet of sea life.

The smallest forms of sea life are phytoplankton and bacterioplankton. These may be considered analogous to the grass of the sea, free-floating, but able to attach themselves to submerged surfaces. The next larger form of planktonic, free-floating life is protozoplankton. Protozoplankton are motile and receive their nutrition by ingesting bacteria and phytoplankton. Metazoplankton are considered the insects of the sea, preying on waste and animal matter of small size.

Microbial life can inhabit almost any surface introduced into the ocean, creating a thin film which provides food and attachment points for the preying animals. The extent to which a surface foreign to the ocean will foul is strongly dependent upon the depth it inhabits. The introduction of the Aquanautics Gill system into the ocean raises concern that the microbial attachments, or biological fouling, and geological factors do not change the performance of the gill system.

Fouling of the gill system may affect its performance in two ways. First, it will coat the membrane surface with a film of biologic and geologic material which can potentially inhibit the flux of oxygen gas across the membrane. Second, microbial growth can create a partial blockage between the membrane surfaces which would raise the energy needed to pump seawater across the surface of the gill membrane

DEFINITION OF BIOLOGIC FOULING

Submerged surfaces in the sea provide an environment for potential colonization by many types of organisms. There is a clear sequence of events which define the fouling process. Bacteria are the first organisms to colonize new surfaces. This is characterized by two distinct mechanisms. One process is an instantaneous but reversible adsorption of the bacteria onto the surface. This reversing process seems to have a mechanism which loosely holds the bacteria in place with a combination of van der Walls forces and repulsive electrical charge.[8,9] This phenomenon explains how glass and polycarbonate surfaces allow for immediate adsorption of bacteria onto the surface while still allowing for easy bacterial removal for counting.

---

[8]Marshall, K.C., Stout, R., and Mitchell, R., "Mechanism Of The Initial Events In The Sorption Of Marine Bacteria To Surfaces," *J. Gen. Microbiol.*, **68**, 337-48 (1971).

[9]Egan, B., "Marine Microbial Adhesion And Its Consequences," *Microbes In The Sea Sleigh*, M. A. ed., John Wiley & Sons, New York (1987).

The second process is an irreversible adsorption of bacteria onto surfaces. This is a time-dependent process of bacteria adhering with polymeric fibrils.[10] Different types of surfaces are colonized at different rates. With this mechanism the wettability, or critical surface tension, and the modification of the surface by organic polysaccharide-protein complexes, determines the rate of colonialization. The colonialization of bacteria will plateau and larger protozoa will appear, apparently keeping the bacteria healthy by balancing their productivity.

The first type of fouling is reversible. It can be eliminated by constant water velocities that keep the bacteria from forming more than a few cells of thickness before being washed away from the surface. The second irreversible process, can be slowed down by choosing a surface that is "slick" and has a surface tension which inhibits the growth of micro organisms. If needed, synthetic inhibitors can be attached to the membrane surface in the manufacturing process to help prevent the second type of biological growth.

DEFINITION OF GEOLOGIC FOULING

Marine sediment has been collecting on the bottom of the ocean at a rate of four to five meters per million years for the last seventy-two million years.[11] The oceanic sediments in some places in the ocean are well over 400 meters thick. Little characterization of sediment diffusion has been undertaken, however the sediment stratification has been reported to be very low. The diffusion stratification of the sediment layer is reported to be confined to the bottom three meters of the ocean floor.[12]

The type of geological sediment found on the ocean floor is mostly silt and sand. Except in places where the ocean bottom is rocky, the bottom is mostly a fine muddy silt. The design of the gill will have to take into account the make-up of the ocean floor so that the gill is not clogged with fine geological particles.

THE ENVIRONMENT OF THE DEEP SEA

The environmental conditions in the ocean habitat dictate the composition of the fouling microorganisms. At depths greater than 200 meters, phytoplankton do not have the proper amount of light needed to survive. Seawater temperatures below ten degrees Celsius also inhibit biological fouling.[13] The effects of depth on plankton biomass can be seen in Figure 37.

Figure 37 is a vertical distribution of plankton biomass found in three deep ocean trenches. The upper most line is the Kurile-Kamchatka Trench.[14] This trench has been used as an example because it can be considered a worst case example of the biomass constant of the ocean. The other two lines are for the Mariana trench and the Bouginville Trench.

---

[10] Egan, op cit.

[11] Menzies, R.J., George, R.Y., and Rowe, G.T., *Abyssal Environment and Ecology of the World Oceans*, John Wiley & Sons, New York (1937).

[12] Petterson, H., *The Ocean Floor*, Yale University Press, New Haven (1954).

[13] Sieburth, J.M., *Sea Microbes*, Oxford University Press (1979).

[14] Menzies, George, and Rowe, op cit.

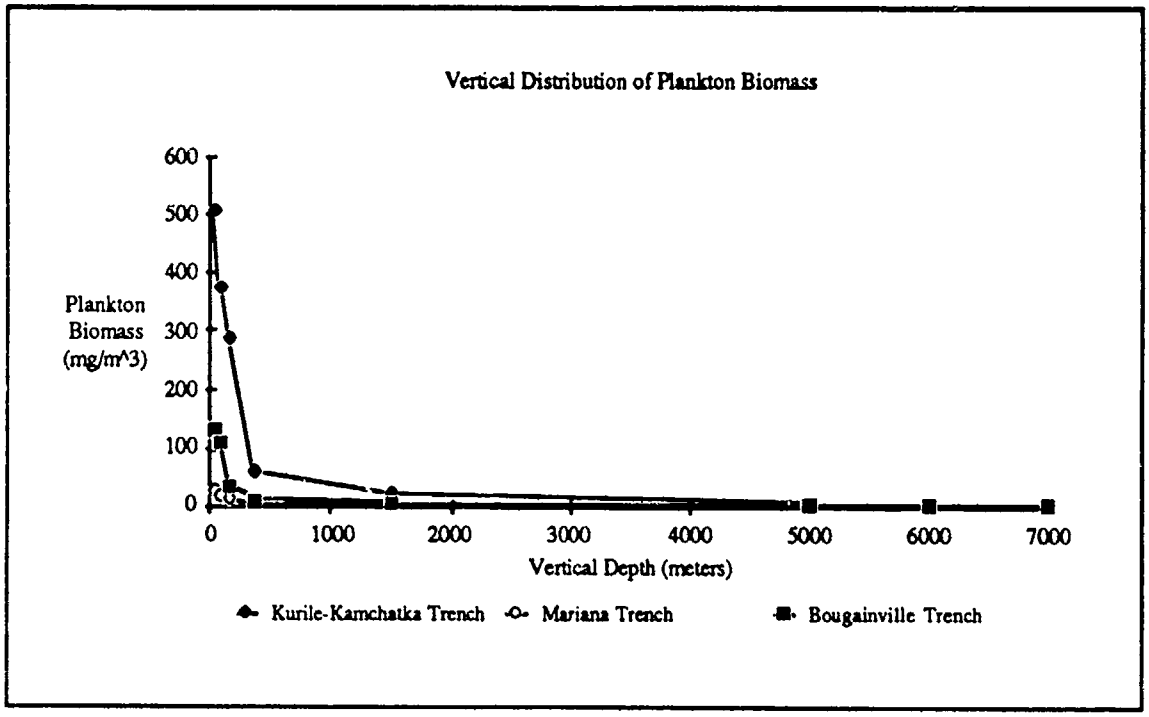

FIGURE 37
Vertical Distribution of Plankton Biomass

The ocean has a mean depth 4000 meters. This accounts for eighty five percent of the area of the ocean. The deep sea has a uniform and constant temperature averaging 2°C. Salinity of the ocean floor is also constant at 35 °/oo.The primary energy source on the ocean floor is sedimented fecal material which falls from the eupathic zone on the first few hundred meters of the ocean surface. This fecal material makes its way to the ocean floor because of the unique membrane which surrounds the feces. Bacteria on the ocean floor feed on this and any other sediment which makes its way to the bottom.

There is strong evidence that there are invertebrates on the ocean floor that feed directly on the sediments of the abyssal floor. These are classic filter feeders that feed directly on the sediments rather than by filtering seawater. In fact, except for the relatively small number of sestonophages in the deep sea, most of the fauna is made up of animals that eat and live in the bottom sediment. This key factor points toward the majority of the life found deep sea being communities which live and depend upon ocean sediment for their nutritive life.

Deep sea bacteria are unique to the bottom environment. They have adapted to the life on the ocean floor and cannot survive at sea level. The bacteria do not seem to be at all specific toward any one food source. They are capable of attacking virtually all kinds of organic compounds.[15]

BIOLOGIC FOULING IN THE DEEP SEA

At the depths where Aquanautics is planning to utilize the underwater power stations, the evidence points towards an environment which is hostile to biologic growth. In 1968 Alvin, the deep sea submersible of the Woods Hole Oceanographic Institution sank in 1504

[15]Peterson, op cit.

meters of water when a cable holding the submarine to its mother ship snapped. Ten months later food, which was to make up the diver lunches, was recovered with the vessel and found to be in an almost perfect state[16]. It was determined by experimentation that the rate of microbial degradation 10 to 100 times slower in the deep sea than at sea levels at similar temperatures using the same recovered food.[17] The apples were so well preserved, that when a bite was taken out of an apple, the taste and crispness had changed little over the ten months.[18] There was no evidence that the dissolved oxygen content of the seawater inside of the hull or the pressure in the hull was anything other than normal for the ambient conditions. The plastic lids of the sandwich boxes and the lids of the thermos flasks were crushed by the pressure, exposing the food to the deep sea environment.

It has also been found that the water pumped from a depth of 540 meters in the ocean, off the coast of Ke-ahole Point in Hawaii, to an Ocean Thermal Energy Conversion Heat Exchanger had much slower fouling than warm water pumped through the system. Bio-fouling in one cold seawater loop contained a barely detectable layer after one year in contact with seawater flow.[19] The cold water inlet was located about 580 meters deep about 20 meters above the ocean floor and 1400 meters from the shoreline. Scanning electron microscope photographs on the deep water stainless steel loops showed insignificant bio-fouling and most of the deposits were mainly inorganic. The two aluminum loops showed considerable corrosion , but not biologic growth.

When the submersible Alvin dove into 3750 meters of freezing sea water to survey the wreckage of the ocean liner "Titanic", which had been sitting on the bottom of the ocean for the last 73 years, Robert Ballard and his crew found a mix of perfectly intact and clean surfaces bordering a rusty and worm infested environment.[20] All the wood and biological materials on the ship had long since been eaten by worms. The iron hull of the ship was a giant blister of rust while the glass surfaces were clean and free from fouling. Interestingly, the debris field of wine bottles, children's dolls, porcelain chamber pots and bathtubs were clean and pristine looking and not appreciably fouled by biologic organisms or covered with silt and mud.

CONCLUSIONS

There is no significant evidence to show that biological fouling of the gill membrane should be an inhibitor of oxygen flux across the membrane. Both the cold temperature and lack of nutrients in the deep sea should keep biologic growth from inhabiting the gill. Using the freshness of the food recovered from Alvin and the lack of fouling found on the Titanic as models of what to expect on the floor of the ocean, decay and corrosion of organic and easily oxidized metals appears to be a larger problem than biological growth.

The issue of geological fouling appears to be more of a concern than that of biologic fouling. According to reports by Petterson, the diffusion layer of mud and silt on the ocean floor appears to be confined to the bottom three meters of the ocean floor. This can be

[16]Jannasch, H.W., Eimhjellen, K., Wirsen, C.O., and Farmanfarmaian, A., "Microbial Degradation of Organic Matter in the Deep Sea," *Science*, 171 (1971).

[17]Jannasch, Eimhjellen, Wirsen, and Farmanfarmaian, op cit.

[18]Ballard, R., Interview with Terry Gross on Fresh Air, WHYY Radio March 23, 1989.

[19]Berger, L.R., and Berger, J.A., "Counter-measures To Microbiofouling in Simulated Ocean Thermal Energy Conversion Heat Exchangers with Surface and Deep Ocean Waters in Hawaii," *Appl. Environ. Microbiol.*, 15 (1986).

[20]Ballard, R., *The Discovery of the Titanic*, Warner/Madison Press (1987).

overcome by constructing the gill membrane so that the inter-fiber gaps of the membrane are an open enough weave that it will not clog with geological materials. The other design consideration for the gill will be to locate the gill membrane off the surface of the sea bottom to keep it out of the diffusion zone of silt-like sediments.

6.0 HYDROGEN GENERATION

Aquanautics has in the past looked into many methods of hydrogen generation or storage for the UPS. Two of these methods were found to be favorable. They are:

1) Cryogenic Hydrogen Storage, and
2) Methanol Reforming.

For the direct carrier feed fuel cell (CFFC), the second option is not viable. The reason is that for direct feed fuel cells, a solid polymer electrolyte needs to be used as described in an earlier section. Methanol reforming normally leads to Hydrogen with contaminants which poison the electrodes in the fuel cell.

Another option which has been recently discovered by Aquanautics is the commercially available Alwatt system produced and marketed by Alupower, Inc., Bernardsville, New Jersey. Originally designed as a power source, this simple system also generates hydrogen in a stoichiometric ratio to the amount of Aluminum consumed. It is the second characteristic of the Alwatt which is being considered in the Aquanautics development of an undersea power source.

Alupower has been awarded a small research contract by Aquanautics to look into the feasibility of using their system in the context of the present program. Their report has been included in the quarterly report submitted to DARPA for the October '88 - December '88 period. The main conclusions of the program:

1) Hydrogen would be produced as a gas after reaching saturation in the flowing seawater in the Alwatt system,

2) Some seawater flow to the battery is required to avoid clogging of the battery, and

3) There will be some power generated by the Alwatt at the ocean bottom, although the voltage and therefore energy will drop as temperature goes down and the pressure increases.

The reactions in the Alwatt battery are:

$Al \rightarrow Al^{+++} + 3e^-$ at anode

$3 H_2O \rightarrow 3(OH)^- + 3/2 H_2 - 3e^-$ at cathode

$Al + 3H_2O \rightarrow (OH)_3 + 3/2H_2$ overall cell reaction

Considerations that dictate the use of the Alwatt battery to produce H_2 are:

1. H_2 generation

   27 g. of Al produces 3/2 moles of H_2

   or 1 g. of Al produces 1/9 g. or 1.24 l. of H_2(STP)

This is equivalent to carrying 1 g. of H_2 in 9 g. of Al gravimetrically or 1 g. of H_2 in 3.3 cc of Al. Cryogenic hydrogen needs 14 cc for 1 g. of H_2. Therefore it is quite clear that Al provides a very distinct advantage with regard to the volume requirement. From the consideration of weight, Aluminum will not be a good option. But for the application on the ocean floor, this is not a disadvantage.

2. Power Generation

a) Aquanautics fuel cell

1 g. of H_2 will generate power that is given by,

1 Faraday x fuel cell voltage (V), which computes numerically to,

$3.06.10^{-3}V$ in Watt-years.

Since 1 g. of H_2 = 9 g. of Al,

1 g. of Al will generate $3.4.10^{-4}.V$ of power in Watt-years via the Aquanautics fuel cell.

b) Alwatt battery

Battery will generate about 0.25V, and

Aluminum generates about 1.5 a-hr./g. This is equivalent to $4.3.10^{-5}$W-yr/g.

Energy generated per g. of Al in Watt-years:

Alwatt	$4.3.10^{-5}$
Aquanautics CFFC	$3.4.10^{-4}V$

At a fuel cell voltage of 0.6V, the total system would generate $2.47.1^{-4}$ W-yr per g of Al out of which 17% is due to the Alwatt and the remainder is from the fuel cell.

In the last quarter Aquanautics has obtained a 1 watt, 1 month endurance Alwatt battery/hydrogen generator. The size of this unit is 6" x 6" x 2" with capacity of 15 ml/unit of H_2 for a period of one month. This corresponds roughly to a size of 0.0009 liters per liter of H_2 capacity. This includes a void fraction of 50% in the battery. In the longer duration, the Aluminum plates will be made thicker and the void fraction will be reduced to at least 75% which will lead to a size factor of 0.0006, which is the final performance target.

PLAN FOR THIS QUARTER

1. The procured Alwatt battery will be tested.

2. A 10-watt battery will be ordered.

7.0 TECHNICAL ISSUES

7.1 Carrier

EOC LONGEVITY TESTING

Two new families of carriers were screened this quarter. The performance of the first family was very disappointing, especially as an almost identical family of compounds had given reasonable oxygen output. No good explanation for this has been formulated as yet.

The second new family of ligands is relatively cheap. It is also possible to achieve higher concentrations and yet retain reasonable conductivities of the solutions. As with the earlier series surprising differences have been noted in behavior upon changing the ligand structure by only one group. The same effect was also noted in a tridentate ligand family where only one group makes all the difference between oxygen production and no activity at all.

At present these new families are undergoing preliminary screening since they are not pure enough to undergo proper lifetime testing. However, it should be noted that one compound obtained commercially in 95% purity produced oxygen for 6 days. These materials will be purified next quarter for careful longevity testing.

During set up time in the new laboratory some equipment check-out experiments were run with 33SP carrier. These experiments showed different behavior for 33SP over previous experiments in that the carrier performed satisfactorily for 140 hours rather than the previously observed 70 - 80 hours. It was noted, however, that due to heating problems with the new building the average temperature was about 15-16°C as opposed to 23-25°C. This indicates that the lower temperature decreases the rate of the degradation reactions. It may be expected then that a further decrease of temperature to 0-5°C will lead to further lifetime extensions. Unfortunately, the lower temperatures also lead to reduced output and current. In the next quarter these temperature effects will be investigated.

SPECTROELECTROCHEMISTRY LONGEVITY TESTING

Last quarter this section reported on a device which simultaneously measures UV/VIS spectra and cycles a solution between oxidized and reduced states. The purpose of such a device is to mimic EOC operation, provide for a great number of electrochemical turnovers, and require low volumes of carrier. This quarter three carriers were evaluated in the thin-layer cycling apparatus.

Of the three compounds examined, 24-2 LM was most successfully cycled. This carrier appears to mimic EOC behavior when cycled in the thin-layer cell. Some difficulties with 33SP were encountered. The problem lies in assignment of the oxygen-metal charge transfer band after a few cycles were performed. The usual band at 340 nm disappears while a shoulder at around 300 nm appears to track oxidized/reduced forms. Another similar compound, 23SP, continues to 1) give small spectral changes, 2) not give a re-oxygenated spectrum upon reduction, and 3) is plagued by very low currents.

CARRIER KINETICS

Overview/Main Objectives

The main objective for this section was to determine the electron rate constant of a specific electrocatalyst at carbon fiber electrodes. Last quarter some preliminary results for the installation of the high-speed data acquisition hardware and software were reported. However, the use of that instrumental set-up was diverted to running the longevity by Professor C. William Anderson (Consultant, Hampden-Sydney College). An order-of-magnitude divergence between exchange current densities calculated by Anderson and those obtained in a half-cell (EOC-25 cm^2) Tafel plot are reported. The difference may be due to the assumptions used in constructing the Tafel plot or mass-transfer complications in the EOC cell.

Results, Discussion and Summary

A) Background: The method for evaluating electron rate constants at single carbon fiber electrodes (SCFEs) begins with mounting a single fiber to a wire. The assembly is tested using simple cyclic voltammetry. Once a precise formal redox potential (E^o) is established, small potential steps are made. Potential steps of 10-20 mV past the E^o are applied to the catalyst solution until the mass-transfer limited current is obtained (unstirred solution). A current vs. time profile is generated and recorded to disk.

Each data set of current vs. time is normalized to the mass-transfer limited current. The current data was acquired over 55 msec. These normalized current vs. time profiles are used in an algorithm and the heterogeneous rate constant is calculated from fitting the above data to a working curve, generating a rate for each over-potential employed, and extrapolating back to the case of zero over-potential.

B) Results: See Figures 38 - 40. Figure 38 is a cyclic voltammogram of a Hercules SCFE in a solution of DAMF. This cyclic confirms a viable electrode. Figures 39 and 40 are samples of the current vs. time plots after applying a potential step. Using 0.372V vs. Ag/AgCl as the E^o (determined from cyclic voltammograms at a button electrode, 59 mV peak separation), and diffusion coefficients provided by Aquanautics, Professor Anderson calculated a rate constant of 4.8×10^{-3} cm/s. "Alpha", or reaction symmetry, is calculated to be 0.5 (for oxidation). This rate constant is consistent with those estimated using cyclic voltammetry of DAMF on a glassy carbon electrode.

For comparison, Tafel plots on a half cell (EOC/25 cm^2 using only 8 mM electrocatalyst resulted in a "flat" plot. Since this plot follows non-ideal form, the very low over-potential region was employed to obtain an exchange current density ($2.92 \times 10^{-4} A/cm^2$ true surface area). The low over-potential region disallows any information on "alphas". The above exchange current density translates to a heterogeneous rate constant of 3.7×10^{-4} cm/s. Although the Tafel plot was performed on Ultra Carbon felts and Professor Anderson's work is on Hercules, an order of magnitude difference indicates the assumptions employed in calculating exchange current densities on the low over-potential region may be invalid. Additionally, the non-ideal Tafel plot may be due to mass-transfer complications (channeling, etc.). Further work is being performed by Professor Anderson using Ultra Carbon SCFEs as well as FMI and National VDG electrodes.

FIGURE 38

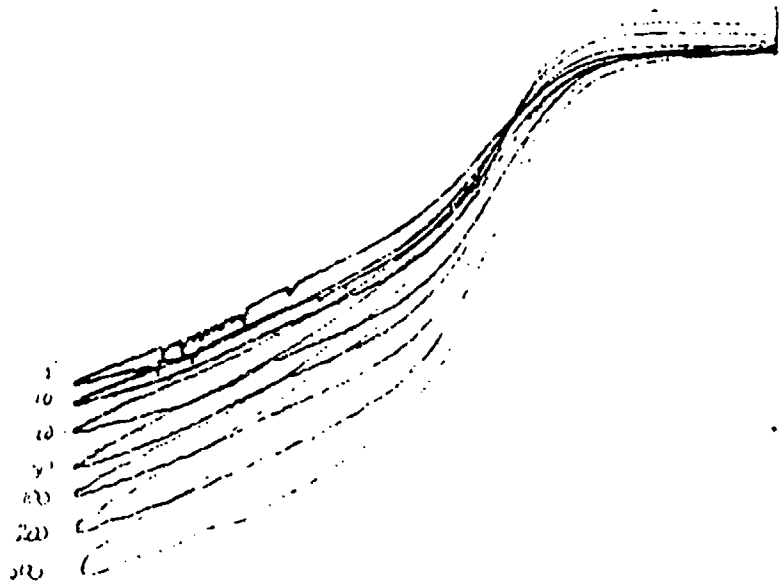

FIGURE 39

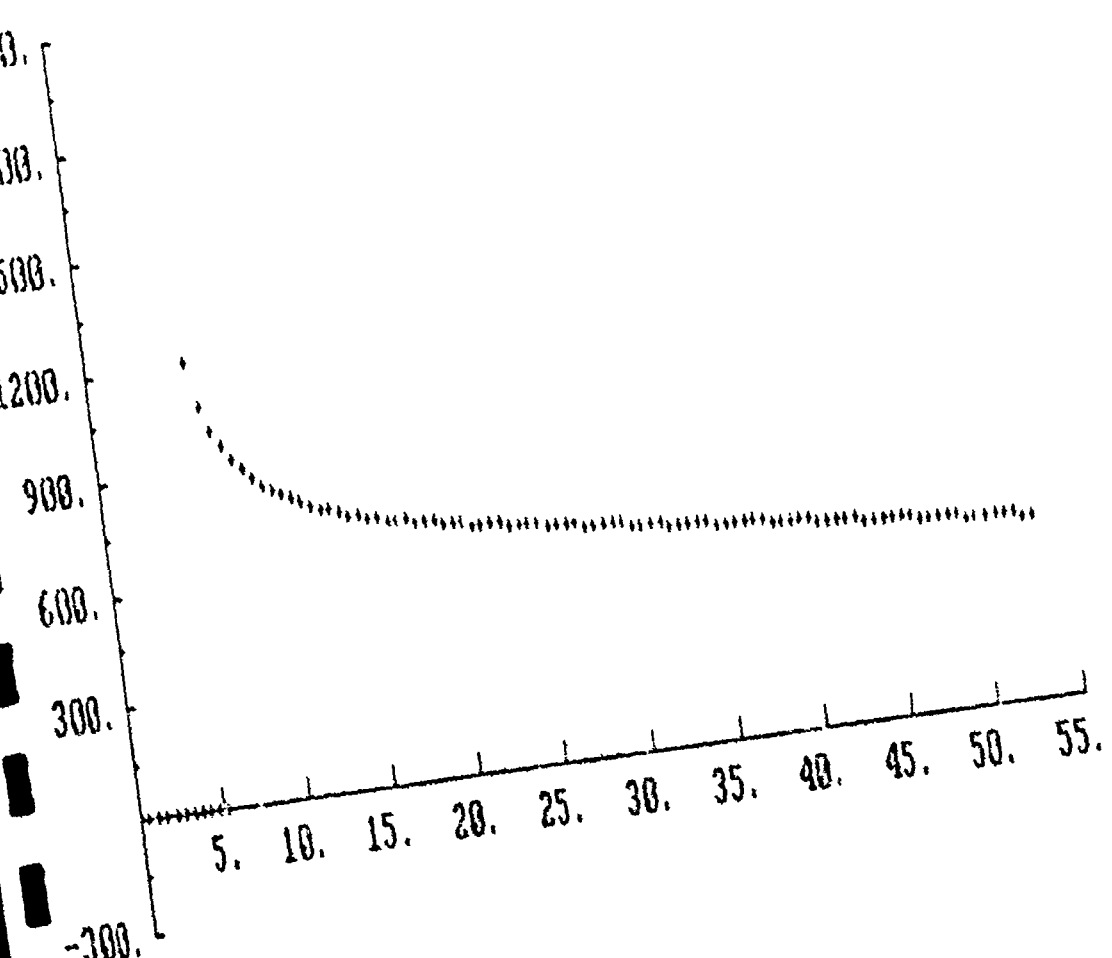

FIGURE 40

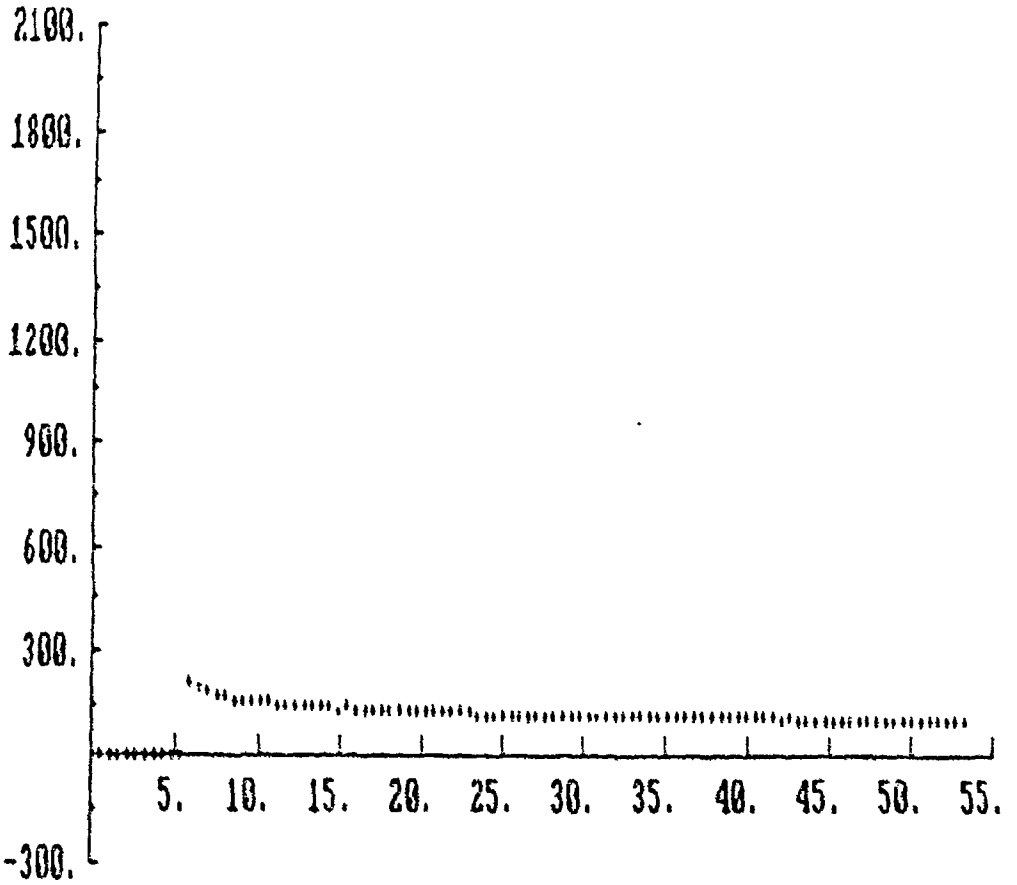

Future experiments

A. Continue rate measurements on the three felt types.

B. Explore the possibility of using this technique on direct feed fuel cell type carriers.

C. Apply method to an oxygenated Laura carrier at low pH.

FUEL CELL FUNCTION

Work was completed on a feasibility study on the use of carriers fed directly to the cathode of a fuel cell. (See Final Report for SBIR contract DAAH01-88-C-0413.) An engineering study considered a number of different schemes whereby oxygen bound to cobalt coordination complexes might be fed directly into a fuel cell in order to generate electricity in situations where gaseous oxygen is not available, for example underwater. Of the schemes considered only the one which involved direct reduction of the oxygenated carrier molecules at the cathode of the fuel cell seemed feasible. For this to be practical the carrier molecules must be able to withstand the conditions in the fuel cell, the bound oxygen must be reduced in a four-electron process to water and the process should occur at potentials sufficiently positive of the potential of the hydrogen anode to give a practical power output from the fuel cell.

Experiments were carried out to test these points. It was found that some of the Aquanautics carriers could indeed withstand the conditions of the fuel cell, at least for a period of days. The bound oxygen was reduced to water and that the reduction took place at a potential which would give a fuel cell voltage of about 0.6V. The concept of using the oxygenated carrier molecules to feed oxygen to the fuel cell is therefore feasible and the next step is to build and test a full prototype.

Although the results of this feasibility test show that the carriers can be used in the fuel cell directly, the EOC longevity testing will still be necessary. This is because the degradation of the carrier appears to occur from the reaction of oxygen with the carrier and this is common to both the fuel cell and EOC system.

PLAN FOR NEXT QUARTER

1) Continue with an accelerated EOC testing program. New sources of carriers are anticipated to become available in the next quarter.

2) Test carriers which display a reasonable EOC lifetime in the fuel cell mode. Determine from electro-analytical measurements the likely products of the fuel cell reaction and whether the oxygen reduction recurs at a reasonable voltage.

3) Investigate the use of radical scavengers in extending lifetime.

4) Investigate the effect of temperature on carrier lifetime.

5) Determine the effect of purification on carrier lifetime.

6) It is anticipated that progress in the area of kinetics will be possible this quarter due to help from a new consultant.

7.2 Design and Fabrication of a System for High Pressure Testing of Membranes

INTRODUCTION

This section describes the work done towards designing and fabricating a system for testing the integrity of gill and fuel cell membrane samples at pressures commensurate with operation at ocean depths of up to 6000 meters. This work was done as part of the feasibility study being undertaken into the use of the Aquanautics Oxygen Extraction system for generation of electrical power undersea. The integrity of membranes becomes an important technical issue when operation of the system at great depths is envisioned. The foremost issue is the prevention of liquid-liquid contact in the gill between the carrier and the seawater so as to avoid dilution of the carrier solution.

BACKGROUND

The gill is a major component of the underwater power system being conceived. The gill is the location at which the seawater and the carrier come in contact with each other through a gas-permeable membrane, allowing the dissolved oxygen in the seawater to be absorbed by the carrier. The design of such a gill must take into account various environmental factors that are determined by the depth of application, in this case assumed to be a maximum of 6000 meters. The most important environmental condition that comes into play at these depths is the overburden pressure which increases by roughly one atmosphere every 10 meters of depth. Pressures of up to 600 atmospheres must therefore be considered as the design point.

Normally, in applications at a pressure of one atmosphere, membranes used for the purposes of oxygen transport from the feed to the carrier are hydrophobic and microporous where the oxygen is transported across the membranes through the pores by diffusion. Since the pores are usually full of air, such transport is fast and not controlled by the membrane permeability itself. However under pressure, the pores tend to contract as the air within them is compressed and at sufficient pressures the liquids on both sides come in contact with one another causing mixing. This would be unacceptable to the Aquanautics system because the carrier would then get diluted over a period of time causing degradation in system performance.

To avoid this possibility, Aquanautics has been investigating the use of solid membrane technology in the gill. Usually this would involve the deposition of thin layers of a solid oxygen permeable material on a support substrate consisting of a conventional microporous membrane. While the presence of the solid layer is expected to degrade the oxygen permeability of the membrane, this degradation is not expected to affect the overall mass transfer coefficient of the system, given the predominance of hydrodynamic effects on the seawater side. Instead the solid layer will help keep the two liquids from mixing while allowing oxygen to permeate through. The depth capability of the membranes under consideration, is an important property that needs to be determined in the membrane selection process. Hence, a system was designed and fabricated to conduct such testing in-house.

DESCRIPTION OF SYSTEM

Measurement Principle

The testing principle that will be employed to test the membrane's ability to withstand hydrostatic pressure will incorporate use of the electrical conductivity of seawater. The membrane sample used in this case will be a flat sheet which will have seawater on both sides. The pressure of the seawater on both sides will be increased in steps and the resistance between the two sides measured. As long as there is no liquid-liquid contact across the membrane, the resistance across the membrane should be high. At the moment any breakthrough occurs, the resistance should drop due to the fact that there will be a ionic conduction path from one side of the membrane to the other.

The reason flat sheet samples will be used - as opposed to the hollow fiber configuration that is to be employed in an actual gill - has to do with ease of testing. It is easier to construct a device for testing a reasonably sized flat sheet membrane samples than to test a minute hollow fiber. On the other hand, testing entire hollow fiber cartridges would make the whole system too bulky and heavy.

System Schematic

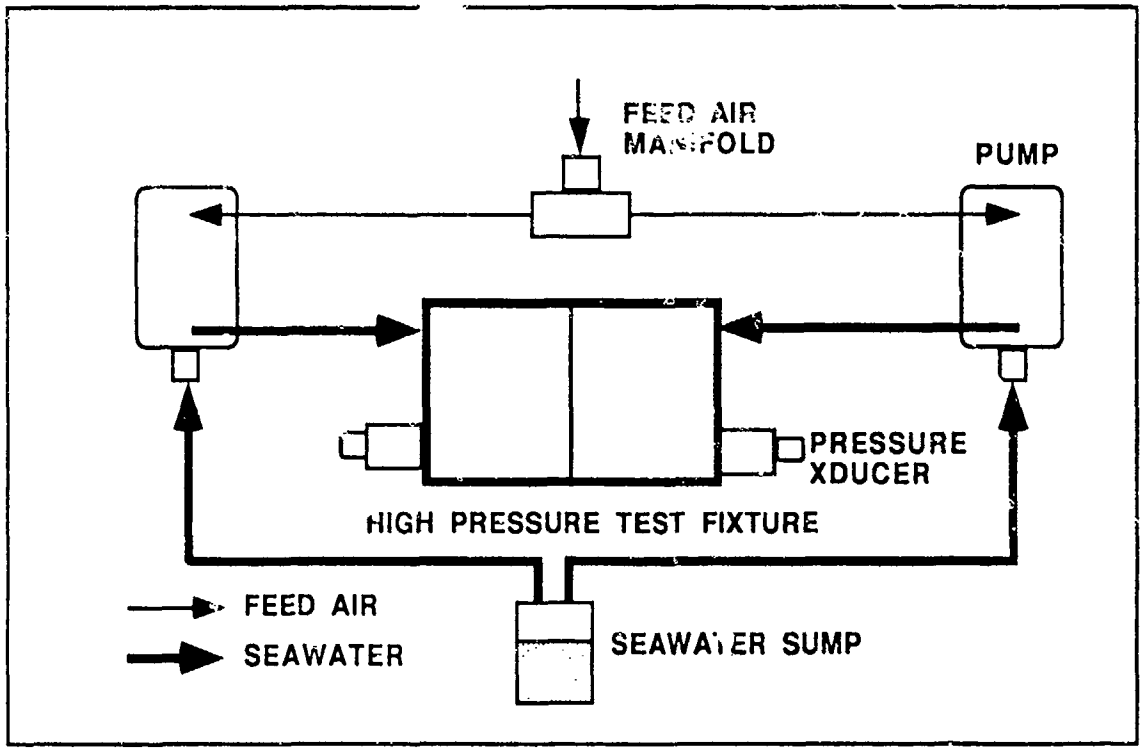

FIGURE 41
Schematic for Proposed Membrane Test Setup

Figure 41 shows the system schematic. The membrane testing fixture which consists of two chambers separated by a membrane shall be connected to two high pressure hydraulic pumps through high pressure tubing. These pumps shall be driven by air pressure and shall be controlled by using the same air feed thus ensuring that the pressure exerted by the two pumps on either side of the membrane is roughly equal. Two 0-10,000 psi (0-680

atm.) pressure transducers shall be used on either side to measure the seawater pressures. The electrical resistance shall be measured using a simple multi-meter or by applying a small potential across the two sides of the test fixture and measuring the current. The pumps shall be connected to the same air feed and isolated electrically from one another by using a plastic manifold for the air feed. The pumps shall also be connected to the same seawater sump by plastic tubing ensuring that they do not short in the sump.

Design of Fixture

The fixture for mounting the membrane samples consists of two pressure chambers that can be bolted together with the membrane sample sandwiched in between them. Figure 42 shows the assembly view of the fixture. The two chambers are of equal volume and are separated from one another by the membrane. The membrane itself is mounted on an acrylic holder that consists of two rings as shown in Figure 43. The two acrylic rings are solution welded together with the membrane sample sandwiched in between. The solution weld allows complete sealing between the inside and the outside cylindrical surface of the membrane holder. A number of such holders have been machined so that various membrane samples may be mounted on them and tested individually. The membrane exposed to the seawater is in the shape of a circular disc of diameter 1.5 inches (38 mm).

The left chamber of the membrane fixture has a receptacle into which the membrane holder fits. The right chamber butts up against the holder as shown in Figure 42 and the two chambers are sealed against the face of the holder by O-rings. Bolts are used to assemble the system together and the twelve 5/16 inch bolts used here bear the axial load caused by the pressurized fluid. The bolts that come in contact with both chambers of the fixture present a possible route for shorting the two halves, but by using heat-shrink on the sides of the bolts and by using the bolt insulator shown in Figure 42 to isolate the bolt heads, insulation was ensured. The receptacle of the left chamber is also shallower than the thickness of the membrane holder preventing the two halves from butting against one another.

Each chamber of the fixture is made of 17-4 ph stainless steel and is hardened to condition H 900 (corresponds to a hardness of 43 on the Rockwell C scale). Each chamber has three ports in its blind end, two of them being 1/8" NPT and the other a 1/4" NPT port. The larger port is intended for the pressure transducer, while one of the smaller ports is for the high pressure pump. The last port is a bleed port to be used when preparing the system by bleeding the air from the fixture.

DESCRIPTION OF OTHER SYSTEM COMPONENTS

High Pressure Pumps

These are used to subject the seawater and the membrane samples to pressures of up to 10,000 psi (680 atm.). The pumps used in the system are air-driven hydraulic pumps manufactured by Haskel, Inc. of Burbank CA. They have a piston ratio of 110:1 meaning that the pumps can amplify the feed air pressure by roughly 100 times on the hydraulic side. These pumps can also maintain pressures accurately by stalling. The pumps can therefore be used to ramp up the hydraulic pressure by ramping up the feed pressure gradually or can be employed to increase the pressure in steps by stepping up the air feed pressure. This versatility in conjunction with their level of miniaturization makes these pumps ideal for the purpose at hand.

FIGURE 42

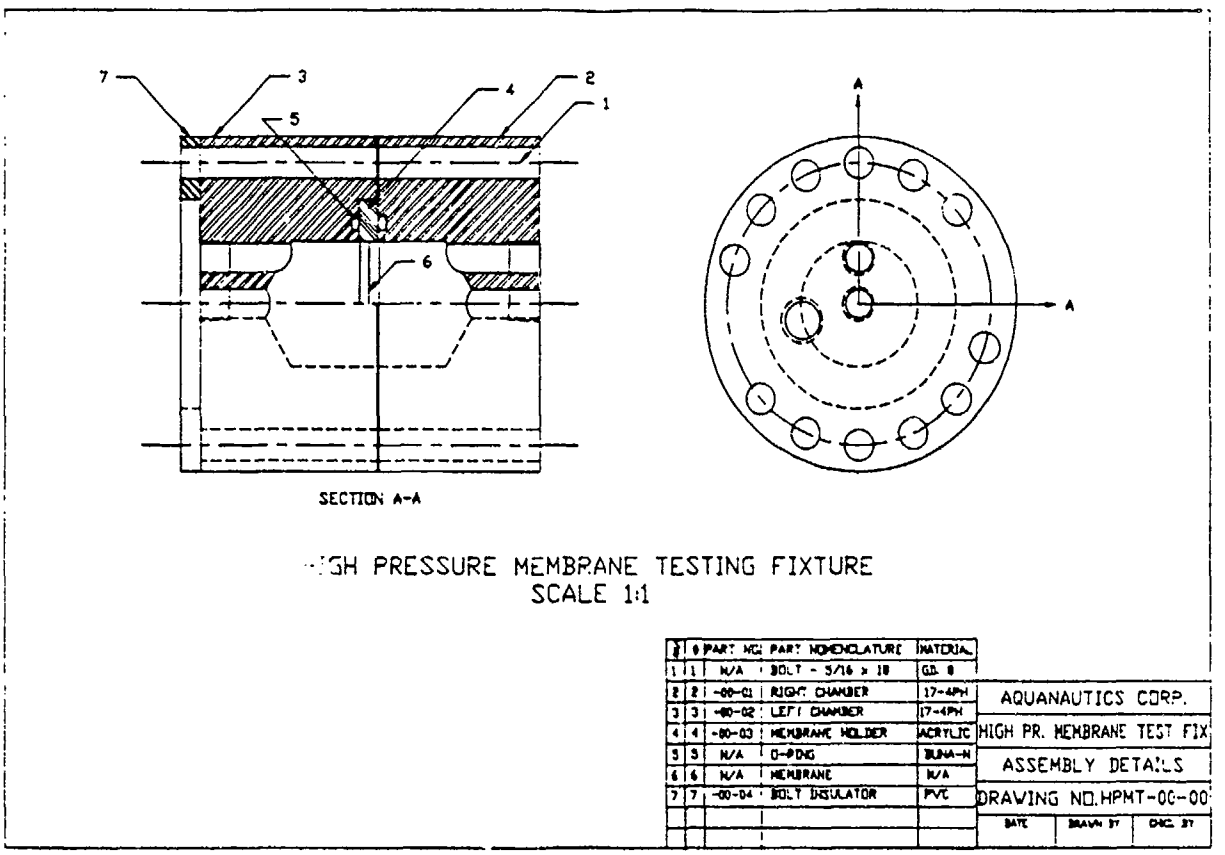

#	ø	PART NO.	PART NOMENCLATURE	MATERIAL
1	1	N/A	BOLT - 5/16 x 18	GR. 8
2	2	-00-01	RIGHT CHAMBER	17-4PH
3	3	-00-02	LEFT CHAMBER	17-4PH
4	4	-00-03	MEMBRANE HOLDER	ACRYLIC
5	5	N/A	O-RING	BUNA-N
6	6	N/A	MEMBRANE	N/A
7	7	-00-04	BOLT INSULATOR	PVC

AQUANAUTICS CORP.
HIGH PR. MEMBRANE TEST FIX
ASSEMBLY DETAILS
DRAWING NO. HPMT-00-00

DATE	DRAWN BY	CHKD. BY

FIGURE 43

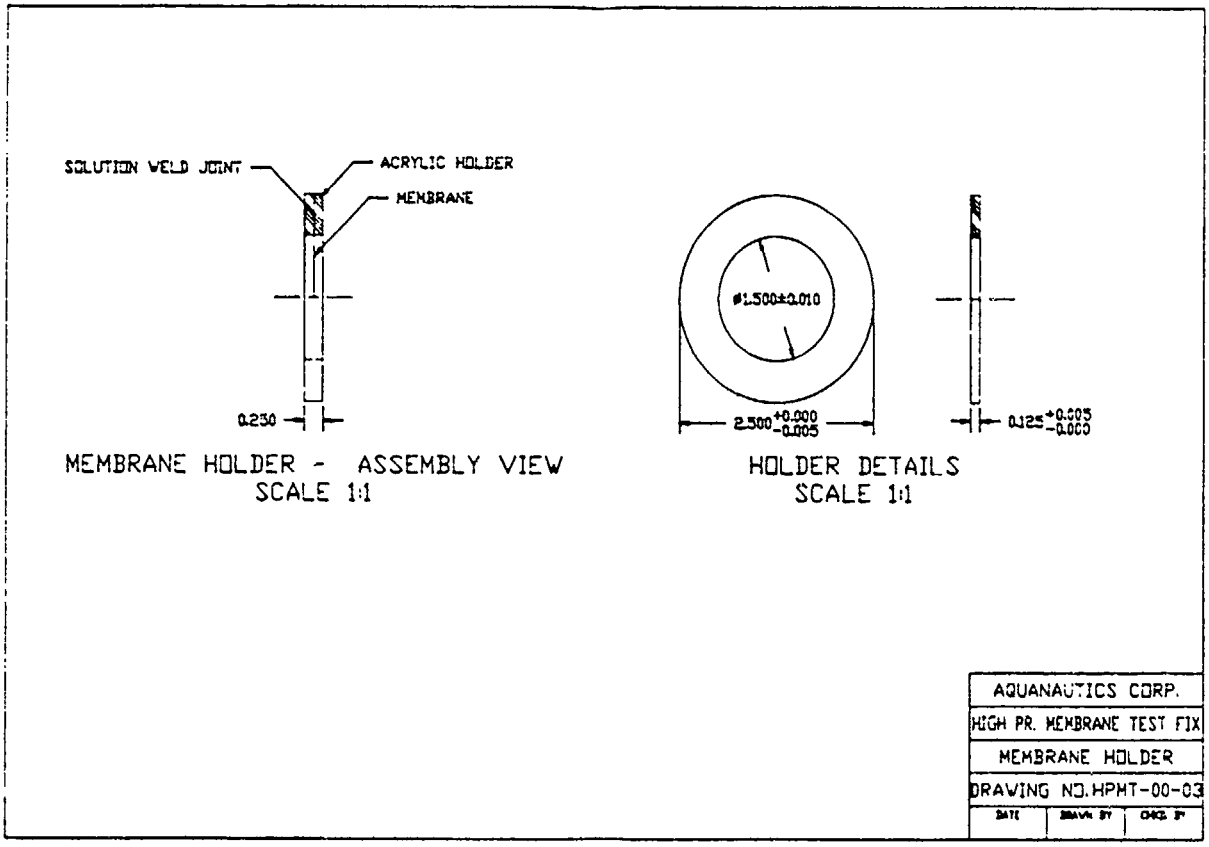
SOLUTION WELD JOINT
ACRYLIC HOLDER
MEMBRANE
0.230
MEMBRANE HOLDER - ASSEMBLY VIEW
SCALE 1:1
ø1.500±0.010
2.500 +0.000 -0.005
0.125 +0.005 -0.000
HOLDER DETAILS
SCALE 1:1
AQUANAUTICS CORP.
HIGH PR. MEMBRANE TEST FIX
MEMBRANE HOLDER
DRAWING NO. HPMT-00-03

Use of this pumping technology also allows maintaining a low pressure gradient across the membrane. This can be accomplished by simply plugging the pumps into the same air feed supply, thus causing their output pressures to be roughly equal within limits imposed by pump-to-pump variations.

Pressure Transducer

The seawater pressure on both sides of the membrane have to be measured for purposes of data recording. This is important to identify the pressure at which breakthrough occurs. The pressure can then be directly used to calculate the depth limit for a given membrane sample. The pressure transducers selected for this purpose are from the Barksdale Controls Division of Imo Delaval, Inc. located in Los Angeles CA. The pressure transducers put out a voltage signal (0-100 mV full scale) proportional to the pressure (0-10,000 psi full scale). They employ a stainless steel diaphragm with strain gages as the transducer element.

Pressure Regulator and Drive Air Parts

A pressure regulator will be used on the air feed side to regulate the supply pressure to the pumps. This regulator will be connected to a compressed air tank which will be used as the air supply. This regulator will feed the drive air to the pumps via a manifold which is made of plastic. The pumps shall be connected to the manifold through copper tubing and brass tube fittings from Gyrolok. The plastic manifold will ensure that the two pumps are electrically insulated from one another.

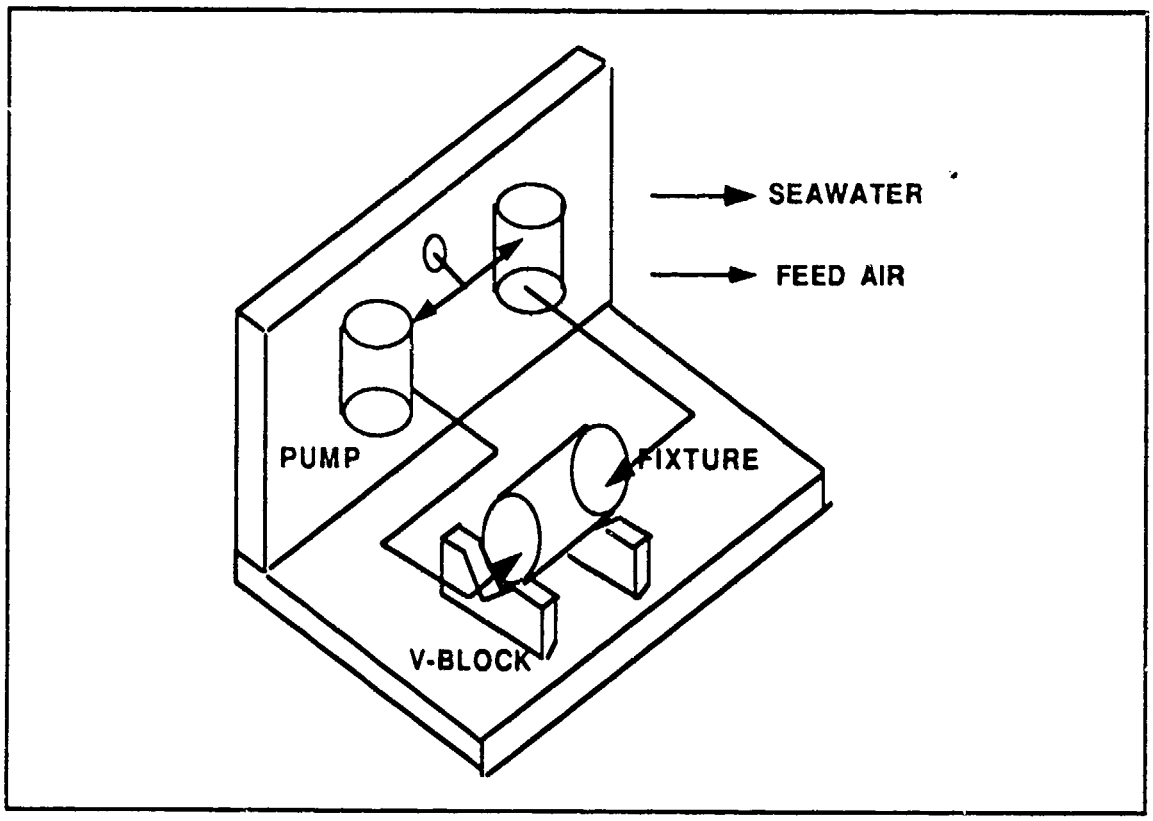

FIGURE 44
Arrangement of Test Apparatus

Hydraulic Components

The pumps are connected hydraulically to the chambers via high pressure stainless steel tubing and tube fittings made by Gyrolok. The second port that is used for bleeding is plugged with a pipe plug. The tubes used to connect the pumps to the seawater sump shall be made with plastic for reasons of electrical insulation. An open tank made of plastic is envisioned for use as the sump.

System Assembly

The system shall be housed in a plywood box for reasons of safety with ports for seawater and air as well as the signal wiring from the pressure transducers and for the conductivity measurement. The system assembly calls for bolting the pumps to an upright while the high pressure fixture sits on V-blocks on a horizontal surface. The schematic of this is shown in Figure 44.

TESTING PROCEDURE

The testing of each membrane sample is expected to follow roughly the same sequence of steps. The important steps are summarized below.

1) Assemble the high pressure fixture with the membrane sample to be tested.
2) Fill the left chamber with seawater through the entry port until the water is seen coming out of the bleed port. Shake out any air bubbles that may be trapped underneath the pressure sensor. Plug the bleed port using a pipe plug wrapped with teflon thread seal. Plug the entry port temporarily with a Gyrolok fitting end .
3) Repeat Step #2 with the right chamber.
4) Seat the fixture on the V-blocks.
5) Start only the pump feeding the left chamber and let it pump seawater out through the high pressure tube. Swiftly remove the Gyrolok fitting plug from the left chamber entry port fitting and connect the tube. Before tightening the fitting and sealing it, turn off the pump. The rationale for keeping the pump running while the tubing is connected to the fitting is to avoid trapping air in either the fitting or the tubing itself.
6) Repeat Step #5 with the right chamber.
7) The fixture and the system are now ready for use. Connect the pressure transducers and the conductivity measurement leads to the data acquisition system and turn the system on.
8) Connect the pumps directly to the air feed manifold and turn on the air supply to the pumps at the lowest possible pressure setting on the air supply regulator.
9) Increase the setting on the supply regulator and therefore the pressure on the membrane, either gradually or in steps until the conductivity measurement indicates that the membrane has been wetted. If this does not happen the test should be concluded at a seawater pressure of 10,000 psi.

TESTING PLAN

Testing is scheduled to begin in the next quarter starting with a sample of membrane that has been ordered from Applied Membrane Technology of Minnetonka, MN. This company supplied the hollow fiber solid membrane prototype that has been tested extensively at Aquanautics over the last two months. The depth capability of this membrane shall be compared to that of a conventional hydrophobic microporous Hoechst-

Celanese membrane sample (Celgard 2400), the latter being similar to the material used in most commercially available microporous hollow fiber cartridges. Further testing is also scheduled with membrane samples from Membrane Technology Research of Menlo Park, CA and SciMed Life Systems of Minneapolis, MN. The last two companies also make solid membranes but do not use the hollow fiber configuration that is desirable for the application at hand. Testing their samples shall however establish a data base of membrane depth capability.